ULTRASONIC REPAIR OF POLYMERS:

FUNDAMENTALS AND MODELING FOR SELF-HEALING

by

John Cody Sarrazin

A thesis submitted in partial fulfillment
of the requirements for the degree

of

Master of Science

in

Mechanical Engineering

MONTANA STATE UNIVERSITY
Bozeman, Montana

May 2009

APPROVAL

of a thesis submitted by

John Cody Sarrazin

This thesis has been read by each member of the thesis committee and has been found to be satisfactory regarding content, English usage, format, citation, bibliographic style, and consistency, and is ready for submission to the Division of Graduate Education.

Dr. Christopher H. Jenkins

Approved for the Department of Mechanical and Industrial Engineering

Dr. Christopher H. Jenkins

Approved for the Division of Graduate Education

Dr. Carl A. Fox

STATEMENT OF PERMISSION TO USE

In presenting this thesis in partial fulfillment of the requirements for a master's degree at Montana State University, I agree that the Library shall make it available to borrowers under rules of the Library.

If I have indicated my intention to copyright this thesis by including a copyright notice page, copying is allowable only for scholarly purposes, consistent with "fair use" as prescribed in the U.S. Copyright Law. Requests for permission for extended quotation from or reproduction of this thesis in whole or in parts may be granted only by the copyright holder.

John Cody Sarrazin

May 2009

ACKNOWLEDGEMENTS

This paper is the result of the cumulated effort of multiple parties and hours of hard work. The research inspiration was planted by Dr. Umesh Korde, currently at the South Dakota School of Mines. Research was completed with assistance from Dr. Steven Rutherford, namely on heat transfer and polymer characteristics, Rukiye Tortop, performing differential thermal analysis tests, and Steffan Francischetti assisting with composition and background in biological self-healing design. Throughout the extensive process, guidance was readily administered from committee members Dr. Ladean McKittrick, especially on the nuances between the complexities of ABAQUS computer code, and Dr. Doug Cairns, elucidating how the ends are only as valuable as the means are concrete. Also, this project could not have come to fruition without the support and assistance of committee chair and advisor, Dr. Chris Jenkins. Whether trudging through repetitive directions and corrections or subtle miscommunications, his aspirations and aid never wavered.

Additional thanks to the entire Mechanical and Industrial Engineering department faculty and staff at Montana State University. And a legitimate apology to the friends and family exposed to the entire process. Special thanks to my office mates who kept things from ever getting dull, and to Dr. Ruhul Amin, my undergraduate advisor, for instilling the possibilities of further education. I can only claim all of the error, for all of the success does not belong solely to me.

TABLE OF CONTENTS

LIST OF TABLES

Table Page

LIST OF FIGURES

Figure Page

LIST OF FIGURES - CONTINUED

Figure Page

LIST OF FIGURES - CONTINUED

Figure Page

LIST OF FIGURES - CONTINUED

Figure Page

LIST OF FIGURES - CONTINUED

Figure Page

LIST OF FIGURES - CONTINUED

Figure Page

LIST OF FIGURES - CONTINUED

Figure Page

LIST OF EQUATIONS

Equation Page

ABSTRACT

Although current research focuses within self-healing materials are advancing, most pursuits are passive systems, unlike the active biological systems they aim to mimic. In this paper an active method utilizing ultrasonic energy is explored. Ultrasonic inspection has served as an effective means toward nondestructive damage detection for decades. Also, a recent method called time-reversed acoustics allows for the redirection of acoustic waves back towards the source.

The active healing method utilizes ultrasonic nondestructive damage detection to locate and categorize damage, and then provide coordinates for the redirection of an amplified ultrasonic energy to heal the material. First, the temperature change as a result of ultrasonic treatment was measured, and then a variety of dogbone samples were tensile tested, including virgin samples, damaged samples, and damaged but ultrasonically treated dogbone samples. The ultrasonic treatment increased the ultimate stress of the ultrasonically treated dogbone samples, which was a result of increased crystallinity. The crystallinity was confirmed with differential thermal analyses. The ultrasonic influence of material temperature and effect of ultrasonically treated damaged samples versus just untreated damaged samples were replicated with finite element models as a means to predict future application and use.

INTRODUCTION AND RESEARCH OBJECTIVE

Engineering, following the general form of its own function, has taken logical steps in development over the last decade. Much like mathematics and physics, engineering was born out of simple concepts, explored for practical advancement, accepted as a science, and is currently being accepted as a branch of physical science. Engineering as is known today flourished out of necessity during the Industrial Revolution when technology was harnessed to make various industries more productive and efficient. This then evolved into a means to make improvements in daily life, clearly exhibited by the expressed need for advertising in the 1950s where different technologies could be selected, compared, and easily obtained in a variety of products. Engineering practice allowed problems to be solved and suited to comply with individual standards and needs. Engineering allowed a bridge for unique problems to be supplied unique solutions.

As engineering evolved and matured, though, the philosophy in design rarely wavered, the motto being, "Apply science to improve standard of living." As a result, the main design philosophy implied nothing of endurance. Designs were meant to function the same as the day created through the entire lifetime of the device or structure. This philosophy, accordingly, is referred to as the 'design for lifetime' strategy (1). But as engineering is still evolving, so is its backbone philosophy. A more realistic approach is being considered where the function decreases even after some limit of damage has been accepted. This is a much more symbiotic approach where design focuses on how to sublimate external influences instead of reject and repel them. The coexistence of

multiple factors has urged engineers to examine and learn from the most diverse example possible, that of nature. Instead of harnessing nature, and producing a synthetic twin of its processes and power, more of an effort to mimic processes that nature has evolved over eons has been undertaken. One such process of extreme importance in the life of numerous organisms is that of healing. The ability to heal oneself allows longer function and lifespan after damage infliction, especially from unexpected and unpredictable sources. Healing, regenerating, and enduring are some of the extraordinary processes in nature.

Being able to include a healing aspect as an engineering design consideration would open numerous possibilities over multiple industries. Currently, self-healing materials are being explored in the forms of polymers and fiber composites. For the most part, these products listed under self-healing contain multiple constituents. Damage to the material will make contact between the constituents evoking a chemical reaction, and the healing, or curing, will be completed. In a more general sense, damage is absorbed by a chemical reaction. Unlike healing in nature, though, the detection of damage needed to initiate healing is not conscious, but a certain degree of damage is the catalyst to healing. While this process is useful and needs to be further explored, this paper seeks to explore the incorporation of damage detection and healing initiation by alternative means. This is performed with the assistance of ultrasonics.

Ultrasonic testing has been used for decades as a means to locate damage in materials without damaging the specimen. Ultrasonic testing can triangulate the size and location of damage within a specimen to varying degrees, but this paper proposes to add an additional step of using ultrasonics to put energy back into the specimen to initiate and

localize healing. If successful, the field of self-healing polymers will have included an additional means to enact healing, and a conscious, albeit intermediate, step in damage analysis.

BACKGROUND

Polymers seemed an easy option for experimentation due to their simple composition. As the name implies, the base molecular unit is a monomer unit that is repeated in long chains with covalent bonds. This means healing is achieved by joining chains together, or creating new chains in the material. Also, polymer creation is relatively easy with low temperature molding and milling easily performed. This makes the inclusion of encapsulated epoxy constituents easily accomplished. Also, the epoxies created have a similar structure which assists the post healing behavior of the material. Polymers have already found large applications in everyday society making their self-healing counterparts that much easier to incorporate in everyday life. Carbon fibers are also choice candidates since it's in their nature to include multiple materials. Changing a lattice matrix and including a supplemental constituent within the lattice matrix is more straightforwardly sought than in a block of 6061 aluminum.

Healing in Nature

The ability to self-heal in nature is often overlooked as simply the status quo with no further investigation. Part of the mentality comes from the separation human beings feel with respect to nature, and therefore the constant changes nature initiates. Also, it is difficult to distinguish between healing, as a result of inflicted damage, and general growth. The healing versus growth argument is especially true of more simplistic life forms. For example, cutting one's lawn, or trimming of landscaping foliage results in repair or death, depending upon the damage inflicted. For the most part, though, it would

be smart to put one's money on a blade of grass cut in half to survive and repair than that of a human in the same situation. There is also a trend in ability to heal and complexity of life form. On the simplest level, single cell organisms can incur relatively immense amounts of damage and still survive. The ability to endure can be attributed to the asexual mechanism for reproduction, though. A unique paradigm is created since most complex organisms, for example, any mammal, lives to reproduce through sexual intercourse while less complex organisms, for example, bacteria, use asexual reproduction to live. Amoebas and Paramecia split in twain in a process called binary fission as a means to reproduce and procreate. It seems damage, although controlled and self-initiated, is actually a means to reproduce.

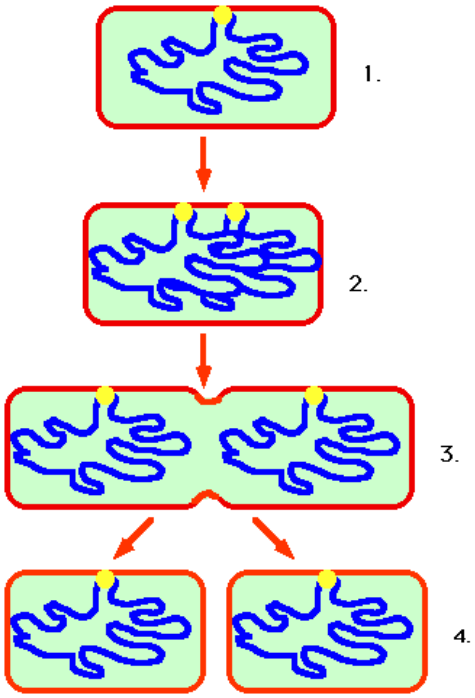

Figure 1: Binary fission diagram. (1)

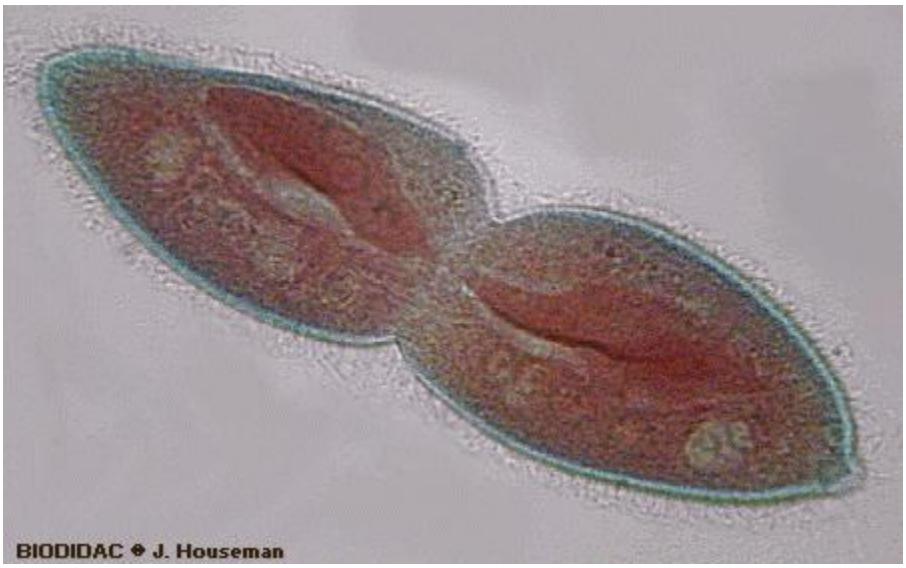

Figure 2: Picture of cell splitting by binary fission. (2)

Studies show that the binary fission process is natural and predictable in splitting and therefore new organism growth rates, but also show that if the cell is split by external means, the resulting pieces can still create two complete and healthy cells. Considering the cell as an entire organism, the ability to heal is extraordinary. The ease of healing also helps to explain the problems caused by bacterial growth, and the extensive measure needed to exterminate them.

As the level of organism complexity increases, healing is still observed, but to a lesser degree. For example, trees in areas of heavy logging and de-forestation commonly have the majority of the above ground organism removed and will perish, but clipping a branch will not greatly affect the rest of the remaining organism while the removed branch will die.

Figure 3: Heavily logged area. (3)

On a smaller scale, an axe cut in a large tree will result in the damage being filled in with tree sap that will harden, and to an extent, 'heal' the axe cut. The sap acts as a band-aid for the axe wound and shows a healing response, albeit a passive response.

Figure 4: Tree leaking sap. System resembles human bleeding. (2)

When speaking of healing mechanisms, passive refers to an act that occurs with little or no external input or energy, whereas the opposite, an active process, does involve additional energy or influence. As an example, dropping a rubber ball on a hard surface

will make the ball bounce. This is a result of the ball with its environment, and the material characteristics of the ball. But, an external influence could direct the ball in a certain direction with increased force or velocity as an active process with a desired result.

To move up another level of organism complexity, certain underwater organisms have been known to exhibit some of the same healing response as the single cell organisms. Although they have no brain or head, starfish do have a mouth and a rudimentary circulatory system. Starfish have five or more arms that radiate out from the center of the body, of which the underside contains the mouth. If a starfish loses an arm, it has the ability to regrow that arm, with the result being identical and of equal or lesser size. Starfish have been the bane of many fisherman's lives by filling their nets, starfish being a useless economical commodity. As a result of angst caused, the fishermen would habitually cut the starfish up into pieces and throw the pieces back into the sea, intending it to be their grave. The damage allowed for the starfish pieces to regrow into new organisms. In a few cases, one arm section regrew the entire starfish body, although the original arm was noticeably larger than the new body. As an ironically tragic twist of fate, the fishermen were in actuality not only perpetuating, but increasing the magnitude of their own problems.

Figure 5: Starfish Regeneration from one severed limb; the larger limb on the right. (3)

Another group of organisms known for their regeneration ability with a complexity above that of starfish are salamanders.

Salamanders are a group of organisms within the amphibian class exhibiting the ability to regrow entire limbs. Even though the lost limb dies, the salamander can repair itself to its same size and appearance as corresponds to before the limb was lost. There are limitations, though. There is a certain area range near where the limb connects to the body within which complete repair can be completed. Outside of this area, the skin and muscle can heal, but no limb regrowth is observed, making the response similar to that in humans.

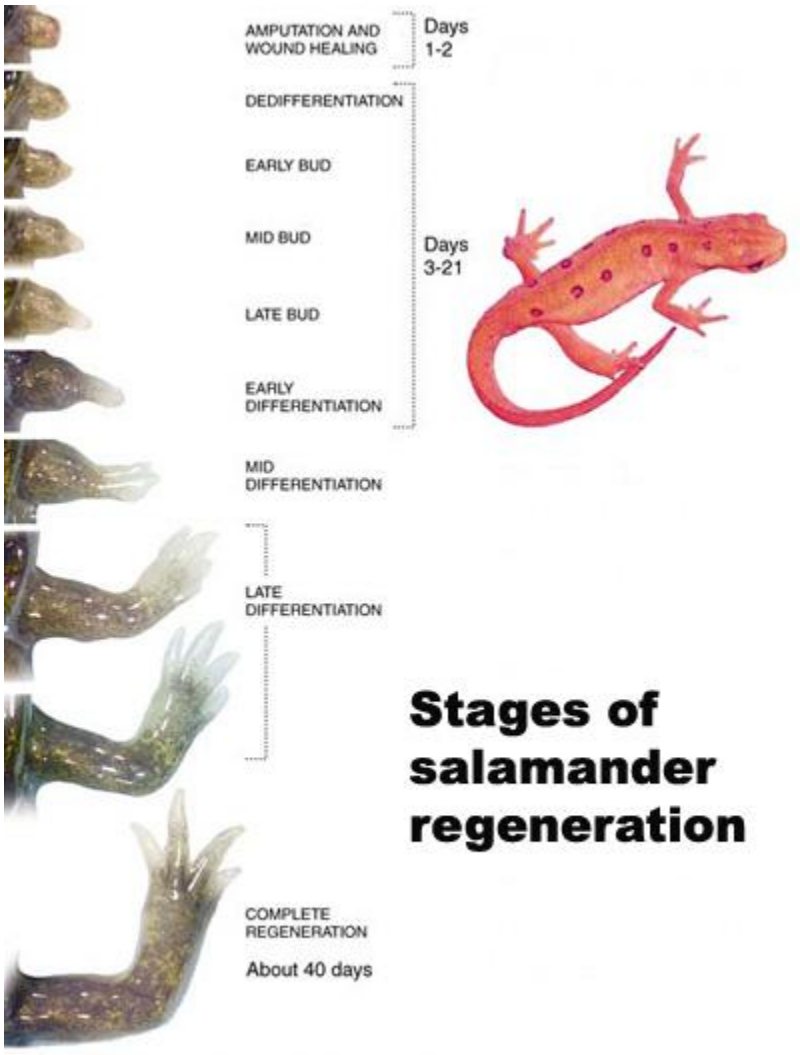

Figure 6: Limb regrowth in a salamander. (4)

Another group of organisms similar to salamanders with an exemplary healing ability are lizards. Many species of lizards have the ability to lose their tales, and then regrow them. As a matter of fact, for some species, losing the tail is a defense mechanism. These lizards will attract the predator to the tail, and when attacked, run away and leave the predator with only a tail as a consolatory prize.

Figure 7: Lizard losing tail. (5)

Although all these healing examples seem commonplace in nature, such abilities dwarf the healing capabilities of more complex organisms such as human beings. Luckily, even though humans cannot regrow limbs, they have the ability to create devices such as prosthetics to aid in optimal function and ease of everyday activities.

Another argument in the ability for regeneration and healing of organisms is the stage of development. Just as ability to heal decreases with increasing organism complexity, the increased development, or age of organisms corresponds to decreasing ability to heal. Specifically to humans, early stages of development are more prone to complete healing or regeneration. This is somewhat ironic seeing as humans develop, they move from single cells into multiple cells and then on to complex multi-cell organisms. As humans develop, they actually become more complex organisms.

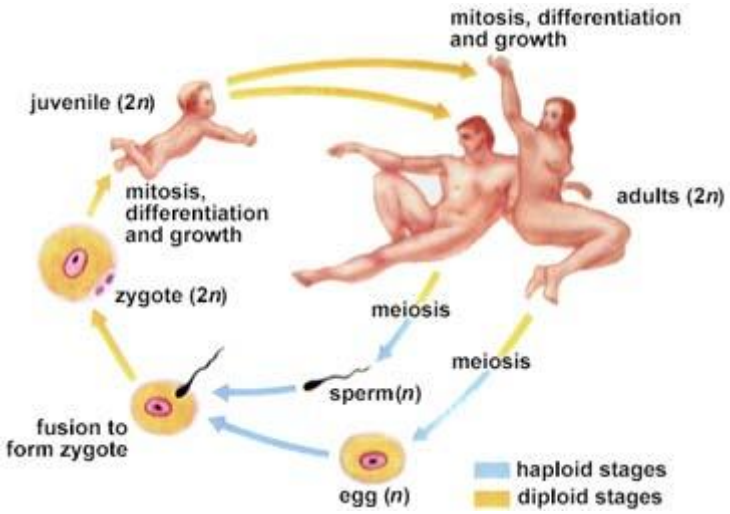

Figure 8: General human growth cycle from single cell to complex, multi-cell organisms. (6)

This concept does make sense, though, since humans in early stages are perpetrating further development, all of the materials and precursors are present and active to repair. Therefore, just a switch in objective from develop further to repair is needed. At the other end of the age/development gamut, older humans have increased difficulty recovering from damage. Natural processes such as regrowth of skin are slowed, and the newly developed skin is less responsive, which is illustrated by the lack of elasticity and formation of wrinkles. Unnatural or externally caused damage takes much more time to heal. A simple fall or trip upon a hard surface will only stun a younger individual while such a fall can cause the breaking of bones in elderly individuals. The trend can also be observed by the fact that the majority of patients needing medical care are elderly (7). Perhaps the decreased healing ability in increased complexity and development of organisms is supposed to be counterbalanced with increased reasoning and experience acquired. As a means to survive, one should learn to avoid damage to oneself. Nonetheless, as nature is concerned, the ability to regenerate and heal is most prevalent in the less complex, and less developed organisms. Giving materials and structures the

ability to regenerate and heal allows an upgrade to smart materials and another aspect of design and maintenance to improve utility, performance, and functional lifetime.

Polymers

Polymers are a group of materials characterized by their repeated molecular chains, just as the derivation of the Greek roots suggests. Each molecular unit, or monomer unit, can be considered a link in the polymer chain. Therefore, overall physical and mechanical characteristics of any one polymer are the resulting behavior of the orientation of the polymer chains, and the monomer unit, or molecular link composing the polymer chain. Polymers are naturally occurring and artificially synthesized. The natural occurring polymers are grouped into three main classes. These classes are polysaccharides, polypeptides, and polynucleotides (8). In more general terms, these classes relate to starches and cellulose, amino acids and proteins, and DNA and RNA, respectively. This paper, though, is only concerned with synthetic polymers.

The synthesizing of polymers is grouped into two types, addition and condensation. Addition polymerization is when all of the atoms of the monomer are included in the creation of the polymer. Most polymers created by additional polymerization are referred to as polyolefins since they are formed from monomers with a double bond between the carbon atoms known as olefins (9). During the other process, condensation polymerization, the monomer units can lose atoms when making the polymer. These lost atoms can form molecules, a common one being H_2O, or water. This helps explain the name, condensation polymerization (9). Since atoms are disregarded in the condensation polymerization process, most polymers resulting from

condensation polymerization are created from monomers that contain two different groups of atoms. This group of monomers can join together to form ester or amide links, hence the resulting polymers are called polyesters and polyamides, respectively. It should also be noted, though, that new methods of polymerization are emerging in technology. One such method is plasma polymerization where gaseous monomers energized from the gas discharge of a separate polymer condenses on substrates (8). This process results in a high level of cross-linking and does not fit well in either the additional or condensation group. Besides the polymerization process, another determining factor in the created polymers is the monomers involved.

The base unit for the polymer is the repeating unit, which is, or heavily depends upon, the monomer used to create the polymer. Also dependent upon the monomer in the polymer is the polymer's name. Homopolymers are polymers that only contain one type of monomer (8). One such example is Polyethylene, which is composed of only ethylene monomers. The mixing and addition of different monomers, though, describes a copolymer (8). One example of this is Polyvinyl Chloride, or PVC which alternates ethylene and chlorine atoms attached to the carbon atoms along the chain structure (9). Within copolymers, monomers can be categorized by their arrangement as alternating, periodic, random, statistical, or block copolymers (8). Although much information is related through the polymer nomenclature, polymers have such a wide distribution, use, and variety of uses, that the proper nomenclature is discarded for an easier name or its acronym. Examples include Polyvinyl Chloride, or PVC, as listed above. Another example is polyurethane, whose common name is spandex, and whose trade name is

Lycra. Some other poplar polymers include polyethylene terephthalate, polyethylene, polypropylene, polystyrene, polytrafluoroethylene, polyacrylamide, and polyamide (9).

Besides makeup, this paper is concerned with general behavior of polymers, and that is, polymers as a solid. As most solid materials, polymers exhibit a crystalline structure, mostly. Different polymers can in fact be of a crystalline structure, or of an amorphous structure. Most synthetic polymers contain regions of both crystalline structure and amorphous arrangement with the amount of crystallinity described as a volume or weight fraction. Polymers with a higher degree of crystallinity will exhibit a higher brittle response and a higher level of light scattering, making them more opaque than their amorphous counterparts (10). Even though the polymer is constructed in long chains, the chains never really stretch out completely. Instead, they fold in an orderly serpentine fashion like wire coils in a toaster. These serpentine chains can then be stacked to create a lamella (10). The lamella accounts for the crystalline structure in the polymer. Folds of the polymer chains can be broken or can lie haphazardly outside of a lamella, characterizing an amorphous region. When the polymer chain has part of the strand that exists outside the lamellae, but still connects the chain, the lamella represents the switchboard model, similar to older phone operations where the operator utilized a switchboard with looping cords. Concurrently, the adjacent re-entry model describes the lamella where polymer chain ends just lie outside of the serpentine arrangement. On the next order of arrangement, sections of lamellae can join to radiate out from a central point called the central nucleus like radii within a sphere. The regions in between the radially arranged lamellae are amorphous regions and may contain tie molecules between separate lamellae groups. This entire three-dimensional radial unit with crystalline

lamellae and amorphous regions is called a spherulite (10). A kilogram sample of polymer contains billions upon billions of spherulites. Keep in mind that increased crystallinity does not always correlate to more, larger chunks of crystalline lamellae because crystallinity is a volume or weight fraction. This means that more, smaller chunks of crystalline lamellae will result in a higher overall crystallinity than fewer large chunks of lamellae since it is a ratio. A good analogy would be a cup filled with water and marbles. The water represents amorphous polymer chain bits and pieces, and the marbles represent the more organized spherulites. Putting a couple of large marbles in the cup leaves a lot of water to the fill the gaps, whereas putting lots of small marbles in will leave less room for the amorphous water and therefore raising the marble volume, or crystallinity ratio. When considering polymers, crystallinity should be equivalent to bits of organized crystalline structure since no polymer is completely amorphous or crystalline. It is almost as if polymers can be considered a composite material. This consideration is especially important when analyzing branching and cross linking.

One polymer feature that influences crystallinity is molecular structure. For a closer look, examine polystyrene. Polystyrene comes in two distinct flavors: syndiotactic and atactic (10). Syndiotactic polystyrene contains a very regular and orderly polymer chain structure where the phenyl groups alternate sides. As an analogy, if the polymer chain was a tree branch, the phenyl groups would be regularly alternating leaves. This regular structure allows for easy regular arrangement, or crystallinity. Atactic polystyrene, on the other hand, has no such order. The phenyl groups, or analogous tree branch leaves, exhibit no regular order making any sort of regular arrangement very difficult. Accordingly, atactic polystyrene is very amorphous and syndiotactic

polystyrene is very crystalline (10). This should be noted when labeling polymers. Some polymers can be grouped into crystalline or amorphous categories, while others can be displayed in both categories simultaneously. Polypropylene, Kevlar, and nylon are highly crystalline polymers, and polycarbonate, polyisoprene, and polymethyl methacrylate are highly amorphous polymers. Another factor in determining polymer crystallinity is intermolecular forces. For example, the polar amide groups in nylon, or polyamide, are molecularly attracted to each other between chains. This ease of regular joining increases the amount of crystallinity in the polymer (10). Other factors in amount of crystallinity include branching, cross linking, and addition of plasticizers.

Branching, much like the name sounds, is the splitting of polymer chains into smaller and smaller polymer chains. Also, branches interact by intertwining and interfering with each other. Long branches get tangled up more and therefore increase bulk strength in the polymer (8). Shorter branches, on the other hand, upset crystalline structure and reduce bulk strength. The purpose of desiring shorter branches, though, is that reduced crystallinity will increase transparency and ductility (8). Polyethylene helps illustrate this point. Low-density polyethylene, or LDPE, has numerous shorter branches and therefore is flexible and transparent (9). As a result, LDPE has uses such as coatings and films. Most people have experienced LDPE in the form of plastic sandwich bags. Alternatively, high-density polyethylene, or HDPE, has a much lower amount of branching. HDPE is brittle, and less translucent than LDPE (9). People have encountered HDPE in plastic milk containers. The branching index is "a parameter, *g*, characterizing the effect of long-chain branches on the size of a branched macromolecule in solution and defined as the ratio of the mean-square radius of gyration of a branched

molecule…to that of an otherwise identical linear molecule…with the same relative molecular mass in the same solvent and at the same temperature…" (11). Special cases of branching exist and are known as dendrimers where every monomer is branched. As with shorter branches in general, dendrimers have lower branch entangling and lower crystallinity (8).

Cross linking is the process of increasing chemical bonds between lengths of polymer chains (8). This process increases the polymer's strength and toughness. The most commonly known cross linking occurs by cross linking rubber with sulfur to manufacture automobile tires, and is referred to as vulcanization. Although discovered by chance, vulcanization of rubber allows the tire to hold air while incurring more damage and use making vulcanized tires more durable than rubber tires without cross linking. An example of not being vulcanized or cross linked rubber is a pencil eraser where the rubber can flake off as to not damage the writing medium.

Plasticizers are a chemical additive to make polymers more flexible. Plasticizers are molecules similar to polymers that are added to keep polymer chains separated (8). The addition of plasticizers is analogous to the addition of carbon black in ferrous metals. The result is an increased durability and reduced ultimate strength. For example, polyvinyl chloride, or PVC, is a common material for plastic pipes, vinyl siding, and plastic bottles. With the addition of a plasticizer, though, PVC can be used for raincoats, shower curtains, and cling wraps (12).

The polymer of the most interest to this paper, though, is nylon, nylon 6,6 to be exact. Nylon is the general name for the group of condensation polymers known as polyamides. Another well-known trademark polyamide is Kevlar, and the first known

nylon application was toothbrush bristles. As these examples imply, nylon is commonly produced as a fiber since its initial creation was to become a synthetic substitute for silk (12). As a solid material, nylon has been used in place of lower stress mechanical components, formerly made of metals, and many simple structure items. The most common commercial grade of nylon is Nylon 6,6 101. Since nylon is a thermoplastic, it can be extruded, casted, and injection molded.

As the name implies, polyamides have amide groups along with carbon configurations as the backbone of the polymer chain. An amide group has the chemical formula, $(CO)NH_2$ (13). The amide links are quite polar and allow for easy hydrogen bonding (13). This combination makes nylon usually assume a regular crystalline structure. Nylon 6,6 is made from the combination of two monomers, a dichloride and a diamine. The dichloride could be hexanedioic acid or hexanedioyl dichloride while the diamine is 1,6-diaminohexane (14). The difference with the dichloride acid is with actual production. The hexanedioic acid is used in an industrial atmosphere where the combination also includes heat and pressure. The hexanedioyl dichloride can be used at room temperature and atmospheric pressure to create nylon with the 1,6-diaminohexane (13). Closer inspection shows the molecular combination does not match up, because nylon is a condensation polymer, so water, a small molecule, is lost.

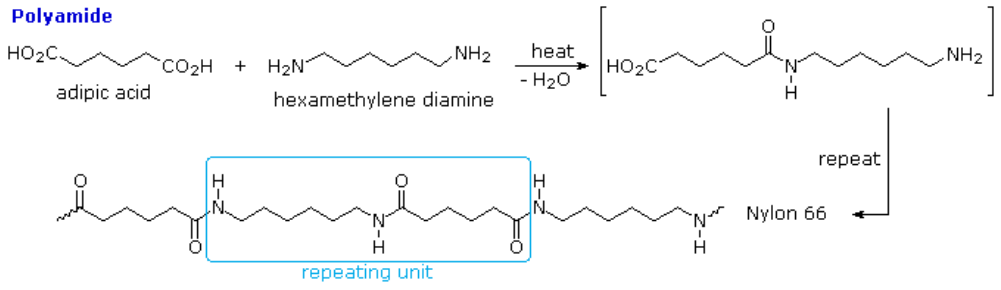

Figure 9: Nylon polymer structure. (9)

The number assignment associated with different nylon types is actually notifying the number of carbon atoms in each monomer group. Nylon 6,6 has two different sets of six carbon atoms in each repeating unit. Due to the combination of its mostly crystalline structure, its commonality, ease of acquiring, and thermoplastic nature, nylon 6,6 was chosen as the polymer to employ for experimentation and further analysis within this study.

Ultrasonics

Ultrasonic waves are acoustic sound waves with a frequency above the audible range of 20,000 hertz. Ultrasonic wave propagation was first deeply studied with the invention of submersible vehicles for purposes of reconnaissance and warfare in the form of sonar. This grew to a study of ultrasonic waves in solids, mainly metallic materials, as a means of identification of internal materials. Since ultrasonic wave propagation could be used to identify different materials through a solid thickness by identifying a boundary, then it was discovered it could also be used for internal flaw detection. Eventually, this use was refined in the 1940's to provide for the pulse-echo technique which is utilized in nondestructive ultrasonic testing used today (15).

In the decades following the application of ultrasonic testing procedures, flaws could be detected allowing for damaged components to be discarded and replaced. This was the practice associated with 'safe life' design. As methods of nondestructive testing became refined and more accurate on smaller scales, fracture mechanics arose as a means to assess damage and specify if a component does indeed need to be replaced or repaired. This new philosophy is referred to as 'damage tolerant' design since function is still

performed and failure avoided while damage has been incurred. Nondestructive testing has evolved as an engineering science regulating the maximum useful life of components, generating maintenance schedules and methods, and advising future operation. It seems the next step is damage recognition and mending.

Ultrasonic testing is rooted in sound wave propagation. In solids, sound waves can propagate in four general modes named by the motion. These modes are characteristic of shear waves, longitudinal waves, surface waves, and plate waves (15). Longitudinal waves and shear waves are the most common, and usually feed off each other. Longitudinal waves are considered the most powerful, or can carry the most energy, which can be attributed to their creation. At this point, it should be mentioned that it is helpful to think of wave propagation as a movement of energy. The atoms and molecules of the material used as a wave transmission medium must not always move in the direction in which the wave is propagating. Longitudinal waves move parallel to wave propagation direction. Longitudinal waves are a series of compressions and expansions in the direction of wave propagation, and are therefore also referred to as pressure waves, compression waves, or density waves as the density changes between compression and expansion steps. Longitudinal waves can propagate through solids or fluids, while shear waves need a solid medium to transmit through (15). Shear waves are also referred to as transverse waves since the particles move perpendicularly to the direction of wave propagation. Just as shear waves can be created from energy derived from the more energetic longitudinal waves, surface waves can be derived from both longitudinal waves and shear waves. The resulting motion of a particle subjected to a surface wave is an elliptical path, and occurs when a surface is hit with a longitudinal

wave at an incident angle. As the name suggests, the surface wave motion is only on the surface of a material or substance, and the elliptical particle motion dies out the further it travels from the surface. Surface waves only permeate to a depth of one wavelength into the material (15). Similarly, plate waves can only propagate in materials as thin as a few wavelengths (15). This makes plate waves suitable for applications in plates and wires. Concerning plate waves, one such type most used for non-destructive testing is referred to as Lamb waves after their founder, Horace Lamb. Lamb waves come in modes, symmetric and asymmetric, whose motions are dependent upon shear wave and longitudinal wave velocities (15). The descriptions express the behavior of opposite sides of the plate. While both faces will have an elliptical particle motion, the wave motion will be symmetric between faces, or equal for Lamb wave propagation. It helps to think of the plate faces as standing waves that are a mirror image, symmetric, or a translated image, asymmetric.

As with acoustic waves, as well as electromagnetic waves, wavelength is a function of wave speed divided by wave frequency. Wavelength and wave frequency are thus inversely related by the factor of wave speed. This fact is important with ultrasonic testing because different wavelengths allow for different size flaws to be observed with ranging sensitivity. Also, usually operators have the ability to directly control frequency input of the ultrasonic source as a means to control detecting wavelength. As a general rule of thumb, the ultrasonic wavelength must be less than twice the discontinuity's length to be detected (15). This means that the smaller the damage to be detected, the smaller the wavelength necessary. This corresponds to a larger frequency. Fortunately, a higher frequency allows for higher sensitivity as well as better resolution. The main

drawback with increased frequency, though, is increased ultrasonic sound wave scattering. On a small enough scale, grain boundaries and imperfections can cause the waves to scatter making resolution and depth of penetration decrease (15). The decrease of resolution is s problem for nondestructive testing methods.

One of the most established methods of nondestructive ultrasonic testing is pulse-echo. As the name implies, an ultrasonic probe pulses an ultrasonic wave through a material, usually with the use of a coupling agent, and waits until the wave hits a boundary. At the boundary, part of the wave will be transmitted through, and some of the wave will be reflected, or echoed. The key to the pulse-echo method is analyzing the difference in time and wave amplitude between wave transmission and reception. The reflection path is shown below in Figure 10. The ultrasonic transducer emits an ultrasonic pulse that transmits through the material until it reaches a boundary. At the boundary the wave reflects back to the ultrasonic transducer. The ultrasonic wave transmission speed is known for the tested material, or can be found by analyzing the time between transmission and reception with the opposite surface boundary, the ultrasonic wave transmission velocity is then twice the specimen depth divided by the time period.

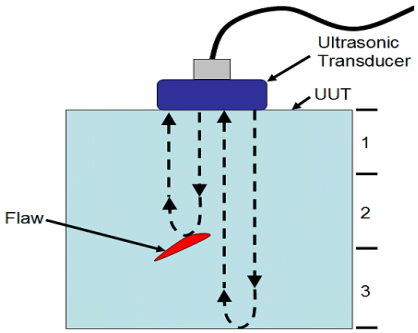

Figure 10: Ultrasonic testing principles. (1)

The ultrasonic pulse-echo output is then a time versus amplitude plot. An example with a transmitter/reciever pair and pulse-echo output is shown below.

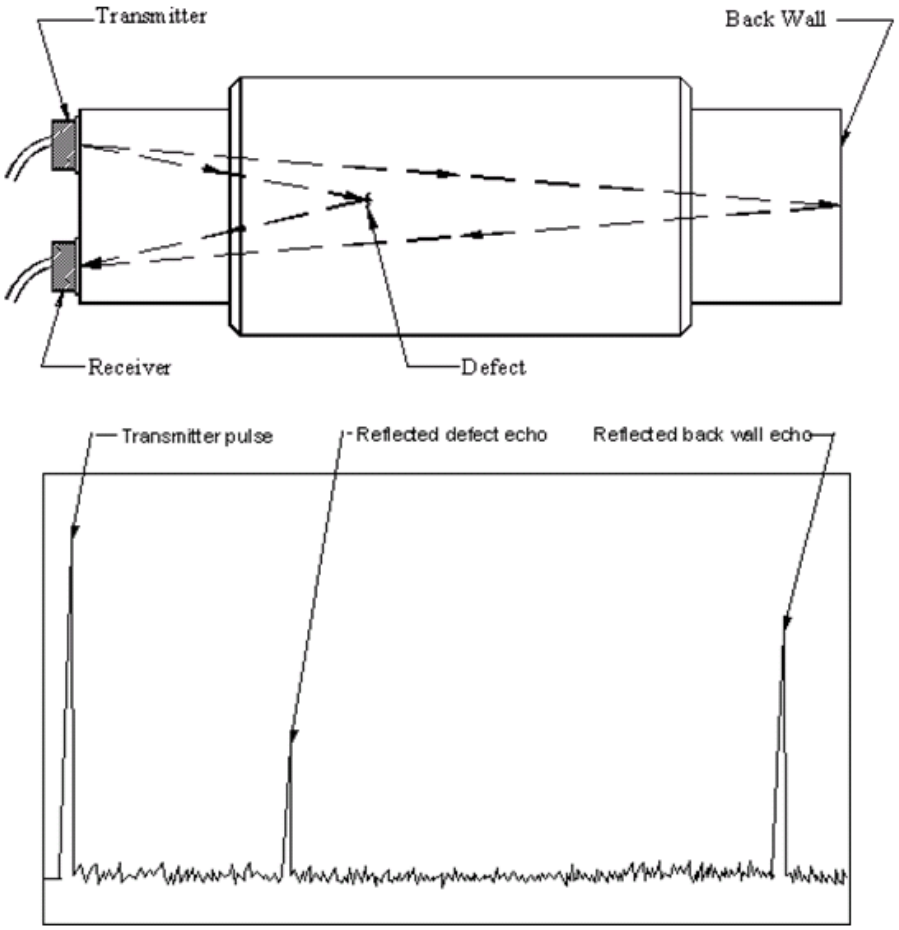

Figure 10: An example pulse-echo setup and response. (1)

The time period between initial pulse and reception echo determines the depth of the crack while the echo amplitude corresponds to the size of the damage. This can be seen from the the previous figure by comparing the peak amplitude of the damage echo versus the peak amplitude of the backwall echo. The pulse-echo technique also allows the analysis of multiple layers of damage to be determined. An example is shown below.

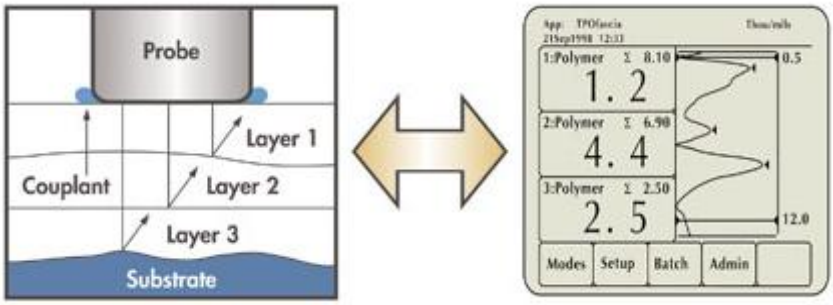

Figure 11: Ultrasonic probe diagram. (1)

The main drawbacks with pulse-echo nondestructive ultrasonic testing are signal dissipation through certain materials, the necessity for large amplitudes on the echo signal, and one-dimensional analysis requiring the probe to be moved around for any sort of three-dimensional view of the damage. Currently, a more recent technique for nondestructive ultrasonic testing countering these problems is time of flight diffraction. Time of flight diffraction (TOFD) uses at least one pair of transmitters and receivers mounted along the same surface of a material. The setup is shown below.

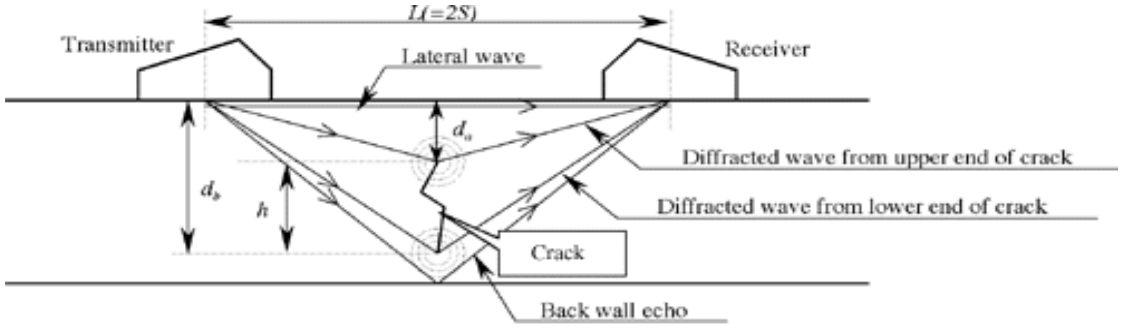

Figure 11: Time of flight diffraction basics. (1)

The transmitter of one pair emits a low amplitude ultrasonic signal that only diffracts off of the back wall of the material and crack tips. This means one signal pulse locates the crack and reveals its size in terms of two crack tips. Also, TOFD is not amplitude dependent since it does not rely on reflected energy that could be dissipated or reduced due to inferior coupling agents. Noticeable boundaries are simply spikes in the received signal, as is illustrated in figure 13, the complimentary receiver plot from the setup in figure 12.

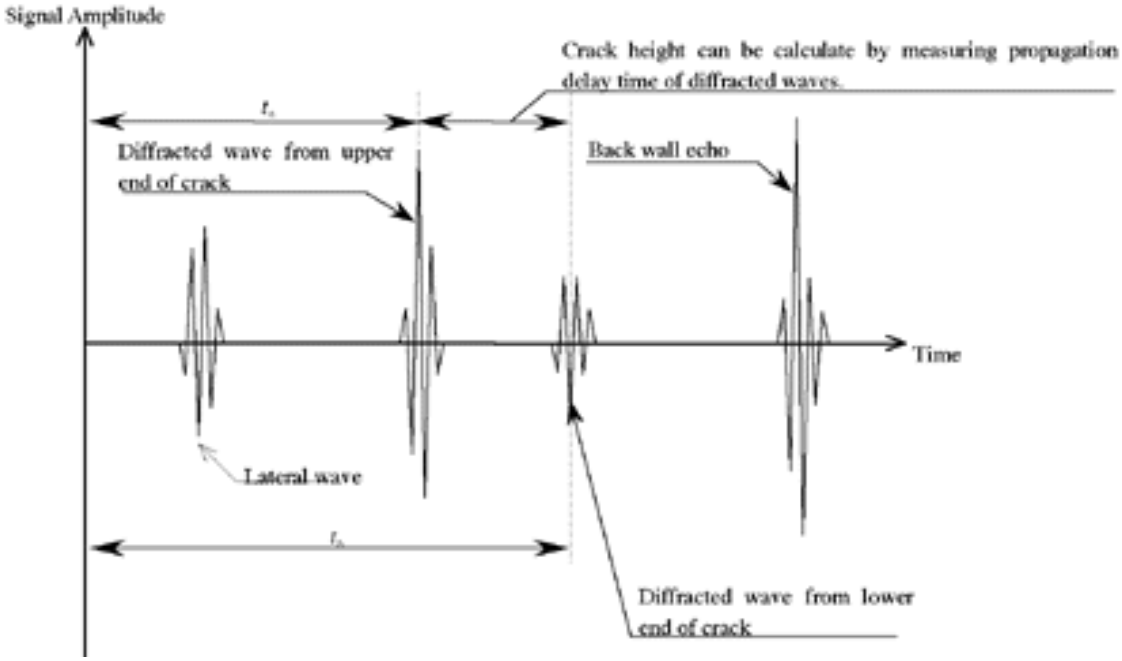

Figure 12: Response plot from setup in figure 12. (1)

As a better illustration, the figure below shows the relationship between the signal response and an associated computer output.

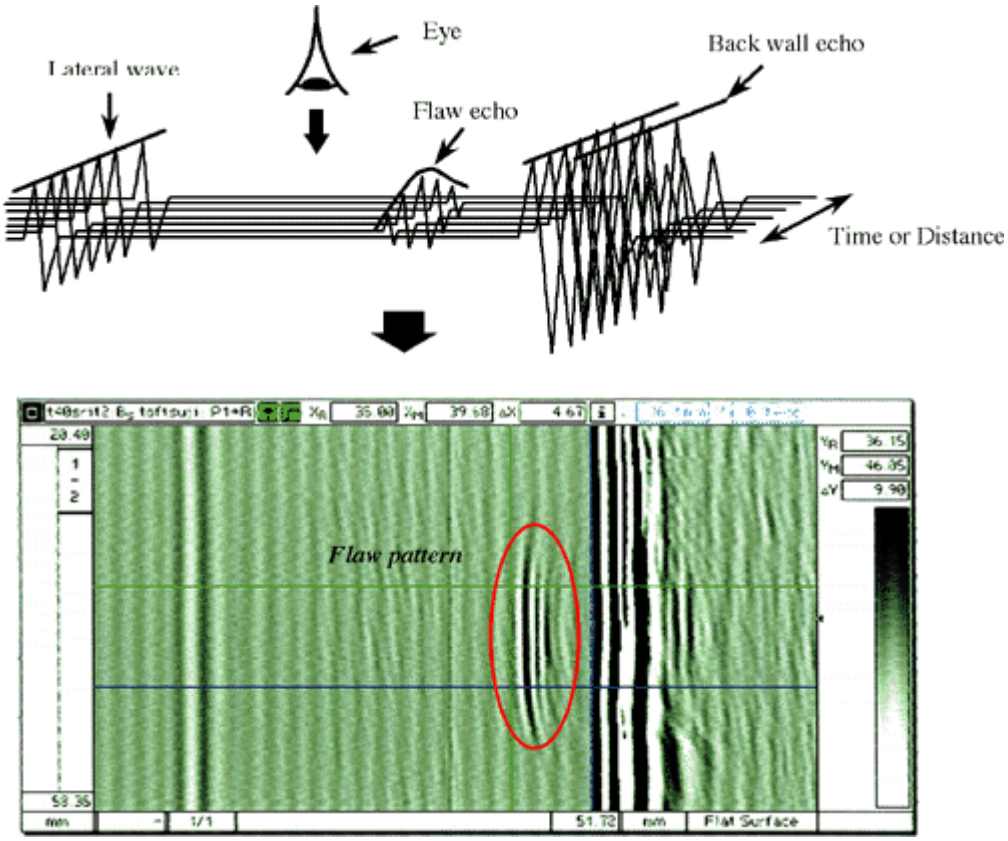

Figure 13: TOFD signal response and associated software output. (1)

Whether pulse-echo or time of flight diffraction is chosen to locate the damage, another key component is putting the ultrasonic energy to heal the crack back into the material at the damage location. This is accomplished using time-reversed acoustics.

Time-reversed acoustics is currently a major field of research for acousticians in applications in multiple industries. The basic principle involves ultrasonic wave conditioning. A transducer, or set of transducers emits a controlled signal. The signal is aimed through a material or region of interest (one of the many applications includes underwater communication). The emitted ultrasonic wave gets changed and manipulated as it passes through the selected region or material. This 'conditioned' signal is then received by a receiver unit, or a bank of receivers. The ultrasonic received wave is converted to electrical signals, much the same way a recording study works for musical

instruments. The electrical signal is then fed through software to create a mirrored signal. The mirrored electric signal is then converted to an ultrasonic wave and transmitted back through the region or material of interest. Since the signal is mirrored it will pass through the material and region and converge on the original transmitter source.

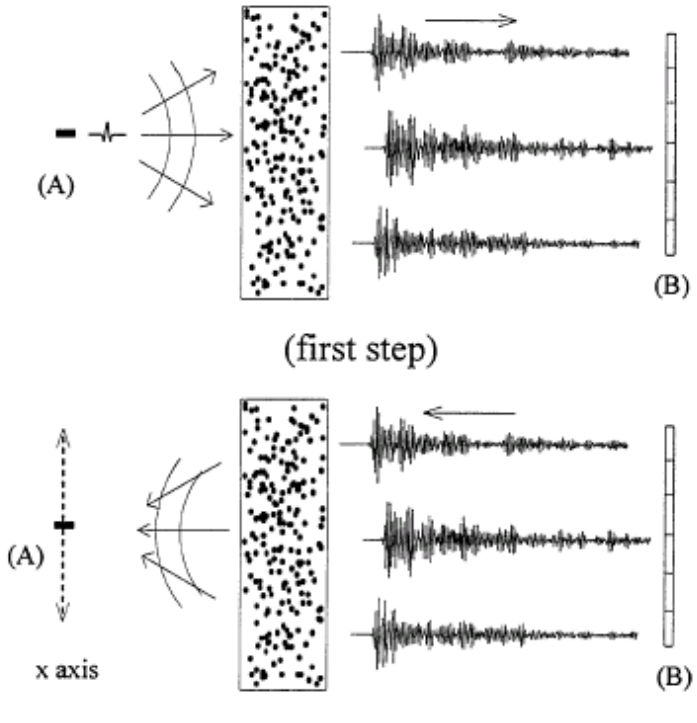

(1)

Figure 14: Time-reversed acoustics principle. The transducer A sends a signal through a material. the signal is manipulated as passing through the material and reaches transducer B. Then, B mirrors the received signal and sends it back through the material to be focused at transducer A. (1)

As a simple analogy, imagine getting into a vehicle and driving through a maze of streets keeping track of turns and distances traveled between turns. Then, to return to the start, simply reverse the order of turns and distances. For example, heading left, right, right, straight would be reversed to straight, right, right, and left to return to the source. In this analogy, the maze of streets is the region of interest, and provides the 'conditioning'

along the route traveled. The effect that the wave experiences from point A to point B is then reversed and sent from B to A.

For some applications, though, this process is all controlled with one single emitter/receiver unit. This one unit will emit an ultrasonic signal, and then read the signal that bounces back, mirror this signal and emit it once again. This method can be repeated in an iterative process to find the precise signal that has any effect on the area or material of interest, as shown below.

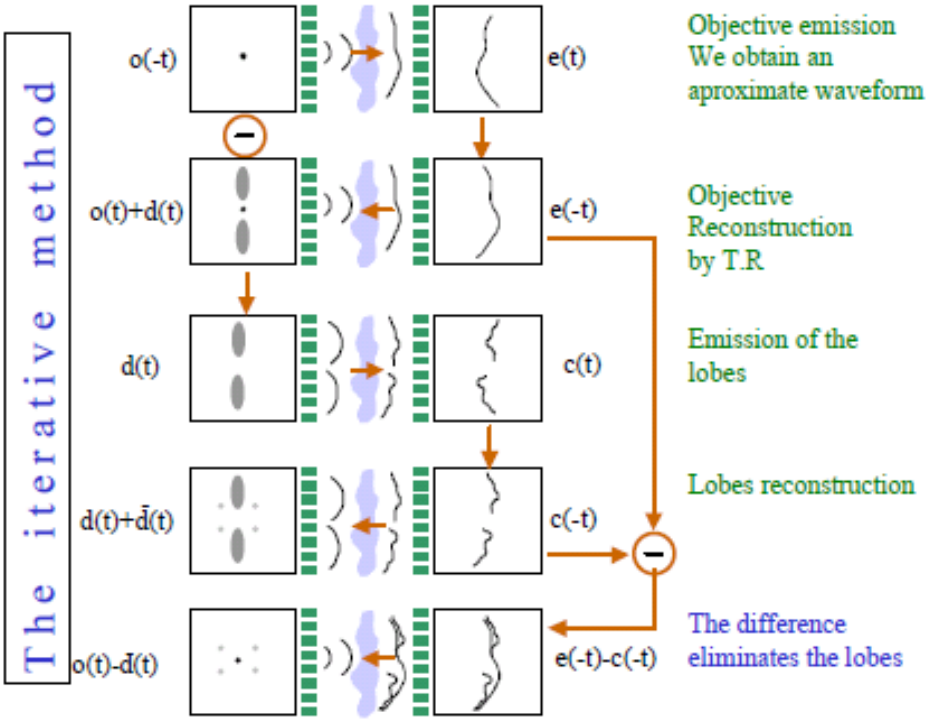

Figure 15: Diagram explaining the iterative method for time-reversed acoustics. (1)

For another analogy, imagine the ultrasonic emitter and receiver unit is a light emitter, a flashlight to be precise. The flashlight emits a white light beam on a glob of interest. Then, the glob reflects only blue light. This means of the entire range of visible light, only the blue wavelength has any effect. To take the analogy to another level, this

information can be used to direct blue light directly towards the glob, or to use alternate wavelengths to not disturb the glob. The concentration of energy idea is currently being examined to breakup kidney stones, especially with pulse-echo ultrasonic treatment (1). The ultrasonic imaging waves reflected from the kidney stones can be mirrored and then emitted again to focus the ultrasonic energy at the kidney stone and locally break it up. The system for destroying kidney stones is shown below.

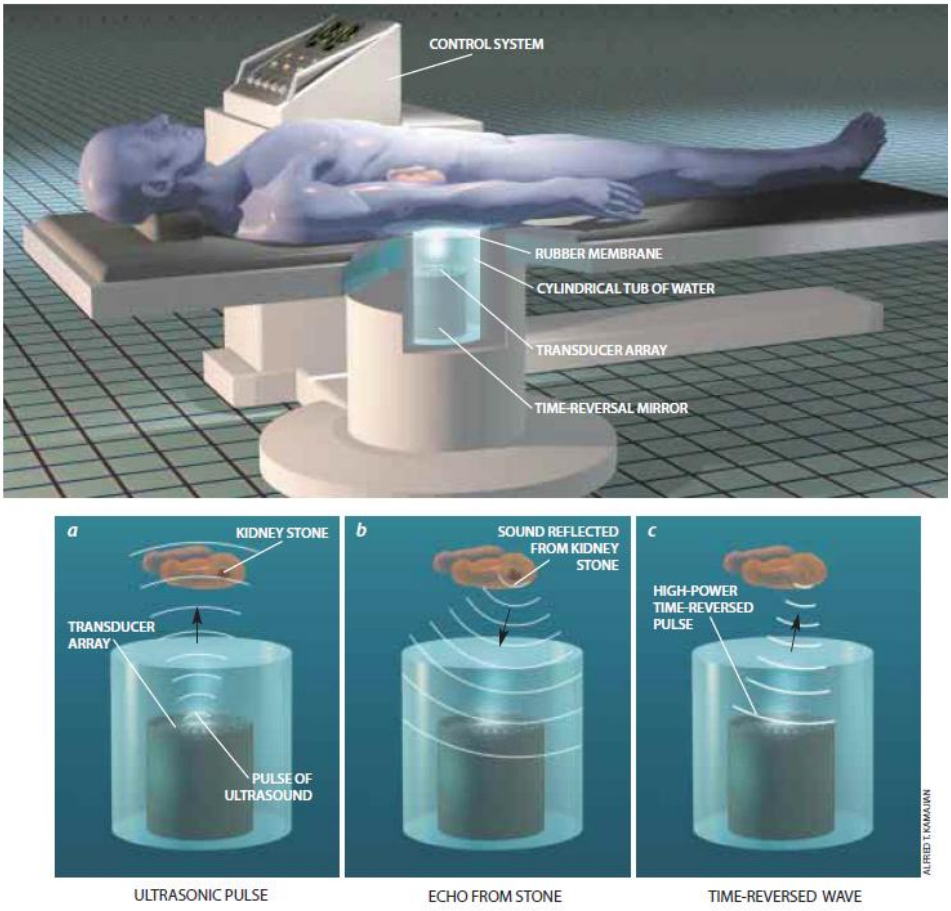

Figure 16: Kidney stone destruction process using time-reversed acoustics. In the bottom series of pictures, (a) is the probe emitting an acoustic waves. (b) shows thereflection wave from the kidney stone while (c) shows the acoustic wave focusing on the kidney stone. (1)

This system works great in biological system analysis because the different densities of the bone and tissue can be identified and tracked real-time (1). One of the major

drawbacks to time-reversed acoustics is a difficulty singling out one of multiple targets. Nonetheless, the uses and applications of time-reversed acoustics is still being explored.

REVIEW OF ENGINEERED SELF-HEALING SYSTEMS LITERATURE

Microcapsules

Much of the work on microcapsule self-healing polymer setups so far has been conducted by White and Sottos at the University of Illinois at Urbana-Champaign. The polymer they created consists of the two components of an epoxy solution separately encapsulated within a polymer matrix. The microcapsules are on the micro scale, with the epoxy capsules measuring abound 20 microns in diameter. It follows that damage to the self-healing polymer, a crack, will propagate through the polymer matrix and crack or break multiple capsules, some with the epoxy resin, and some with the catalyst. At this point, the epoxy constituents will flow to fill in the damaged area, mix, and cure where the damage was. This is shown in a cartoon below, with actual pictures following.

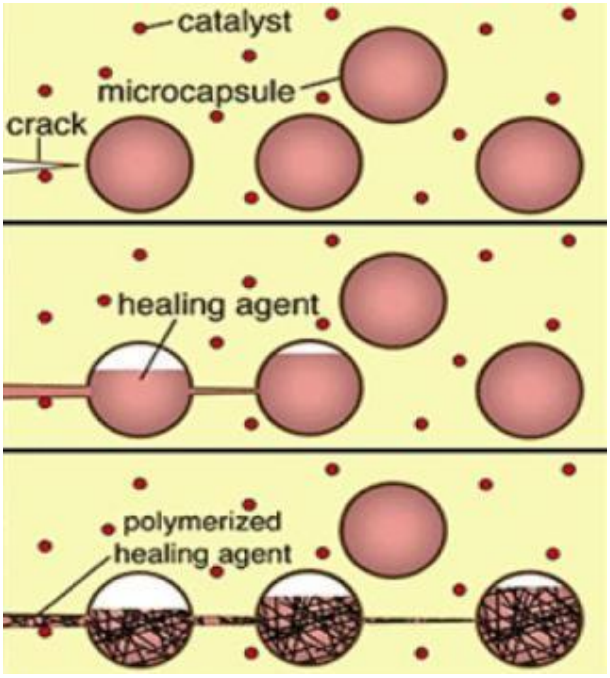

Figure 17: Self-healing polymer with microcapsules.(2)

Figure 18: Actual picture sequence over time of microcapsule healing. (16)

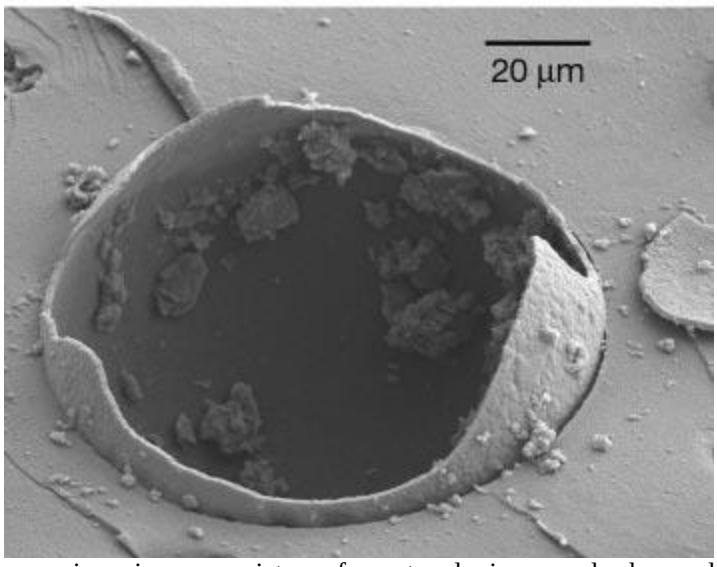

Figure 19: Electron scanning microscope picture of a ruptured microcapsule along a damaged surface. (2)

Layers

Another self-healing polymer created involves separate layers instead of microcapsules. Imagine a piece of plywood where every other layer is a thick fluid type substance. When this 'plywood' setup is cracked, the layers are broken perpendicularly to their lay-up, and the fluid substance will be absorbed by the broken solid layers and expand much like a sponge, but utilizing the capillary effect. An example is shown below.

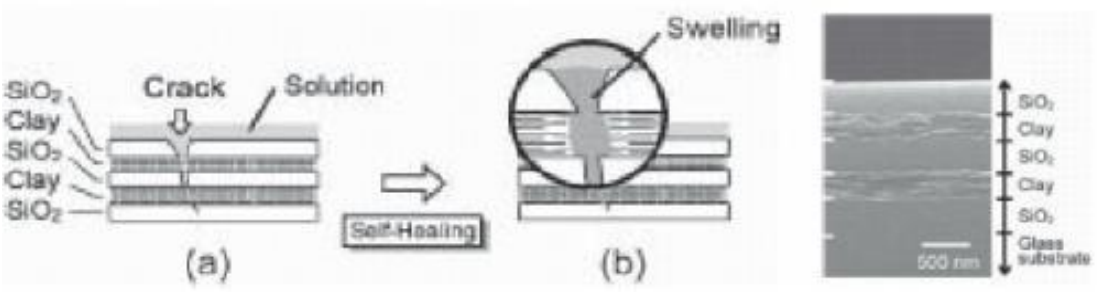

Figure 20: Method of self-healing by the swelling of layers. (3)

While both of the aforementioned self-healing polymers are novel and theoretically appear to work effectively, much more experimentation and modeling is needed before any broad application is applied. Modeling either of these polymers needs to include fluid flow, mass diffusion, and chemical reaction for the microcapsule example. Yet another self-healing polymer has emerged, though, that does not require such complicated modeling approaches. This one cures with acoustic sound waves.

Acoustically Curing Polymer (7)

Dr. Korde and his research team at South Dakota School of Mines are exploring a polymer material that is alleged to cure under applied acoustic sound waves. The preliminary tests explore the healing of a membrane sample. Initial tests affix a polymer membrane with piezoelectric sensors in a clamped apparatus.

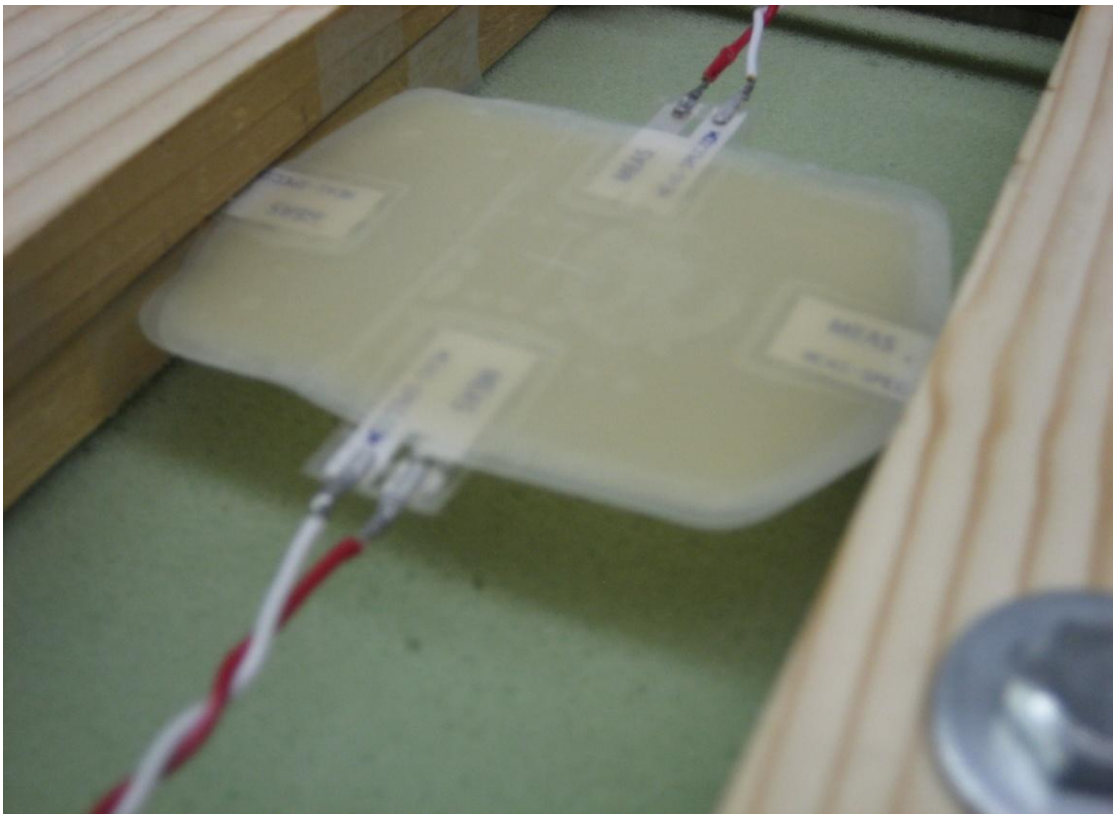

Figure 21: Experimental setup from SD School of Mines & Technology. (2)

The setup allows the sensors orientated across from each other on the non-restrained sides to emit and receive ultrasonic waves. The theory behind wave propagation being that an undamaged sample of a certain material will have identifiable wave propagation characteristics. Next, the sample was damaged by making a shallow cut with a razor blade and the wave propagation techniques analyzed.

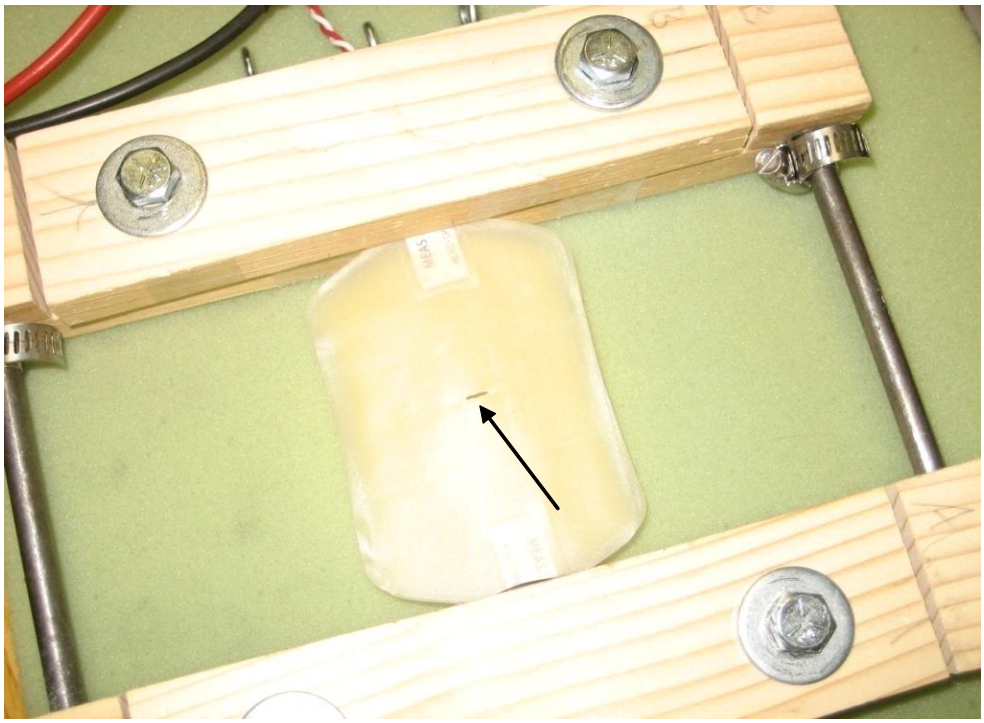

Figure 22: Experimental setup from SD School of Mines & Technology again. Damage in membrane is indicated by arrow. (2)

It was determined that the damaged sample created a phase shift in the ultrasonic wave transmission. The goal of this set of experiments was to determine if the waves transmitted through the damaged sample could cause energy absorption at the site of the damage and therefore trigger some sort of healing or curing of the damage. The next step for Dr. Korde and his team was then to determine how well they could control the wave interference in the membrane medium. This was tested by outfitting a ceramic plate with two pairs of actuators and receivers and using an Agilent Technologies data acquisition system to observe the different wave interference behaviors.

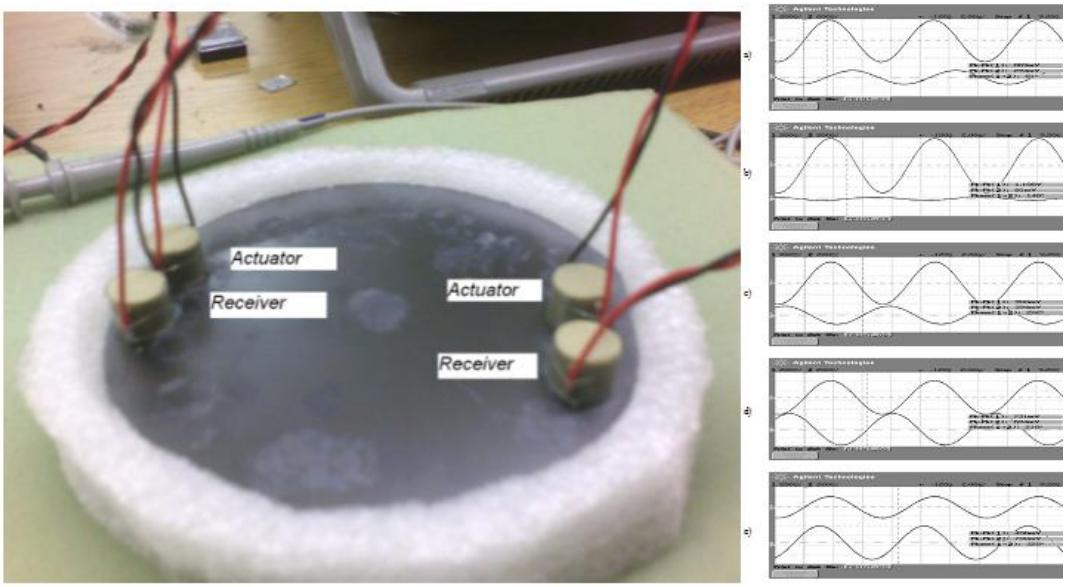

Figure 23: Experimental setup and output from SD School of Mines & Technology. The ceramic plate is fitted with 2 actuator and receiver pairs. (2)

The resulting wave charts clearly show the comparison between emitted waves, and received waves after interference between the two transmitters.

Self-Healing Glass Fiber-Reinforced Plastic

Creation motivation stems from carbon fiber products that are under aerospace industry scrutiny. Products created for the aerospace industry are not allowed much deflection, so over designed and more brittle. Self-healing GFRPs could reduce weight and reduce, or eliminate maintenance check schedule. Different setups for GFRPs are hollow glass fibers containing one-part resin in a polymer matrix, hollow fibers with resin or hardener inside, all contained in a polymer matrix, or resin contained in hollow fibers within a polymer matrix that also contains micro-capsules of hardener.

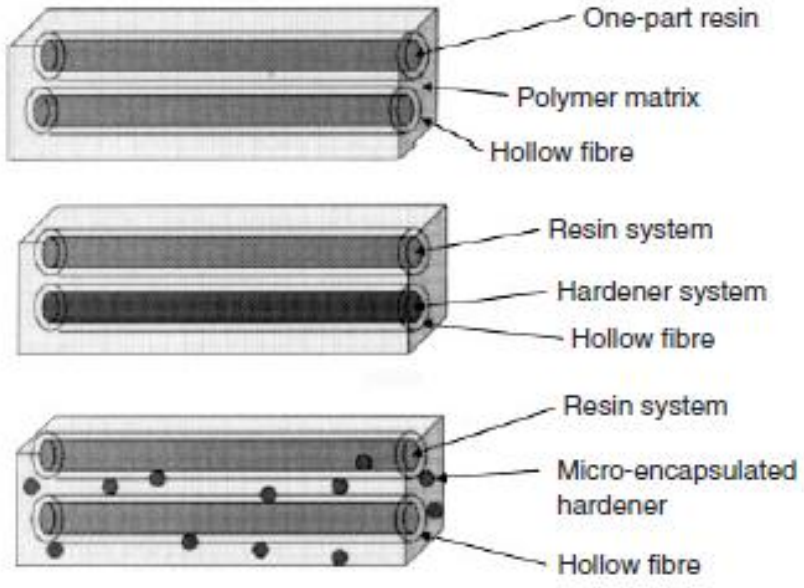

Figure 24: Hollow fiber resin composite structure setups. (3)

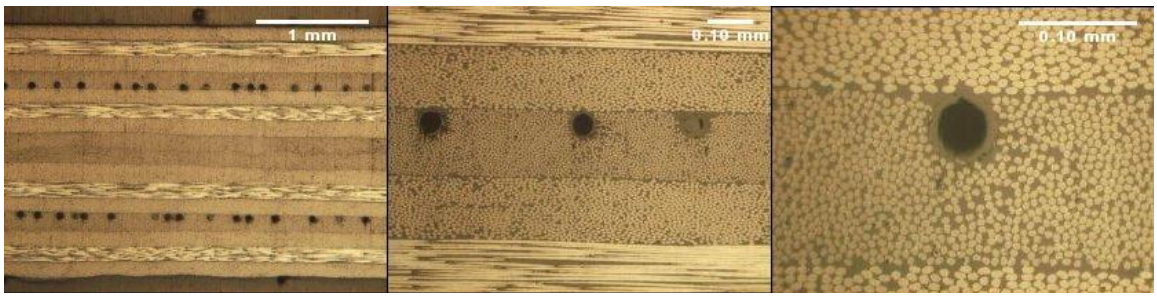

Figure 25: Cross-section pictures from a hollow carbon fiber reinforced composite. (4)

Hollow glass fibers are preferred to embedded microcapsules because they can store functional agents, can be more easily incorporated in a polymer matrix, and assist as reinforcement (3). The fibers are usually between 30 μm and 100 μm in external diameter with hollowness around 50%. These fibers are given the resin treatment for the desired setup and then imbedded in a glass or carbon fiber reinforced plastic.

The working mechanism in GFRPs occurs when the fibers containing the resin are broken, and the resin allowed to leave the fibers and enter the damage area. Once in the

damage area, the resin will interact with the hardener and cure, which is, in effect, healing. The entire process is described as mimicking human thrombosis.

Thrombosis:

> The formation or presence of a blood clot in a blood vessel. The vessel may be any vein or artery as, for example, in a deep vein thrombosis or a coronary (artery) thrombosis. The clot itself is termed a thrombus. If the clot breaks loose and travels through the bloodstream, it is a thromboembolism. thrombobis, thrombus, and the prefix thrombo- all come from the Greek thrombos meaning a lump or clump, or a curd or clot of milk. (7)

The level of actual healing depends upon characteristics and extent of damage, choice of resin used for repair, hollow fiber placement in matrix, and inclusion of environmental factors. Although the damage, material selection, and environmental influence are very intuitive factors, fiber placement is not. It would seem that beta prototypes would include a random distribution of hollow healing fibers dispersed throughout the polymer matrix. Design could be maximized, though, by strategic placement of hollow fibers within the matrix, or between laminates. For example, if the polymer is a relatively thick specimen designed to withstand a certain amount of flexural loading, placing the majority of the fibers near the surface where the tensile and compression stresses are concentrated can allow a quicker and more effective response, especially considering a brittle matrix where smaller brittle fractures are more likely occurring with cyclic moment bending. Another consideration for manufacturing is fiber orientation. It seems much research has been performed including self-healing reinforced glass or carbon fibers that are dispersed

randomly in a chunk of polymer matrix. The fiber in matrix material is cracked with an impact sort of fracture or cracking and then the load removed, but strain and cyclic loading along the axis of fiber orientation and normal to fiber direction need to be analyzed. The figures below shows fracture plane surfaces and the epoxy spreading into the damaged areas.

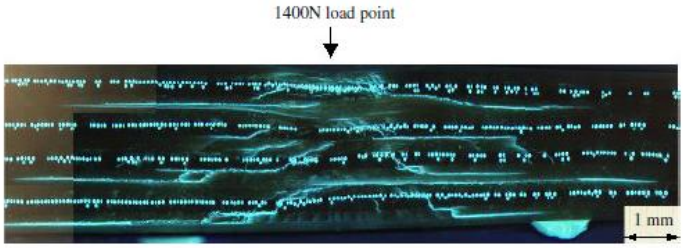

Figure 5. Impact damaged cross-section of $[0°/+45°/90°/-45°]_{2s}$ composite laminate containing healing filaments at the $+45°/90°$ and $-45°/90°$ interfaces containing Cycom 823 and UV dye.

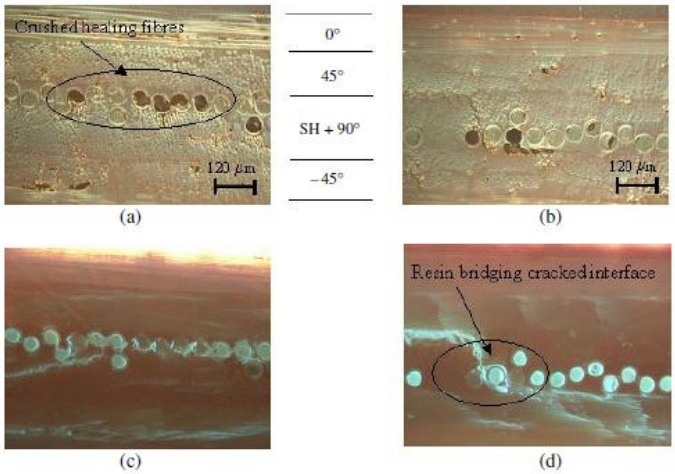

Figure 6. (a) Crushed healing fibres located under the impact site viewed under normal illumination; (b) healing resin bridging cracked interface viewed under normal illumination; (c) crushed healing fibres located under the impact site viewed under UV illumination; (d) healing resin bridging cracked interface viewed under UV illumination.

Figure 26: Cross-section pictures of hollow carbon fiber self-healing composites. (8)

Drawbacks with Current Technology

Although the aforementioned self-healing material attempts seem very promising, there are some inherent problems. First of all, the simplest types of healing systems that

are widely used are passive systems. When designing a self-healing material to mimic healing in nature of complex organisms, healing is not passive, but an active response. For the existing self-healing technologies, a certain amount of damage is needed to initiate healing, but any amount of damage will result in the same level of healing, not exactly the elevated response as may be required. This makes the healing ability not an action of the material, but a mere response to a stimulus. In biological systems, the cognitive healing ability can detect the damage sustained, categorize it by the amount of damage received, and then apply the necessary means to heal the specific damage on a case-by-case basis. This aspect is to be remedied with the inclusion of ultrasonic sensing technology.

The second inherent problem with the existing self-healing technologies is the fact that they are composite materials. This term implies the more general connotation that most self-healing materials being currently explored have at least two distinct components. This means that the damage must be experienced by both constituents to initiate the healing. For the example of the use of microcapsules, it is possible for the matrix containing the microcapsules to experience damage without disrupting the microcapsules themselves enough to set off the healing process. The inclusion of two different materials also means that there is another step in the manufacturing needed to combine them. This makes the creation of self-healing materials more labor intensive and complex than normal materials. Although this seems understandable, reducing this complication by using a single material would decrease manufacturing cost and time.

EXPERIMENTAL ANALYSIS

Testing over the course of this project analyzed thermal and ultrasonic effects on nylon samples. First the temperature change and distribution was tested in nylon samples, then the mechanical response of heated and ultrasonically treated samples was observed during tensile tests, and then the change in crystallinity was tested using differential thermal analysis (DTA). The testing progression, numbers of samples tested, and test motivation is shown below in table 1.

Table 1: Testing progression.

TESTING		
Test Name	# of Samples	Test Motivation
Ultrasonic Influence Test		Determine effect of powerful ultrasonic energy on nylon sample.
30% Power Test	1	
50% Power Test	1	
Tensile Tests		Determine the difference in mechanical response of heated samples and damaged samples with and without ultrasonic treatment.
Virgin Samples	31	
Heated Undamaged	3	
Damaged	2	
Constant Period/Different Power Levels	4	
Constant Period #1/Constant Power Level	5	
Constant Period #2/Constant Power Level	3	
Different Period/Constant Power Level	2	
Overall Comparison	50	
DTA Crystallinity Test		Determine if increased heat correlates to crystallinity.

Testing began after nylon was obtained from McMaster-Carr. The nylon purchased was Tecamid® 6,6, delivered in 1.219 meters by 2.438 meters (4 foot by 8 foot) sheets and was 6.35 millimeters (0.25 inches) thick. These sheets were cut down into smaller, more manageable chunks. Before the dogbone samples were cut, though, scrap pieces were obtained for initial tests. The first test was ultrasonic influence on the nylon dogbones.

Ultrasonic Influence

It is known that ultrasonic testing had been successfully used to detect damage in nylon structures, but the power needed to detect is relatively weak compared to the power needed to change the crystalline structure. The first test was used to determine if a higher power ultrasonic transducer could produce a large enough effect on nylon to produce a material response. The response desired was a restructuring of the material that could be measured as a result of temperature change. Therefore, to measure this change, a rectangular scrap of nylon had J-type thermocouples affixed, and was fitted in an apparatus. The ultrasonic transducer used to heat the nylon was a model 450 ultrasonic probe from the Branson Ultrasonics Corporation operating at 20,000 kilohertz with a power range of 350 to 450 watts.

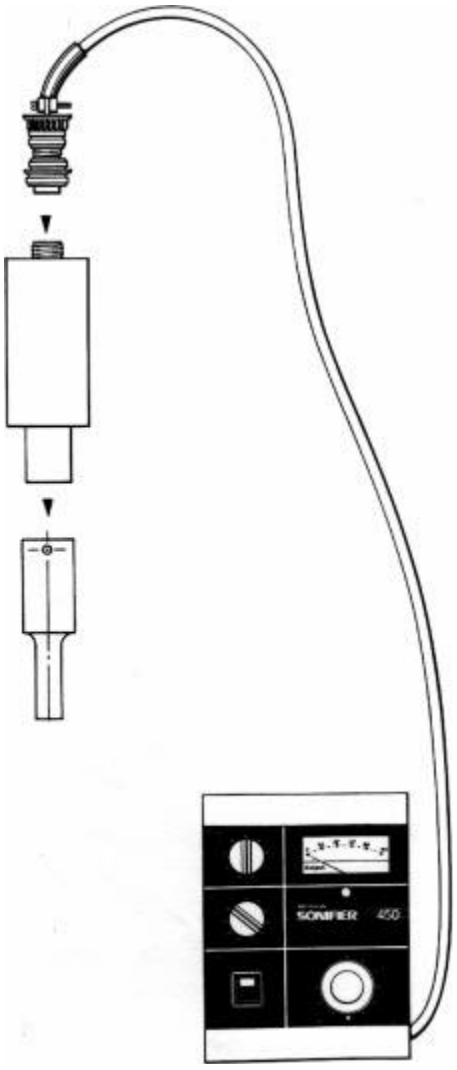

Figure 27: Schematic of ultrasonic probe and its components. (5)

The probe was operated by an accompanying control box that allowed the operator to change the power output and time of operation, and choose between continuous or pulse mode.

Figure 28: Ultrasonic probe control box. (5)

The probe is a common choice used to mix heavy slurries, and has the ability boil water instantly upon contact. The probe could also be used with different probe tips. Although the smallest probe tip, with a footprint diameter of 3.175 millimeters (0.125 inches), was desired, the small discrepancies with creating a flush surface contact between the probe and nylon sample, and the immense power created by the probe made the tight source of ultrasonic power burrow into the material and create multiple uncertainties in the experiment.

Figure 29: Ultrasonic probe tip attachments. (5)

The next smallest tip was used with the contact diameter of 9.525 millimeters (0.375 inches). The probe with chosen tip was a little larger than two aluminum soda cans

stacked end to end, and the control box was slightly larger than a normal car battery. The ultrasonic transducer was suspended by clamps, tip side down, above a plate to hold the nylon sample.

Figure 30: Ultrasonic probe and testing apparatus.

The nylon sample was a rectangle piece measuring 186.7 millimeters by 28.57 millimeters (7.35 inches by 1.125 inches, respectively). It was affixed with four thermocouples equidistantly along its length by masking tape while a fifth thermocouple was used to measure ambient air temperature. The sample was placed on the plate with the length vertically between the plate and probe tip and held by another clamp.

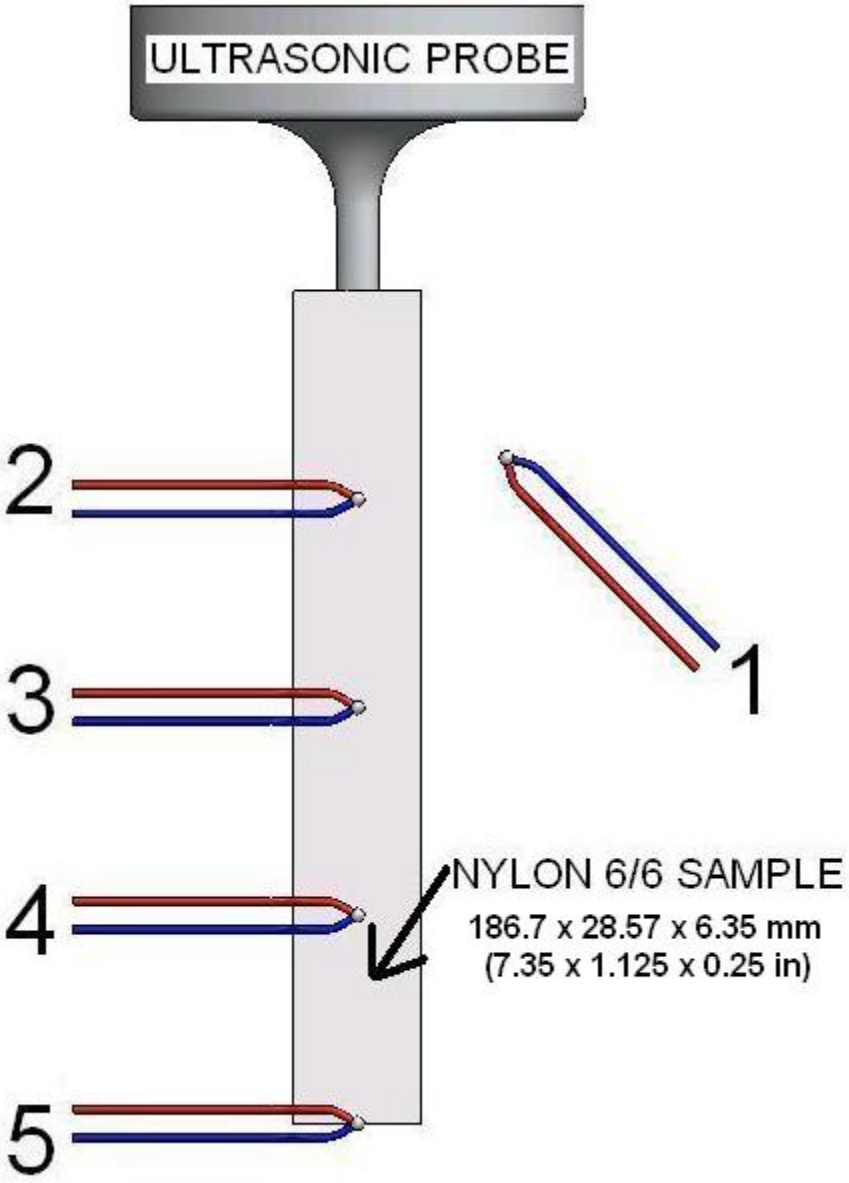

Figure 31: Schematic of ultrasonic influence test setup.

The experiment was meant to best represent a one dimensional heat transfer problem along the length of the nylon sample with the ultrasonic probe tip acting as a heat source. The control box was set at level 5 out of 10 and turned on to continuous operation as the thermocouple temperatures were recorded.

It was observed that the ultrasonic probe produced an increase in temperature in the nylon sample, and a gradient was created along the length. Initially, the ultrasonic probe was operated at a level 3, or 30% of maximum power and the thermocouple temperature readouts were recorded for 5 minutes.

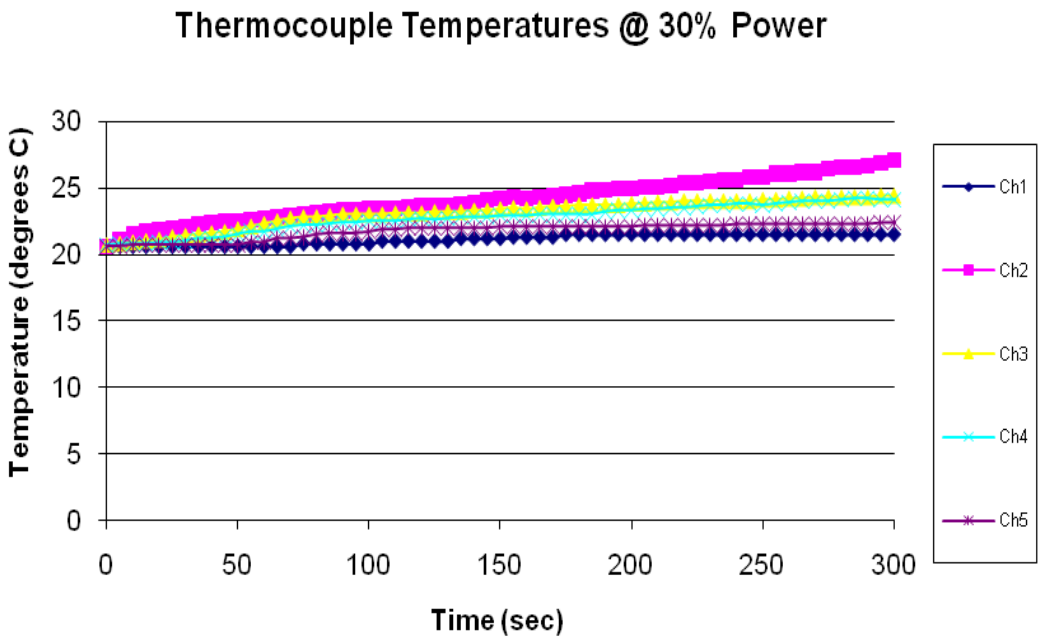

Figure 32: Temperature readout from the thermocouples in the ultrasonic influence test. The ultrasonic probe is operating at 30% of maximum power.

The thermocouple nearest the tip shows the greatest immediate increase in temperature as the ultrasonic energy propagates down to the other probes, but the other probes assume the same response as the probe nearest the ultrasonic probe. After 5 minutes, the probes demonstrate a nearly linearly increase in temperature response. The temperature of the air in the room did slightly increase due to the experimenter's presence and the use of powerful electronic equipment in the confined area of the lab. Next, a higher ultrasonic probe operation level was tested.

Although 5 minutes of operation of level 5, or 50% maximum power, did not bring the nylon sample anywhere near equilibrium, noticeable increases in temperature were monitored. The relatively slow flow of heat through the material was reasonable considering the relatively low thermal diffusivity of nylon compared to, for example, aluminum.

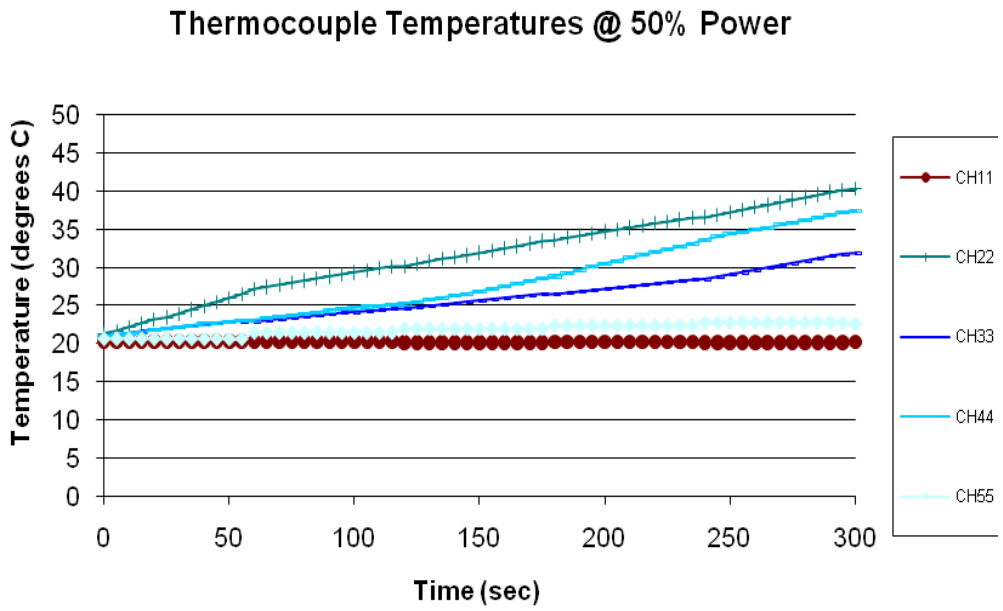

Figure 33: Temperature readout from the thermocouples in the ultrasonic influence test. The ultrasonic probe is operating at 50% of maximum power.

The test at 50% power exhibited the same initial first probe jump and remaining sample probe lag as that of the 30% of maximum power test. The exception between the 2 tests is the higher power ultrasonic probe test displayed a larger increase in temperature response.

Since these ultrasonic probe tests proved that ultrasonic waves could create a temperature change in nylon, the next step was to check the effect of ultrasonic waves on

damaged nylon. This was performed by obtaining dogbones, damaging them, and then exposing them to the ultrasonic probe and observing the tensile test response.

Tensile Tests

The nylon dogbone samples were manufactured by the machine shop at Montana State University. All of the samples were cut from the same order of sheet stock nylon 6/6 ordered from McMaster-Carr. Also, samples from this stock were provided to the undergraduate testing class to reaffirm the general properties. The dogbones are of the overall measure 177.8 millimeters by 25.4 millimeters (7 inches by 1 inch), but the actual tensile section was closer to 76.2 millimeters by 12.7 millimeters (3 inches by 0.5 inches).

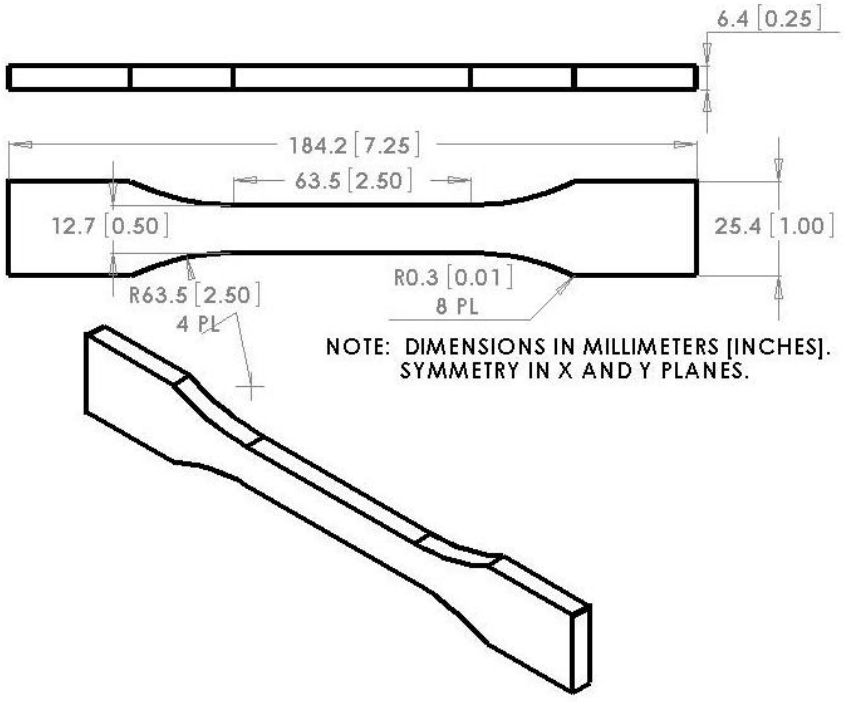

Figure 34: Engineering drawing of dogbone sample dimensions.

Since those nylon dogbone samples provided almost exact replicas, it was important to use a repeatable form of producing the same damage. Damage was produced in the sample by holding a razor blade in a vise with 3.175 millimeters (0.125 inch) of blade showing and the dogbones slowly pressed down on the blade with the head of a drill press until flush with the vise.

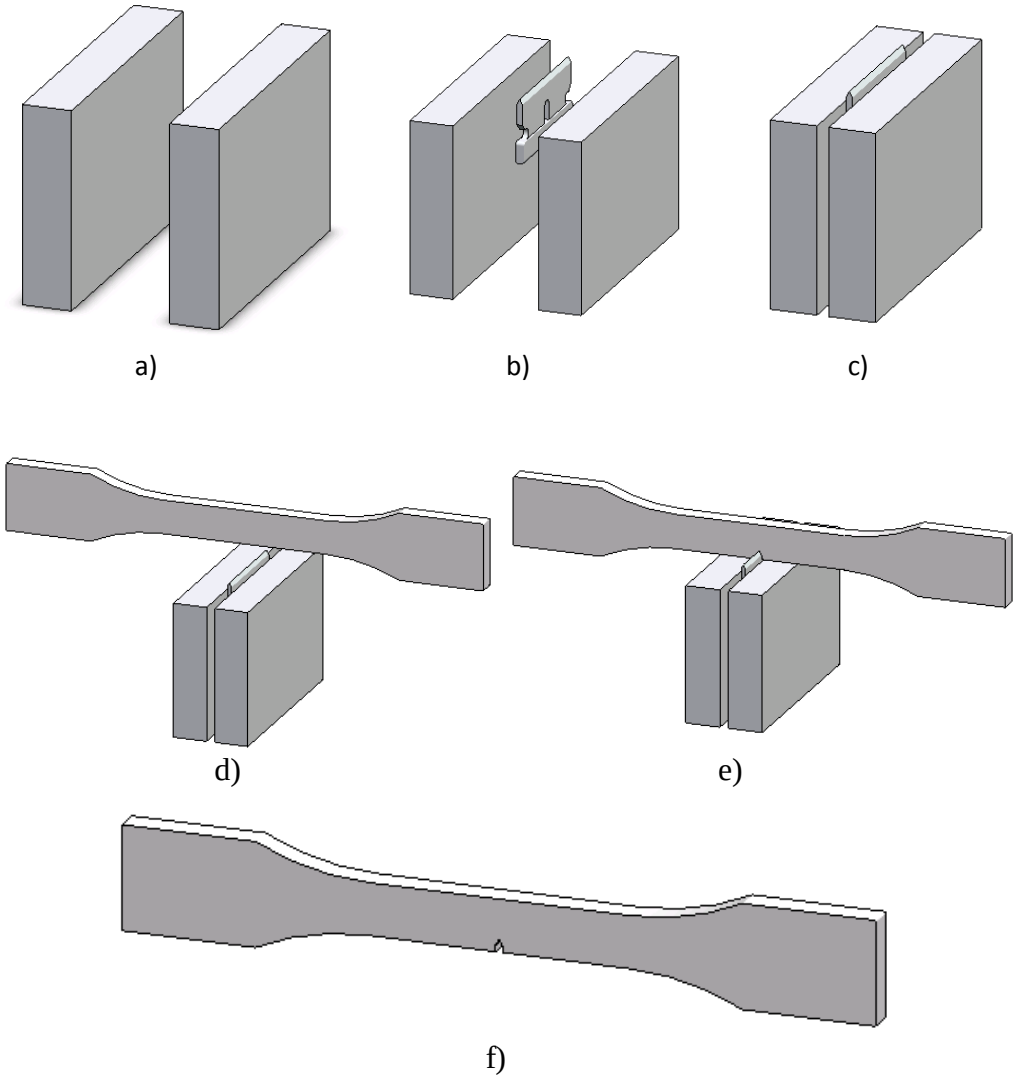

Figure 35: Schematic of damage process for dogbone samples. Parts a) through c) show the razor blade being clamped into place with only 3.175 millimeters (0.125 inches) showing. Parts d) and e) show the dogbone being pressed onto the razor blade until motion is stopped by the top of the clamp. Part f) shows the finished, damaged dogbone sample with exaggerated damage.

This created a specific amount of damage and was easily repeatable. Also, the razor blade was a simple way to create a small crack of determined length without changing material properties, such as heating the nylon or removing material, which a band saw would produce. It was suggested to use a three point bending apparatus to crack the sample, perhaps in conjunction with freezing the sample. This was exchanged for the razorblade idea due to its more precise repeatability. Since this is the first trial with ultrasonic healing considerations, first the principle of operation was sought, and then more realistic approaches could be entertained. Such realistic scenarios include cracks and flaws created by fatigue loading. The exact location along the length of the dogbone samples was not as strictly maintained as the razorblade penetration depth since the cut would be the point of failure in the tensile test and the ultrasonic probe would be placed accordingly. The razorblade was used to create a 3.175 millimeter (0.125 inches) deep cut through the thickness, at the approximate center, of the dogbone samples. Some of the samples were set aside to be tested as damaged controls, and the rest of the damaged samples were treated with the ultrasonic probe.

Ultrasonic treatment of the damaged samples included a prescribed probe power level applied to one side of the damaged sample for a prescribed amount of time. Then, the sample is turned over and the treatment and time of exposure repeated. The circular probe tip is centered about where the crack damage intersects the side of the nylon dogbone sample.

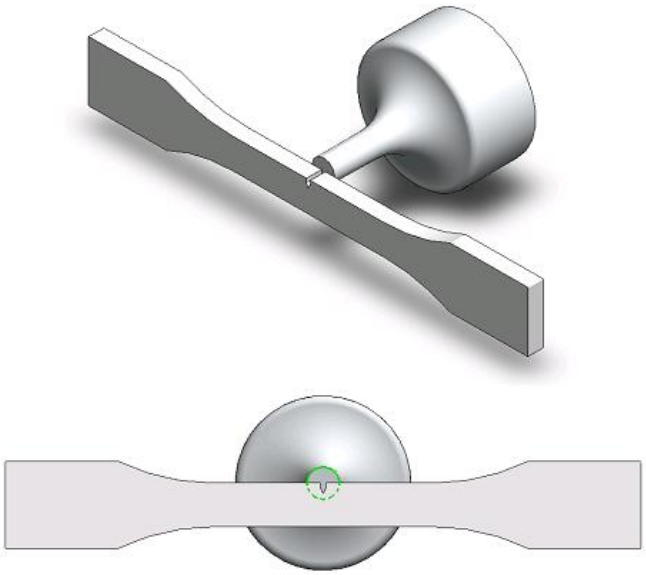

Figure 36: Representative ultrasonic probe tip coverage area of dogbone sample shown over exaggerated damage.

This alignment was simple to repeat, and still allowed the crack to be completely covered by the probe tip. Although this method does not create a symmetric exposure since one side exposure precedes the other, it was determined that sequentially exposing both sides to the ultrasonic probe created a more symmetric response than just exposing one side. The most difficult aspect of the ultrasonic exposure was attempting to keep a flush contact between the probe tip and the nylon sample. The probe holding apparatus could not hold the ultrasonic probe completely still once the powerful probe was activated. Clamps were used to suspend and grip the probe, but movement of the probe tip, which could not be constrained, creating some shifting of the probe in the apparatus. This led to a non-uniform contact area that would allow for more intense exposure where the probe tip provided more pressure. This means an exposure power level that did not cause visible nylon melting could tilt, reduce the contact area, and therefore increase the applied ultrasonic probe pressure. This can be considered more localized heating by

means of an equal power applied to a smaller area. The effect of the different exposure levels on the damage was then tested by tensile testing the damaged nylon samples.

Tensile tests were performed with the use of an Instron model 5882 tensile test machine and accompanying software. This is the same tensile test machine used by the materials property class from which the undamaged nylon tensile test response data was taken, for continuity purposes, and is shown below.

Figure 37: Tensile test experiment setup.

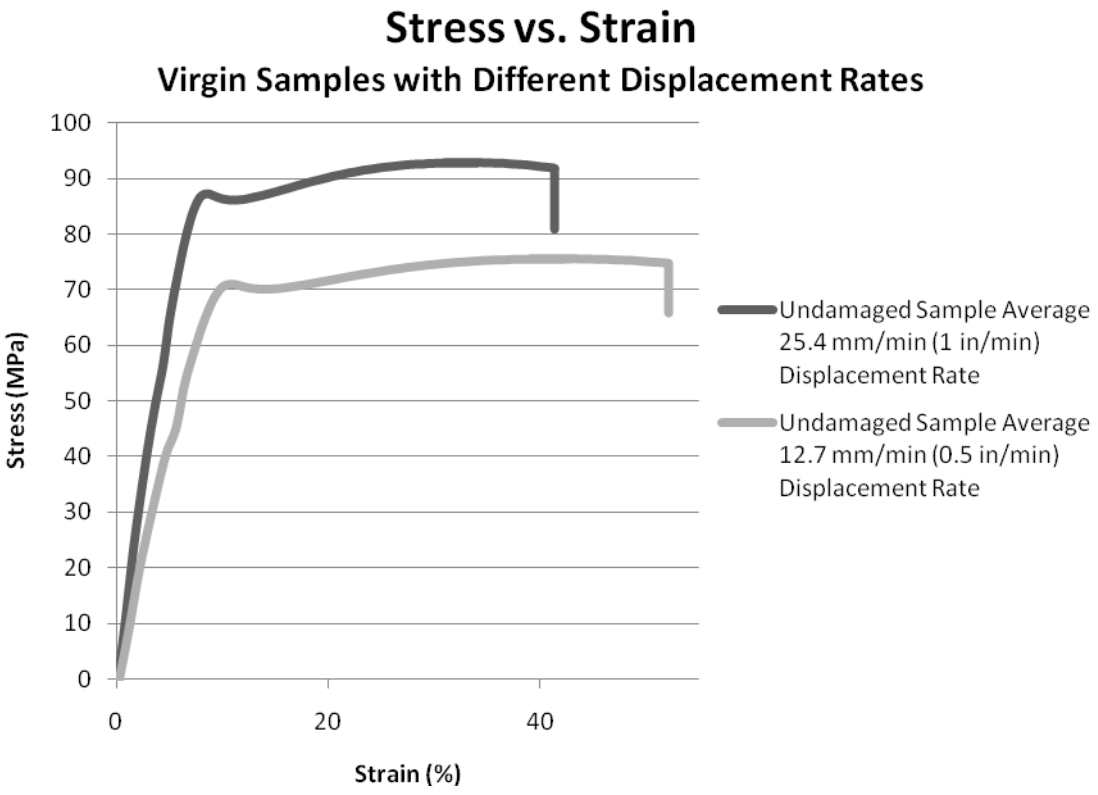

Figure 38: Stress strain plots of undamaged dogbone samples performed at 2 different displacement rates.

The data was collected from the undergraduate class and averaged. Since some tests included gross miscalculations, eighteen samples were averaged for the 8 millimeter per minute (0.5 inch per minute) displacement rate and thirteen samples averaged for the 8 millimeter per minute (1.0 inch per minute) displacement rate tensile tests. The undamaged response was then compared to manufacturer's data sheets, and published values. Although the data does not align with the manufacturer's given values, it is clear from the undamaged test data that tensile test data greatly depends upon tensile displacement rate. The actual test procedures were not listed by the manufacturer.

The first parameter to compare with experimental data and published data was elastic modulus. The three line segments in the figure below represent the range of

elastic moduli for nylon 6,6 and the published elastic modulus provided by the manufacturer. The modulus provided by the manufacturer falls between the high and low limit moduli. The tensile test data shows that the calculated modulus does not fall in this range, but the modulus from the faster rate of displacement pull test is close to the lower limit.

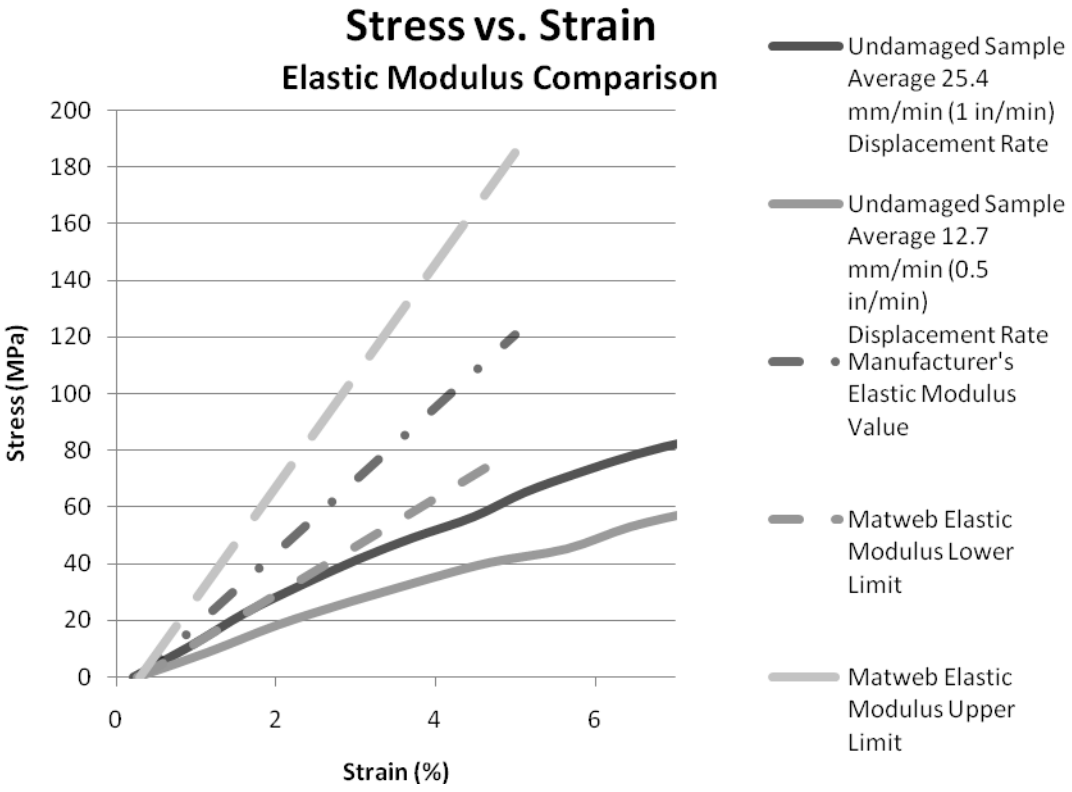

Figure 39: Undamaged stress strain data compared to published elastic modulus values.

This comparison was repeated with yield stress and ultimate stress.

Again, with the comparison of yield stress, the greatest value line is the highest limit of the yield stress range provided by Matweb, the lowest value line is the lowest limit of the yield stress range provided by Matweb, and the line inbetween is the yield stress value provided by the manufacturer. While the data from the more rapid

displacement tensile test was closer to the acceptable range of elastic moduli, it was completely outside the range of provided yield stresses. Alternatively, the yield stress found from the slower displacement rate tensile test was almost equivalent.

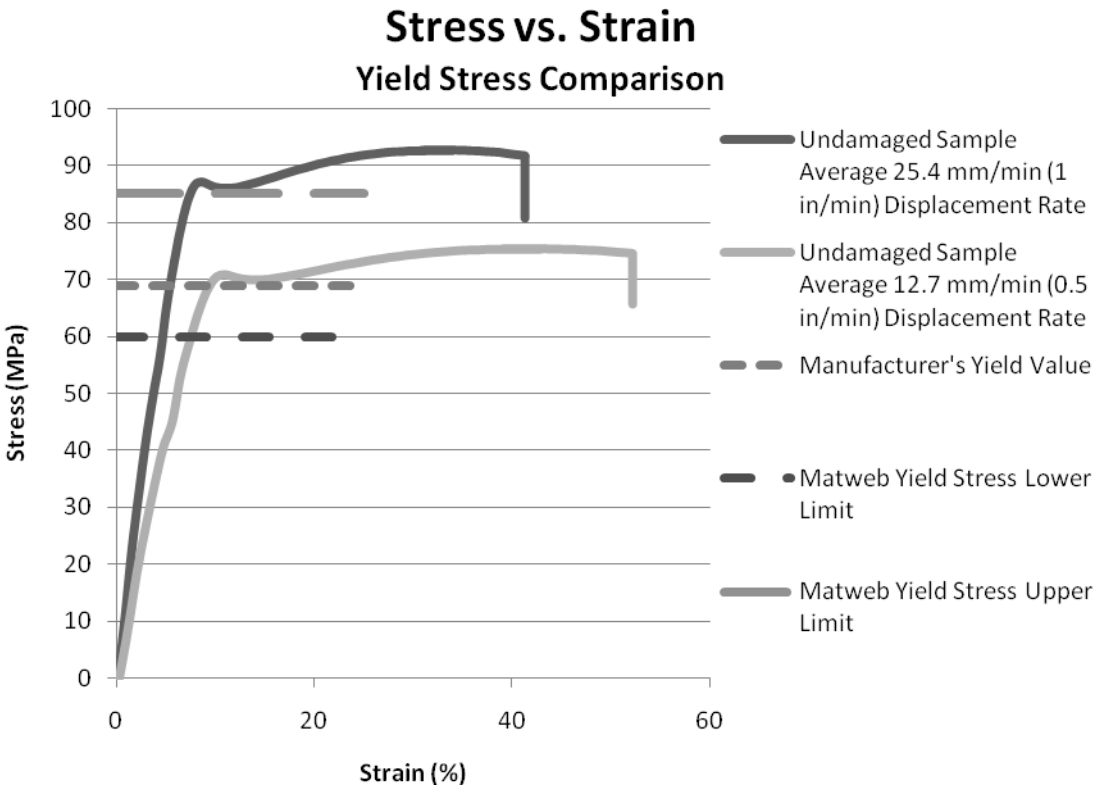

Figure 40: Undamaged stress strain data compared to published yield stress values.

Next, the ultimate stresses were compared between experimental data and published values. The ultimate stress from the more rapid displacement test data is almost equivalent to the manufacturer's ultimate stress, but this time, the test result data from the less rapid displacement test falls outside of the range of ultimate stresses for nylon 6,6 provided by Matweb.

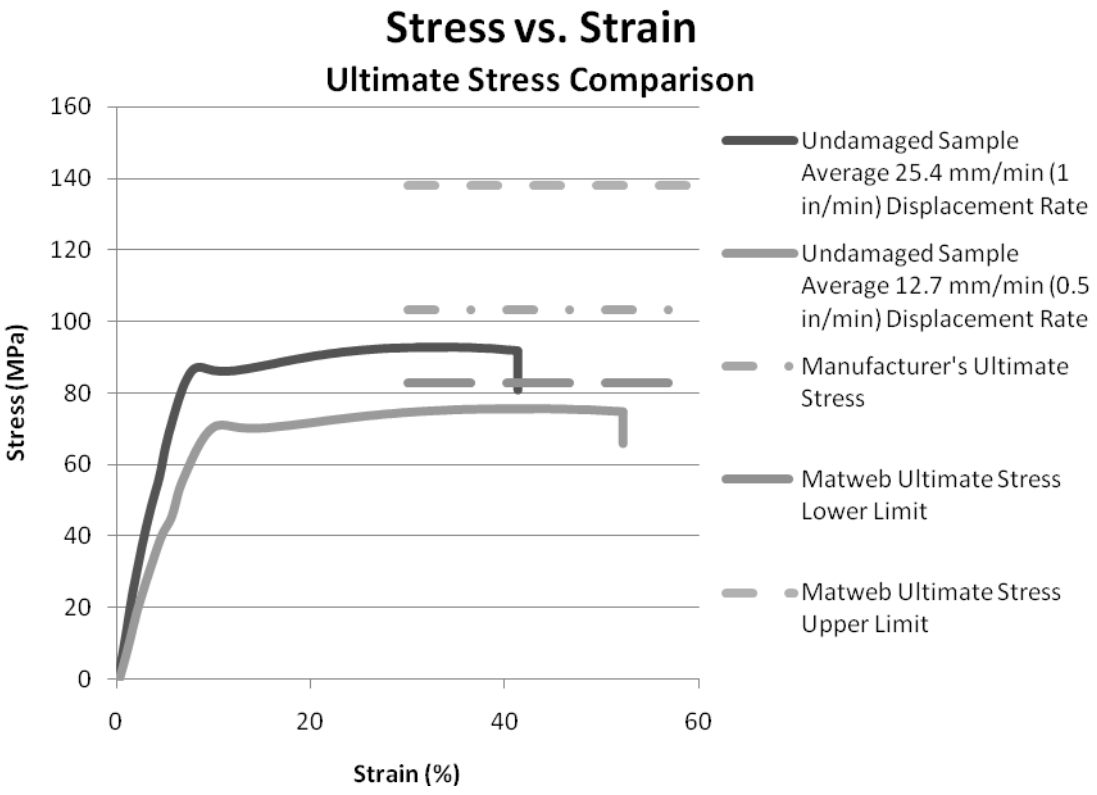

Figure 41: Undamaged stress strain data compared to published ultimate stress values.

Although the comparison of results was discouraging considering the mismatch of published and experimental data, the data from the undamaged tensile tests was used to compare to the tensile tests of the damaged samples.

Since digital thermal analysis was utilized for better understanding of the effect of ultrasonic energy, virgin samples were first heated and tensile tested to observe mechanical response. Three samples were heated, all at a rate of 10ºC per minute. The first sample was heated to 180ºC and the second and third samples were heated even closer to the melting temperature of nylon (~200ºC) at 190ºC. After heating, the furnace was programmed to allow all three samples to cool to room temperature at the same rate as the heating. Research has shown that cooling rate is just as influential, if not more

influential, than heating rate for polymeric materials. According to work by Avlar and Qiao with nylon 6, cold water quenching resulted in a higher tensile strength and lower amount of sustainable fracture work than air cooled samples (17). The cold water quenching reduced the amount of time for the crystalline spherulite regions to form resulting in much smaller crystalline areas. This is analogous to grain boundaries in metals. Quenching metals also produces smaller grain size and therefore a heavier saturation of grain boundaries. Smaller grain sizes or crystalline areas result in less room for dislocation between the boundaries. Dislocation is related to ductility and therefore smaller grains and crystalline areas result in a more brittle material response.

The first noticeable change was the color of the dogbone samples. As the samples were heated closer to melting temperatures, the samples turned a darker color. The darker change in hue is characteristic of an increase in relative crystalline structure. The three samples were then tensile tested at the more rapid displacement rate and compared to the virgin sample tests.

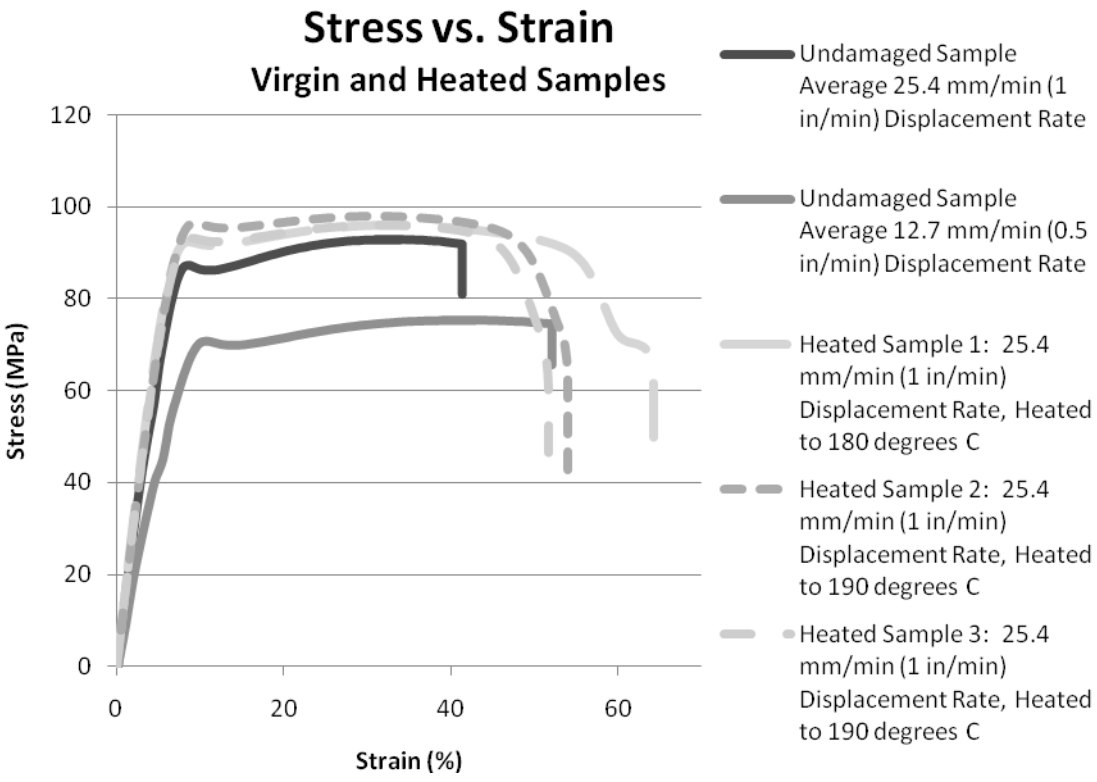

Figure 42: Undamaged stress strain data of virgin samples and heated samples.

All three heated samples show the same general response as the virgin samples, and it is apparent that the tensile test displacement rate is similar to the more rapidly displaced virgin sample. The sample heated to only 180ºC exhibits a more ductile response and a higher ultimate stress. The second and third heated samples, both heated to 190ºC, exhibit a more ductile response than the virgin samples, but a more abrupt, or brittle response than the sample heated to only 180ºC. It is possible the ultrasonic heating relieved any residual stress from manufacturer's treatment or machining. After the residual stress was compensated, an increasing approach to the melting temperature created a more brittle response. Nonetheless, increased temperature has a positive correlation with increased ultimate stress and brittle response.

The first tensile tests of damaged samples were just the damaged samples without ultrasonic treatment. These samples exhibit the same elastic response as the undamaged samples, but fail long before the yield stress and strain of the undamaged samples.

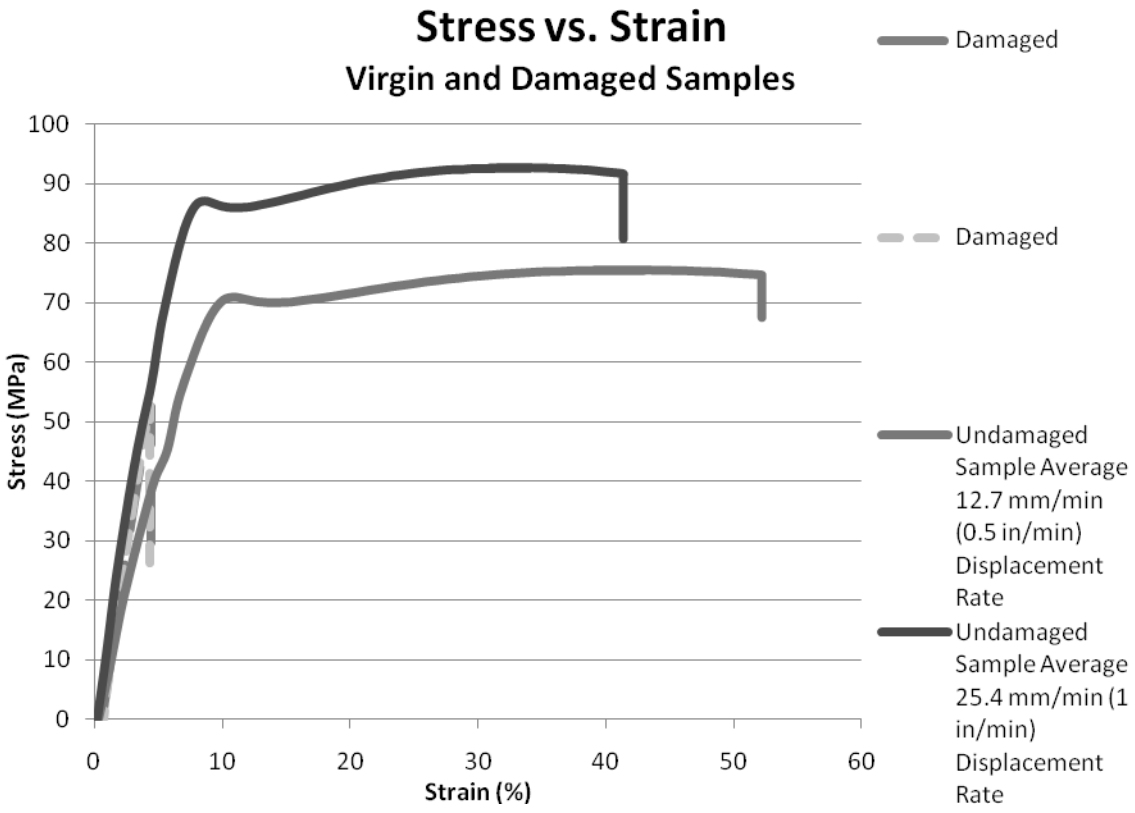

Figure 43: Undamaged stress strain data compared to damaged specimen stress strain data.

The quick catastrophic failure can be explained by the relatively large amount of damage compared to the cross-section of the nylon sample. The large, but known, initial crack length and brittle response warranted a fracture analysis. The damaged samples and the damaged and treated samples were therefore compared by their critical stress intensity factor. The first round of treated samples was exposed for 15 seconds per side for different intensity levels.

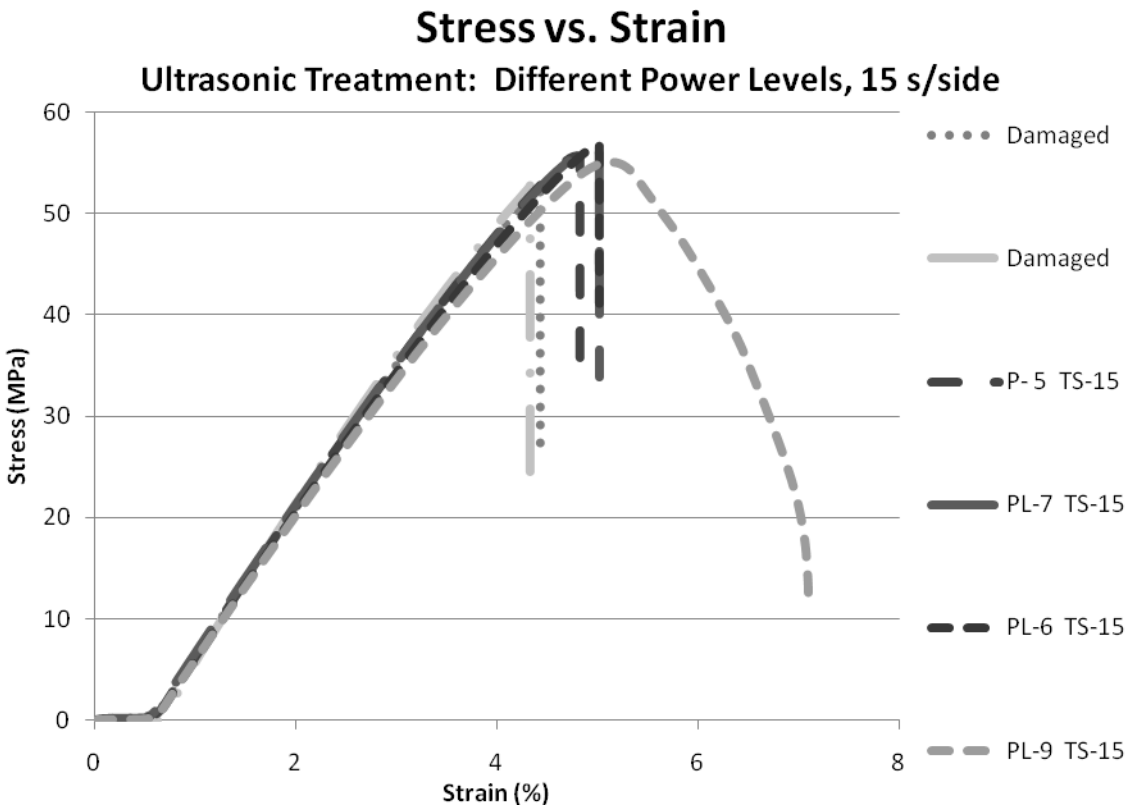

Figure 44: Stress strain data of damaged samples ultrasonically treated for 15 seconds a side at different power levels. (PL) represents power level out of 10, and (TS) is the treatment time per side in seconds.

As the ultrasonic probe power level increased, the samples reached a higher ultimate strength while exhibiting the same elastic modulus as the untreated samples. The unique case displaying a yielding and strain release before failure was one of the aforementioned cases where the probe shifts left an easily visible mark of a local melting near the crack tip. Whether visible melting is present or not, ultrasonically treated specimens show a different response than untreated samples. The next round of tests hold the ultrasonic probe power level constant and change the exposure time on each side.

The next set of tests was used to see the precision of multiple tests at a controlled level. Since melting was visible after a couple of seconds of exposure at level 10, and level 5 produced no visible melting but produced a noticeable effect, level 7 was chose

for the controlled test. Also, the exposure time was increased to 30 seconds per side to increase ultrasonic effect. The results are shown below.

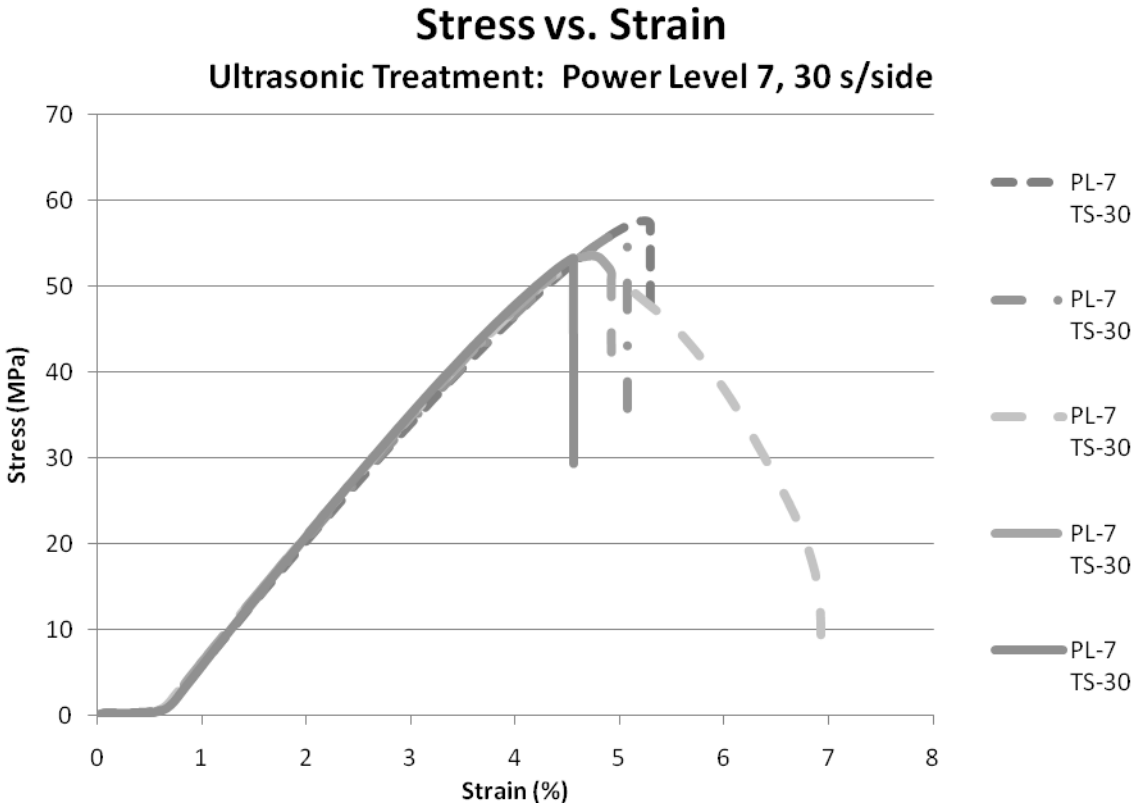

Figure 45: Stress strain data of damaged samples ultrasonically treated at 70% maximum power for 30 seconds a side. (PL) represents power level out of 10, and (TS) is the treatment time per side in seconds.

Of the four samples tested, they all yielded or failed between 53MPa and 57MPa and 4.5% and 5.25% strain. One sample, though, produced a ductile response by yielding and then reducing the amount of stress needed to continue on the same strain rate. Upon examination of the sample, a local melting spot near the crack tip was observed. It seems that although all of the samples in the test received the same level of ultrasonic power exposure for the same amount of time, the test involving this specific sample allowed the ultrasonic probe tip to shift and therefore apply more ultrasonic energy more locally to a smaller surface area and create a small local melting spot. To determine if the local

heating was in fact the cause for the unique ductile response and not just an abnormality, another series of tests was performed at the same level of ultrasonic probe power, but with longer exposure time on each side. The exposure time was doubled to 60 seconds a side. The results from this series of tests are shown below.

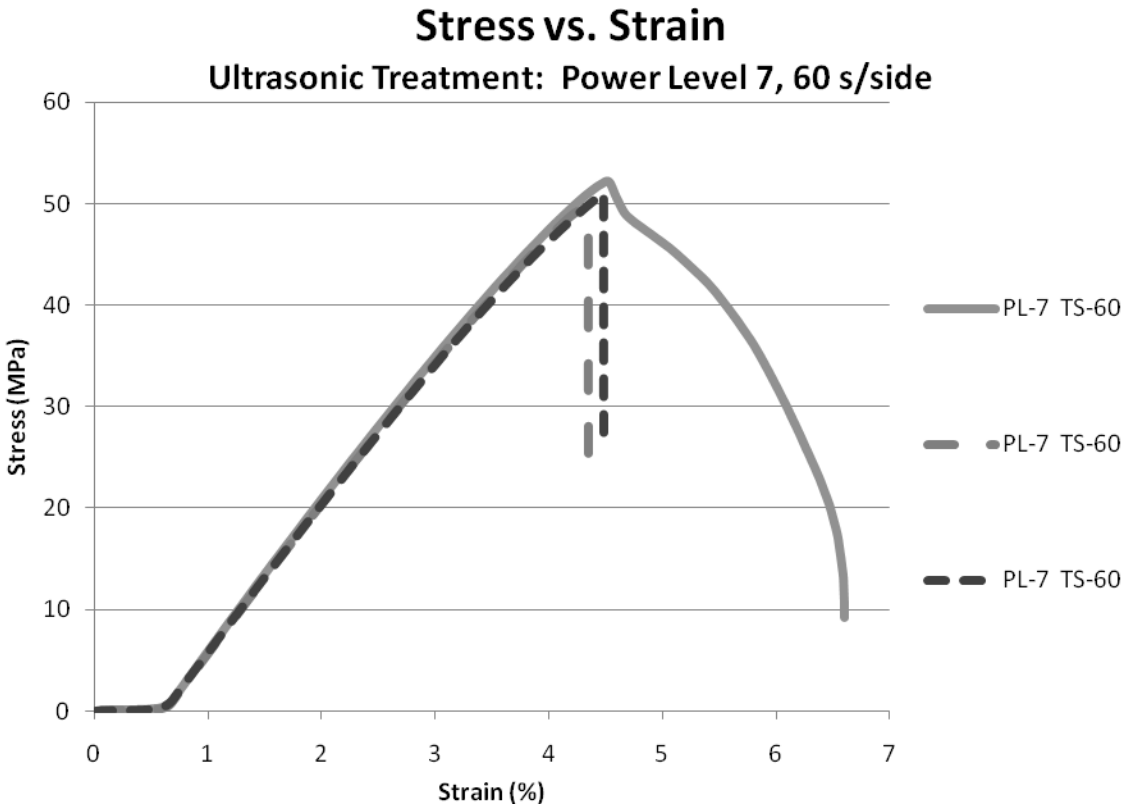

Figure 46: Stress strain data of damaged samples ultrasonically treated at 70% maximum power for 60 seconds a side. (PL) represents power level out of 10, and (TS) is the treatment time per side in seconds.

Just as with the tests with the 30 seconds a side exposure time, the yield and ultimate stresses clumped together, and at a higher stress than that of the lower exposure time. Also again, one of the samples exhibited a similar ductile response where yield occurred at the same stress level that the others failed, and then decreased the force necessary to continue the same displacement rate. To help observe the correlation between ultrasonic treatment and mechanical response, the remaining samples were tested at level 9.

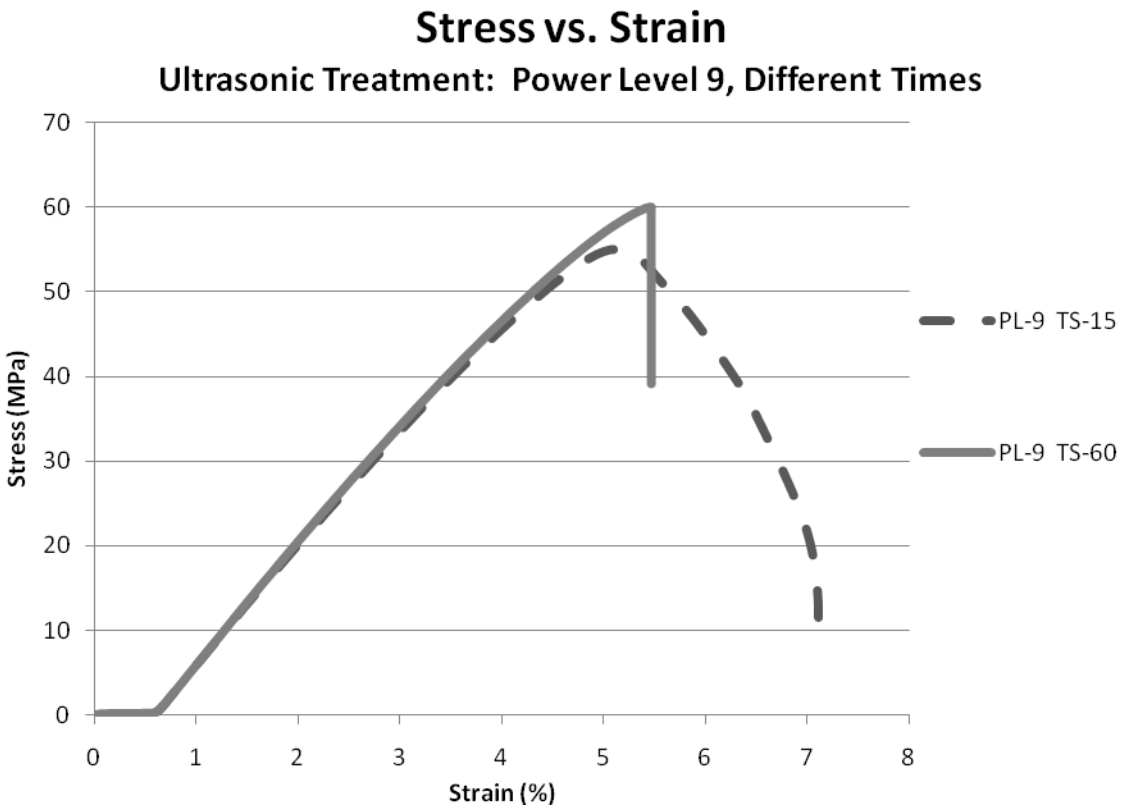

Figure 47: Stress strain data of damaged samples ultrasonically treated at 90% maximum power for 15 and 60 seconds a side. (PL) represents power level out of 10, and (TS) is the treatment time per side in seconds.

Level 9 treatments offered an increase in ultimate stress and an increase in yield stress.

The next figure shows all of the damaged samples on one plot.

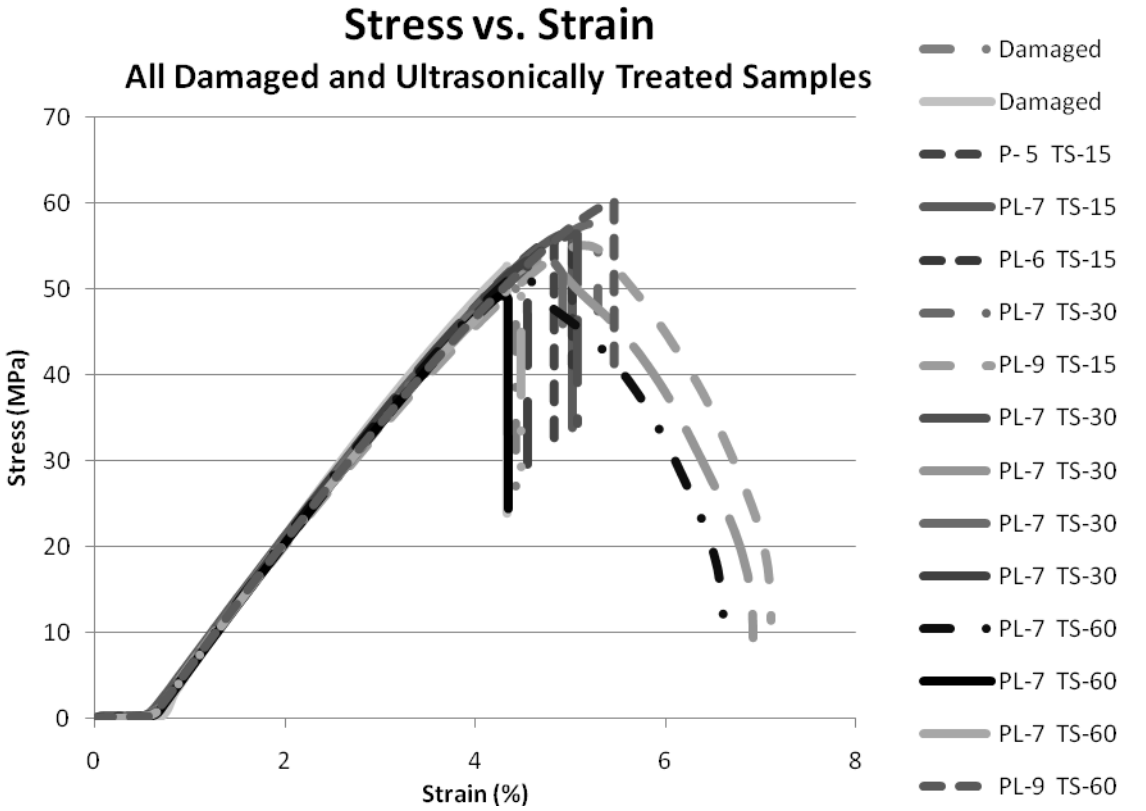

Figure 48: Stress strain data of all damaged samples ultrasonically treated. (PL) represents power level out of 10, and (TS) is the treatment time per side in seconds.

This comparison illustrates that as exposure time and power level increase, the ultimate stress also increases. It also shows that the ductile response from the local spot melting occurs at different exposure times and levels. This means that the ultrasonic probe influence depends upon ultrasonic power level, exposure time, and exposure area.

To get a better idea of the bigger picture, all of the damaged samples are shown in the plot below along with the undamaged sample tensile test data.

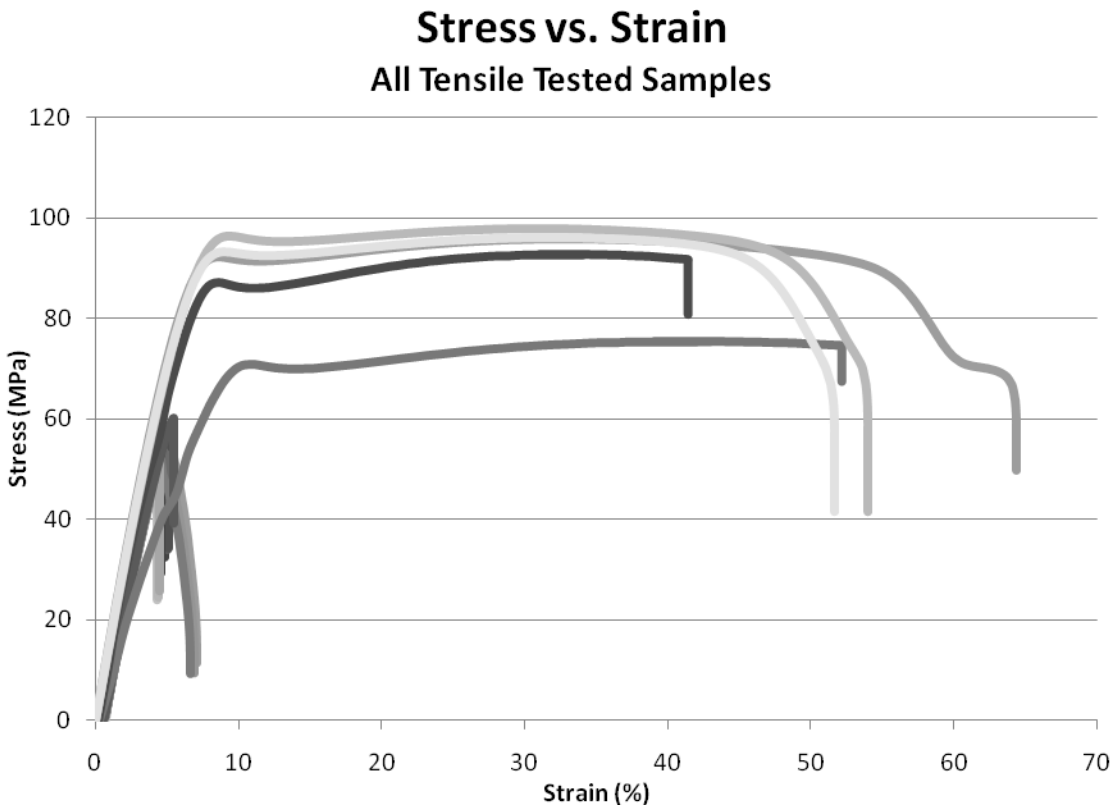

Figure 49: Stress strain data of undamaged, undamaged but heated, damaged, and damaged but ultrasonically treated samples.

Although the effect of the ultrasonic energy can be observed when comparing damaged and ultrasonically treated tensile test specimens, looking at the big picture shows that the effect seems limited compared to undamaged samples. It is important to remember that the damage in the samples was a 1/8 inch edge cut, which means that ¼ of the material was removed in the cross-section of the cut. This accounts for the extreme reduction in ultimate stress, and for the common brittle fracture behavior. The brittle fracture can be observed by examining the fracture surface of a failed specimen, as seen below. The crack area shows little to no necking, as is common in undamaged nylon 6,6 tests, and a rough fracture surface, which is associated with brittle failure, seen below.

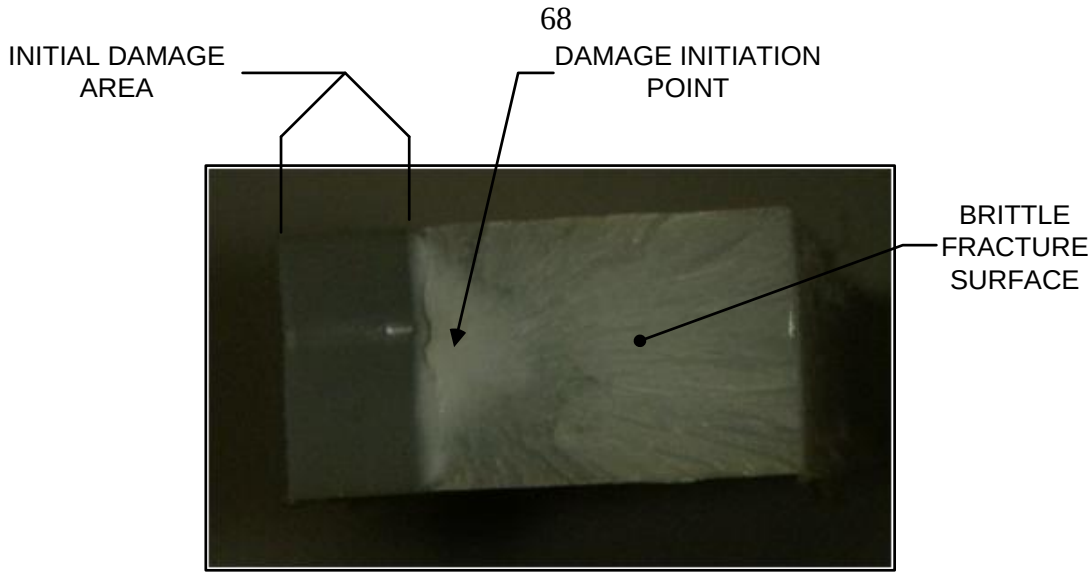

Figure 50: Picture of fracture surface of damaged dogbone.

This fracture surface was compared to the surface of a virgin sample, and a heated virgin sample. The results show the virgin sample showed noticeable necking, the heated sample showed less necking and the damaged sample showed a brittle fracture surface. The larger relative amount of necking between the virgin and heated samples was also exhibited by the tensile test results where the virgin sample dips lower after yielding. The larger dip corresponds to more necking because more energy is being used to reorient the polymer chains to create the necking.

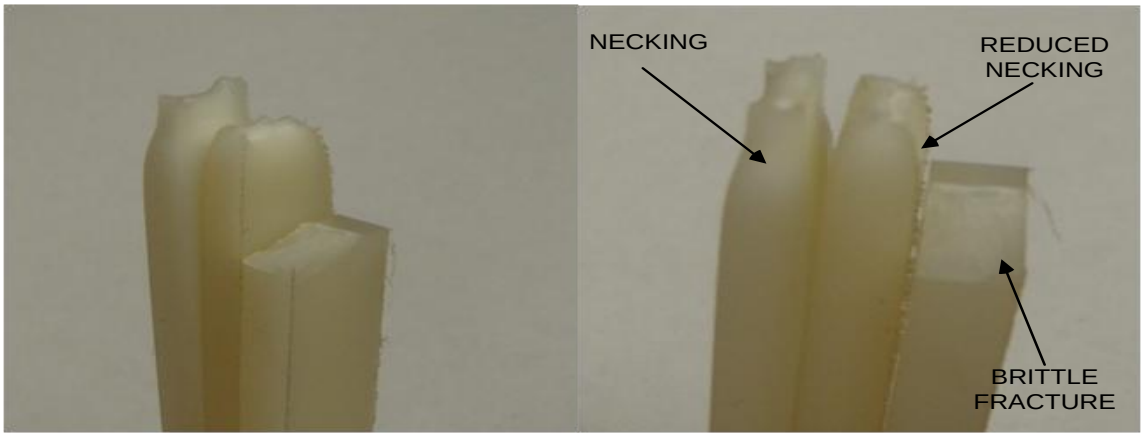

Figure 51: Comparison of fracture surfaces of, from left to right, a virgin sample, a heated but undamaged sample, and a damaged but untreated sample.

Differential Thermal Analysis

Differential thermal analysis (DTA) examines the difference in temperature between a test specimen and a control specimen. Both samples are heated simultaneously in the same vacuum chamber, and their temperature monitored with thermocouples. A sample setup is shown below.

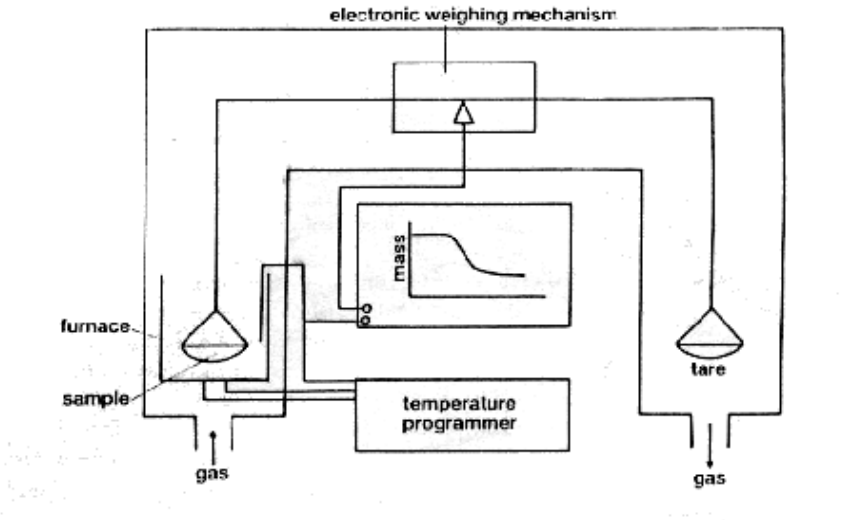

Figure 52: Schematic for DTA testing apparatus. (18)

The key to DTA is heating the control specimen at a specified rate and measuring the difference in thermocouple output. The actual sample temperature is not as important as the difference between the actual sample and the control. The test sample will not increase temperature at the same rate as the control since different materials contain different rates of enthalpy exchange. This also means that certain output behaviors can be interpreted to represent certain thermomechanical changes. Specific spikes represent glass transition, phase change, and other changes in crystalline structure. A sample DTA output graph is shown below.

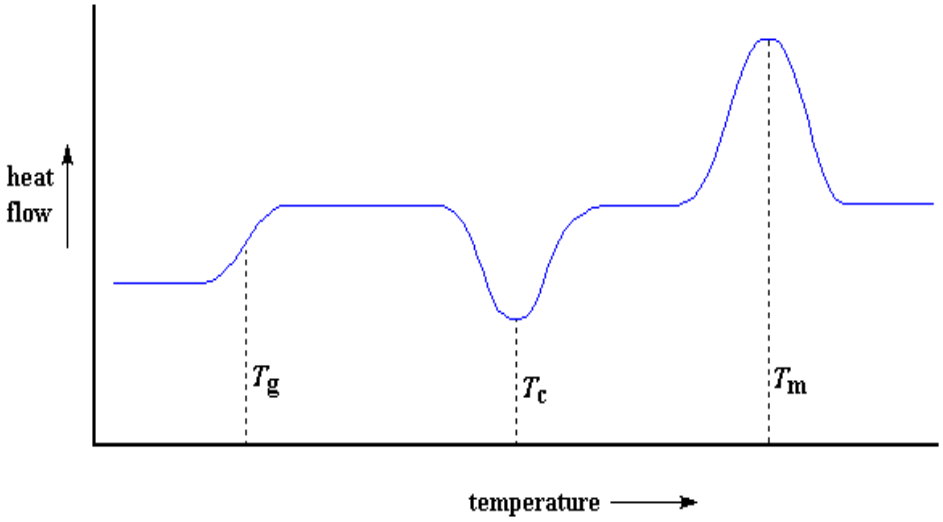

Figure 53: Sample DTA output graph. (19)

As the temperature of the sample increases, the thermal response adjusts to accommodate different phase changes. These changes are represented by peaks and valleys that correlate to glass transition temperature (T_g), crystallization temperature (T_c), and melting temperature (T_m).

These tests used aluminum oxide (AlO_3) as the control material. The test speciemens of nylon were all about 50 mg. The test vaccum chamber was heated at a rate of 10ºC a minute. The figure below shows the relative sample size of the specimens used.

Figure 54: DTA sample specimen shown for scale.

The DTA tests were also used to determine melting temperature and glass-transition temperature. The resulting specimen, being taking beyond the melting temperature, turned an opaque black color.

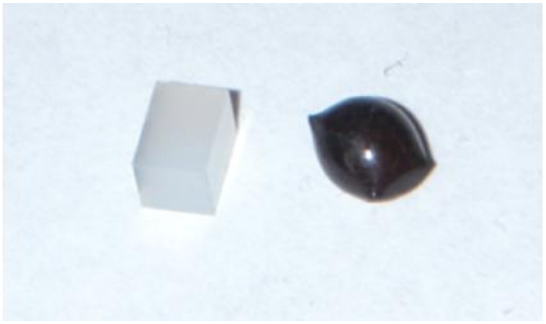

Figure 55: DTA virgin sample versus DTA sample heated to melting.

The DTA results below demonstrate the comparison between differently treated samples. Although every sample exhibits a similar response, the magnitude of the peaks and values discriminates between different samples. The first divergence between samples occurs at around 45˚C. At this point, the level of ultrasonic influence determines how high the DTA curve will rise during the glass transition phase. As the signals all decrease, slight dips seem to represent increasing levels of crystallization, especially around 170˚C. Then, all samples seem to melt around 270˚C. The results are shown below.

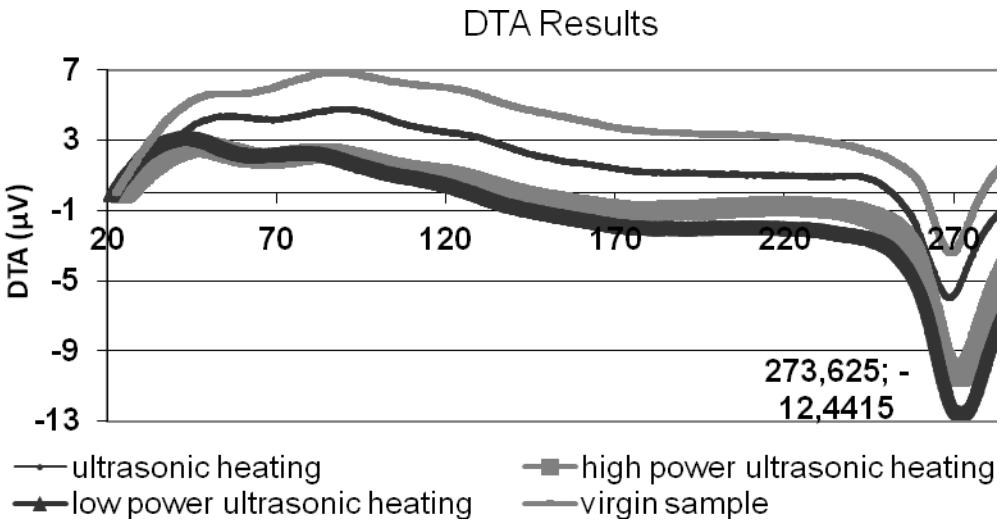

Figure 56: Experimental DTA results.

The level of crystallinity can be calculated from these results by finding the areas under the crystallinity change and melting spikes, and incorporating the mass of the sample in a series of equations as shown in Appendix B. Differential thermal testing showed a correlation between increased heating and increased crystallinity, as well as a correlation between ultrasonic treatment and increased crystallinity.

MODELING

Modeling consisted of validating the finite element code, ABAQUS, accurately representing the experimental data, and then using the correlated models to predict future behavior and results of ultrasonically activated self-healing polymers. The general modeling progression is shown below in table 2.

Table 2: Modeling progression.

MODELING
Model Validation Validate Heat Transfer Case 1 Case 2 Case 3 Case 4 Validate Heat Generation
Ultrasonic Influence Model 30% Power Model 50% Power Model
Heat Distribution Representative Semicircular Area Localized Area
Cohesive Zone Model
Relative Crack Representation

Thermal Modeling of Self-Healing Polymers

It is commonly understood that the acoustic sound waves applied to the polymer create mechanical impedance where the acoustic wave energy is absorbed by the polymer atoms creating localized relative motion, friction, and therefore, heat. This localized heat forces the polymer to expand, begin to change phase, and then cool, cure and heal when the acoustic sound waves cease. Since ABAQUS was used as the modeling program, and acoustic elements are used primarily to determine resonant frequencies and mode shapes for sound in confined spaces, acoustic elements were ignored, and an internal heat generation model was created.

Before heat generation models could be created and confidently utilized, heat transfer validation of ABAQUS was performed. Specific thermal loading situations were setup and ABAQUS results compared to the model results from a program called COMSOL and analytical results. Four different transient loading situations were compared involving constant boundary conditions or convective boundary conditions. For all tests, though, the same material properties were used, and these are shown in Table 3.

Table 3: Nylon 6,6 material properties used for model validation.

Property	**Value**
k	0.237 W/mK
C_p	1.674×10^3 J/kgK
P	1140 kg/m^3
C.T.E.	8.1×10^{-5} m/mK
Melting Temperature range	200 C to 265 C

The first case analyzed involved an initial temperature of the sample, and then once the model was started, one side had a constant boundary condition of a higher temperature than the initial. Both the top and bottom of the sample were insulated, making the problem one-dimensional. The setup for case 1 is shown below.

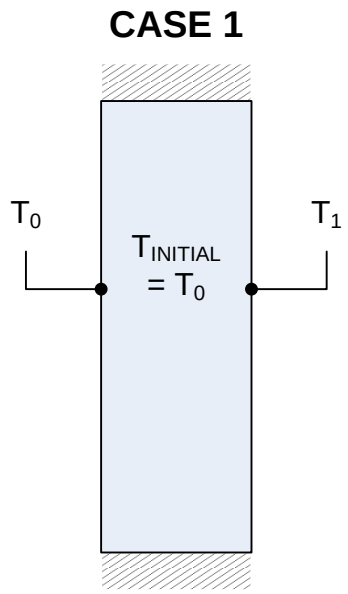

Figure 57: Model setup for case 1.

The COMSOL and analytical results for these four cases were completed by Dr. Steven Rutherford, and his results are contained in appendix A. His results were normalized to decrease confusion between different codes and for purposes of comparison. For these reasons, the ABAQUS results were also normalized. The three following figures are the exact, analytical results, the COMSOL results, and then the ABAQUS results. The values in the legends on all graphs are the normalized time values. This was done to illustrate the heat transfer progression for the transient analyses.

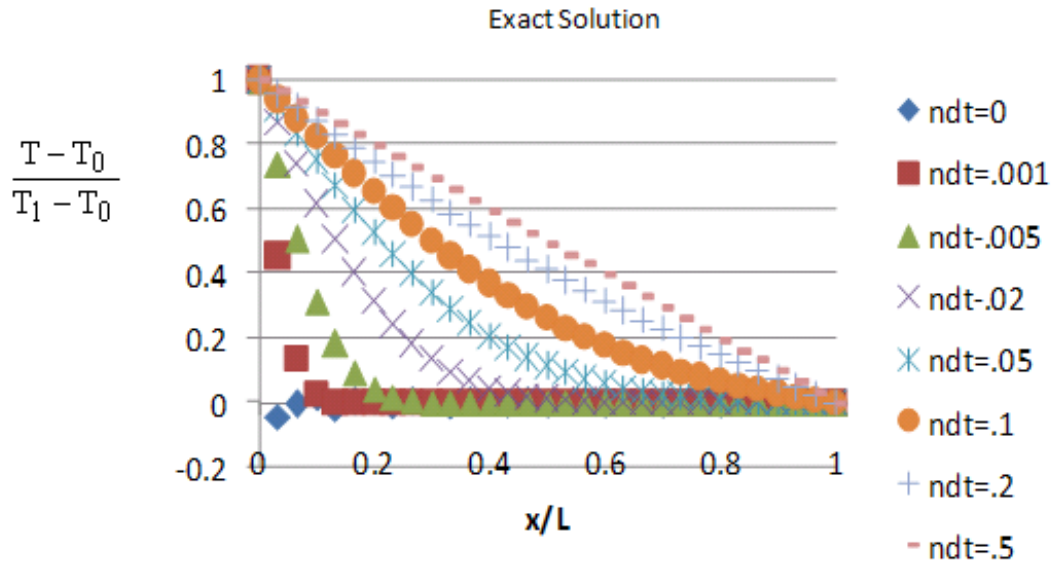

Figure 58: Analytical results for heat transfer validation case 1.

The analytical results show a clear temperature increase as time progresses until a steady-state is reached at normalized time equal to 0.5. The equations used, though create a discontinuity at time equal to zero, and this continuity can be seen in the graph above for normalized time equal to 0.

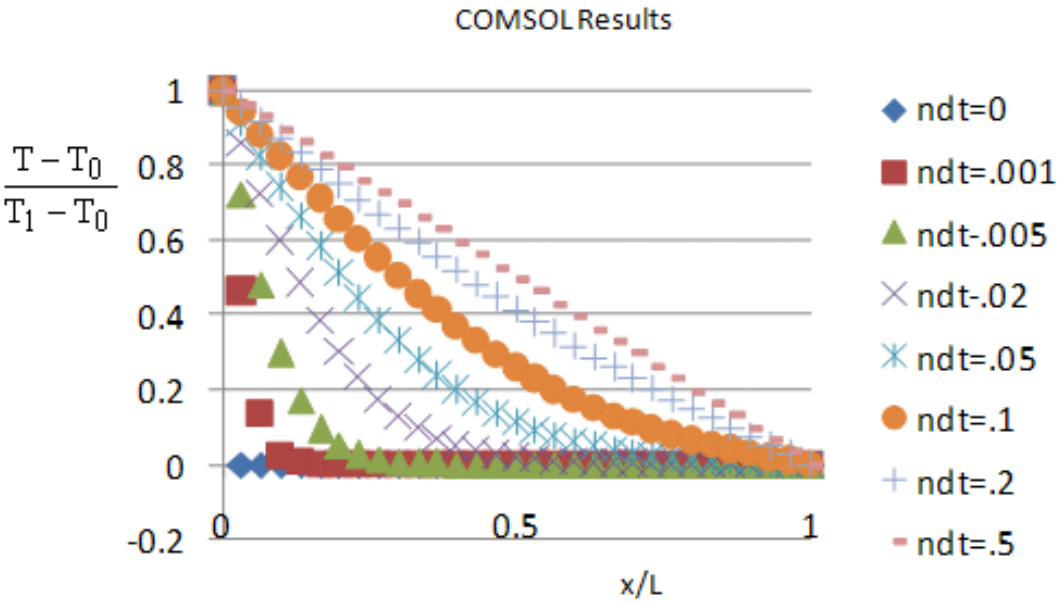

Figure 59: COMSOL results for heat transfer validation case 1.

The COMSOL results agree quite well to the analytical results. This makes sense since the COMSOL solver is programmed with the same general heat transfer equations. The real test is the comparison to the ABAQUS results, below.

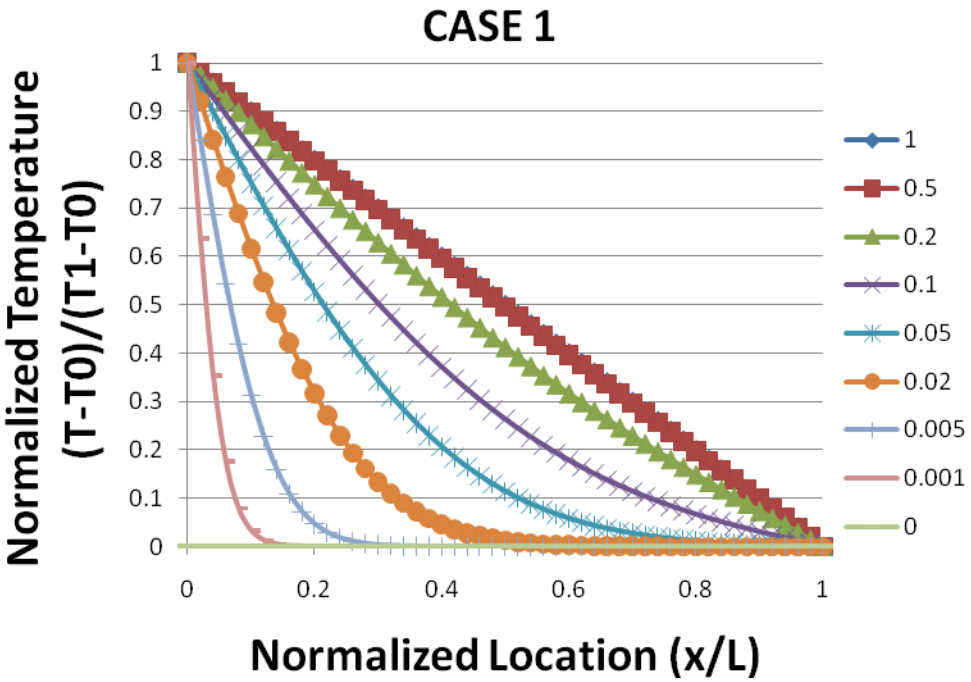

Figure 60: ABAQUS results for heat transfer validation case 1.

The ABAQUS results reveal the exact same temperature response as the analytical solutions and the COMSOL solutions, so the next case was analyzed.

The next case is similar to case 1, except both sides of the sample are held constantly at the same elevated temperature. The setup for case 2 is shown below.

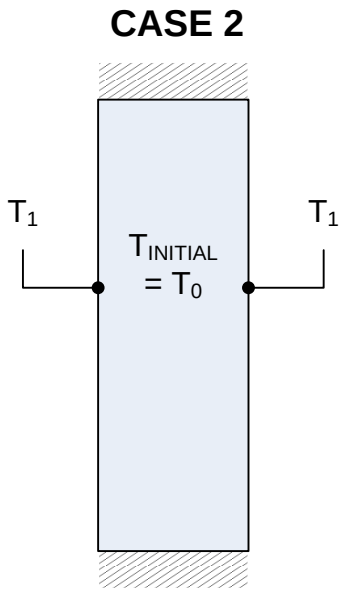

Figure 61: Model setup for case 2.

This setup allowed for a thermally and spatially symmetrical analysis. The resulting plots for case 2 are given below.

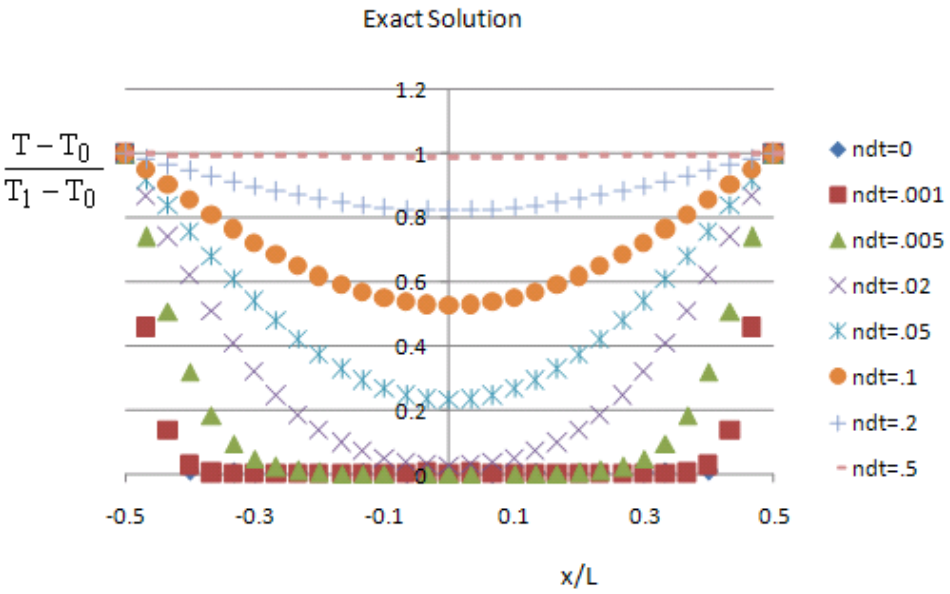

Figure 62: Analytical results for heat transfer validation case 2.

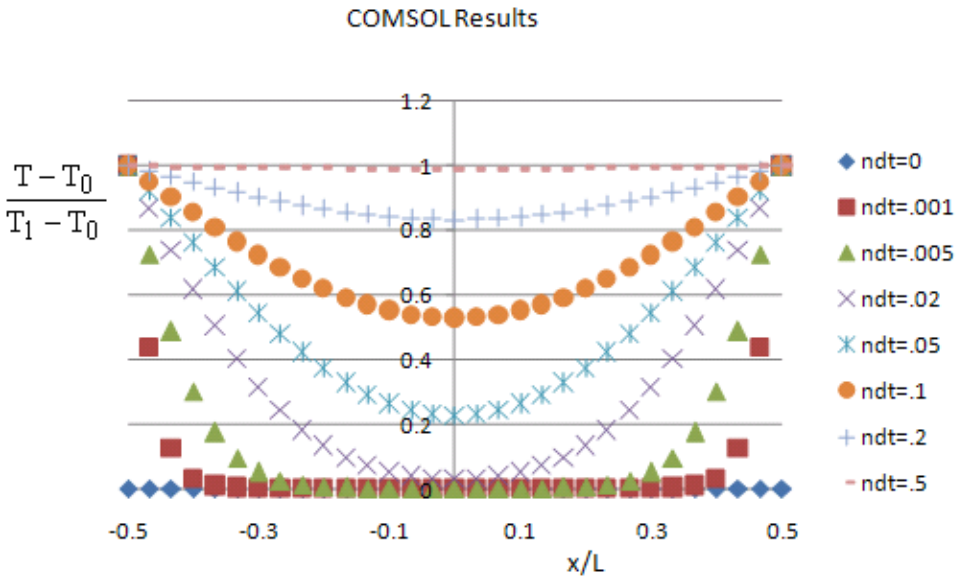

Figure 63: COMSOL results for heat transfer validation case 2.

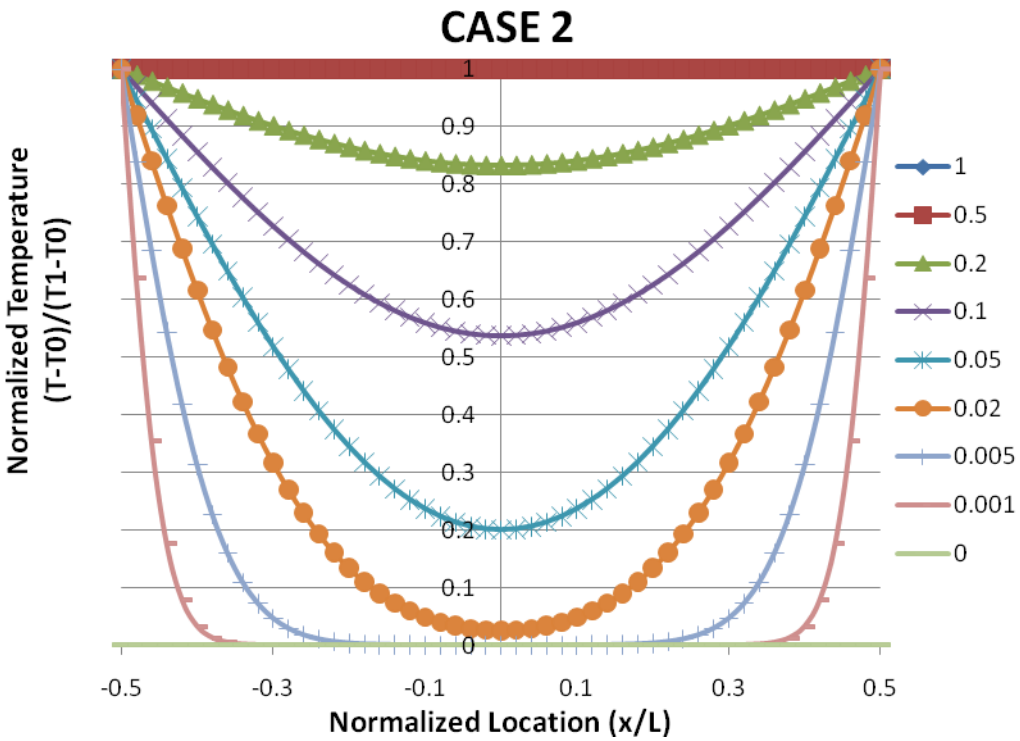

Figure 64: ABAQUS results for heat transfer validation case 2.

Again, the results from the analytical model, COMSOL simulation, and ABAQUS model all agree. The thermal loading situation for case 3 analyzed involves symmetric

convection loading on the left and right sides while the top and bottom are still insulated. The model loading for case 3 is shown below.

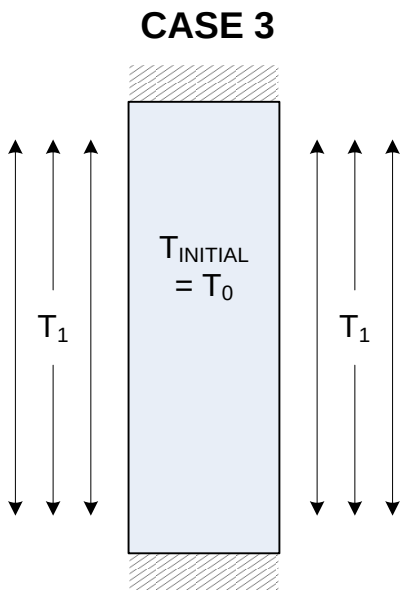

Figure 65: Model setup for case 3.

Since a relatively large coefficient of convection was chosen, the results from case three are identical to a loading situation where the left and right sides are held at the convective sink temperature. The results are shown below.

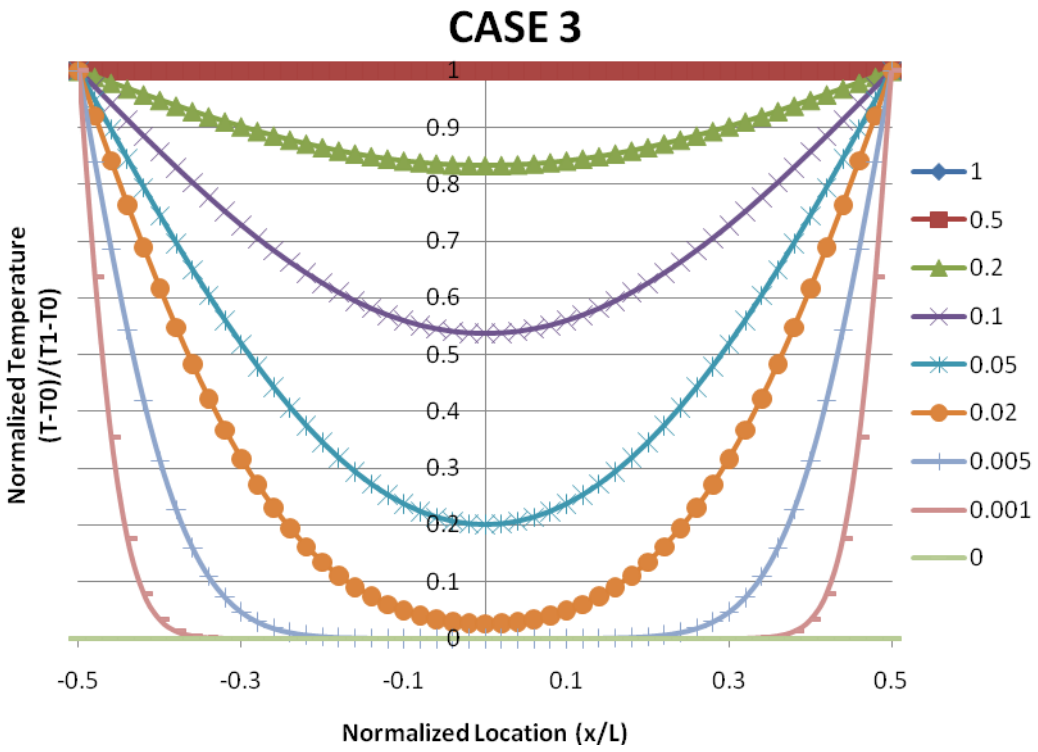

Figure 66: ABAQUS results for heat transfer validation case 3.

Further inspection proved these results to be identical to case 2 results for analytical, COMSOL, and ABAQUS simulations. For this reason, the other graphs are not repeated.

The next, and final validation loading situation is two-dimensional since it allows convective loading on all four sides. For this reason, the generalized dimensions were changed to represent the modeling area ratio of length to height of 6 to 1. Next, this model had the initial temperature of the model just below melting at 200˚C (473 K) and convecting to a room temperature sink temperature of 20˚C (293 K). The thermal loading setup for case 4 is shown below.

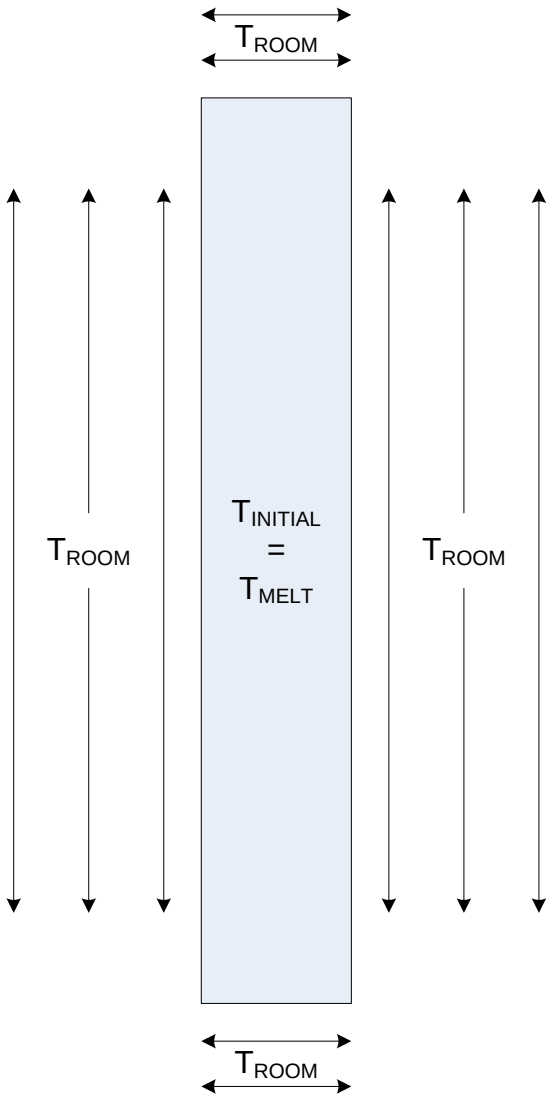

Figure 67: Model setup for case 4.

Since this was a two-dimensional model, results had to be compared as temperature gradients at different times. The results are shown below in increasing time steps with COMSOL results on the left and ABAQUS results on the right.

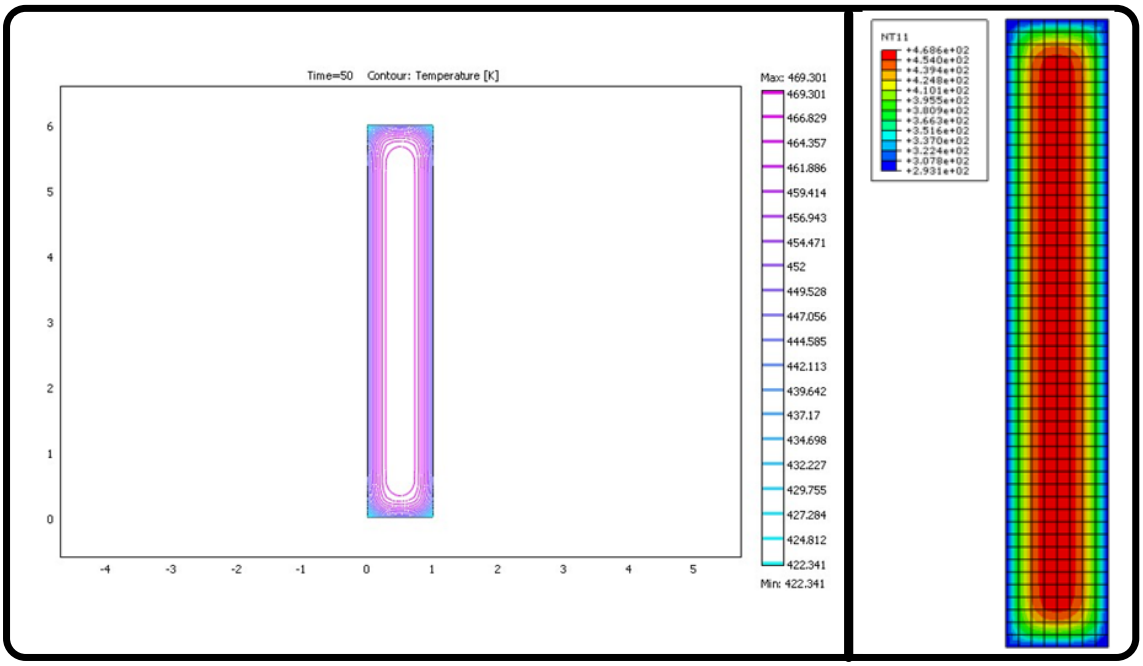

Figure 68: Results for case 4 loading at 50 seconds elapsed time. COMSOL results on the left and ABAQUS results on the right.

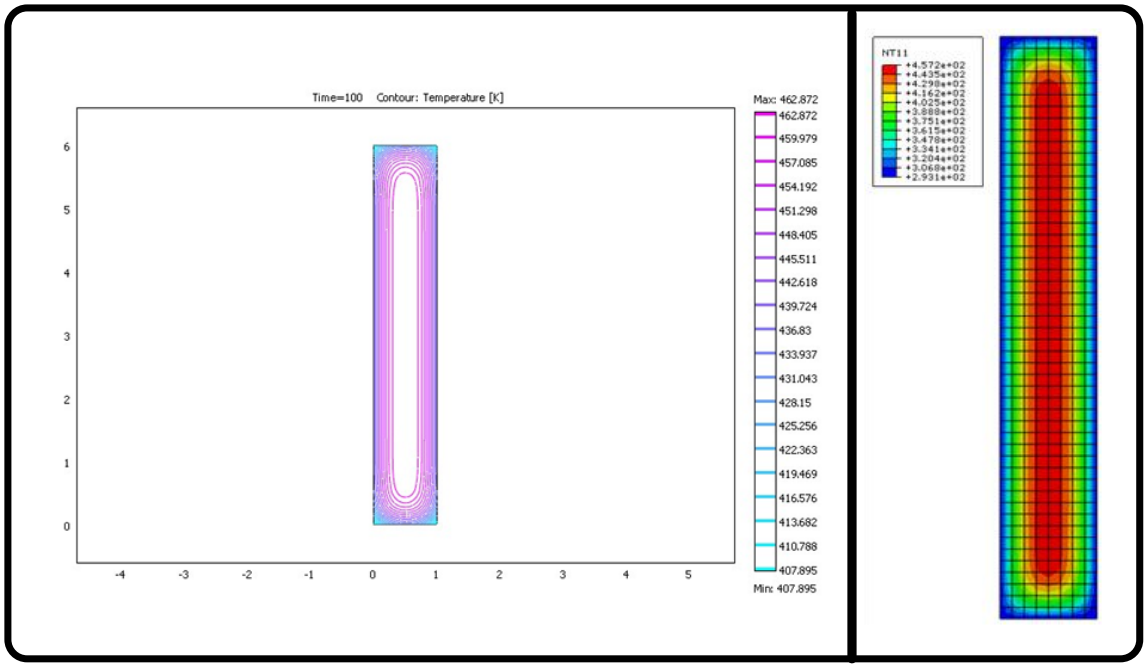

Figure 69: Results for case 4 loading at 100 seconds elapsed time. COMSOL results on the left and ABAQUS results on the right.

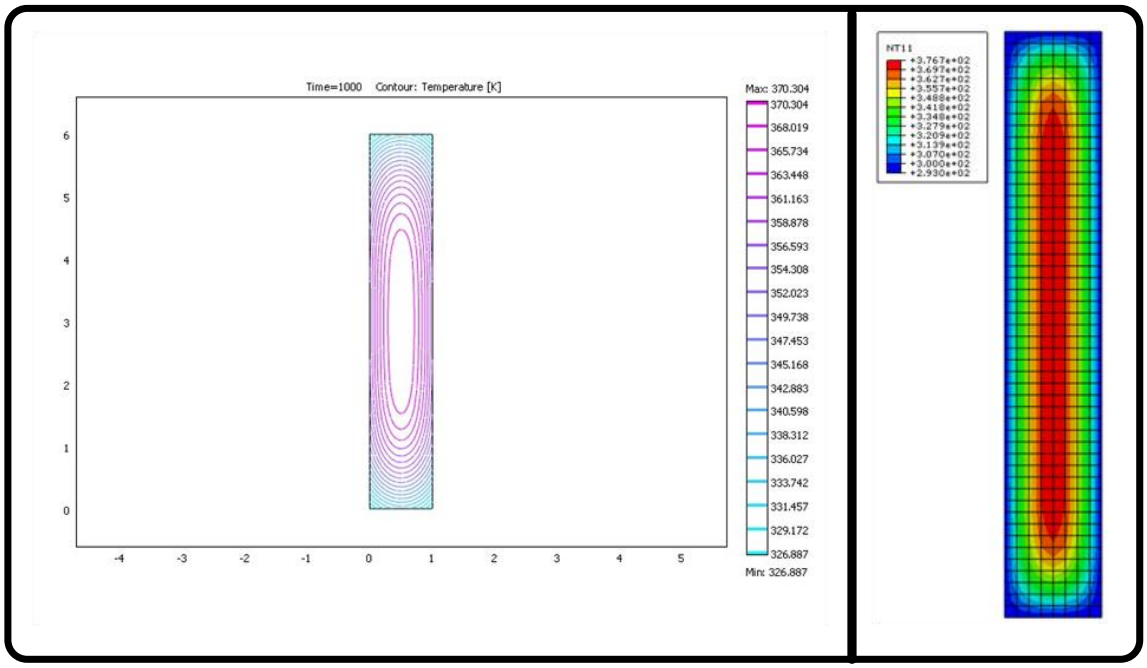

Figure 70: Results for case 4 loading at 1000 seconds elapsed time. COMSOL results on the left and ABAQUS results on the right.

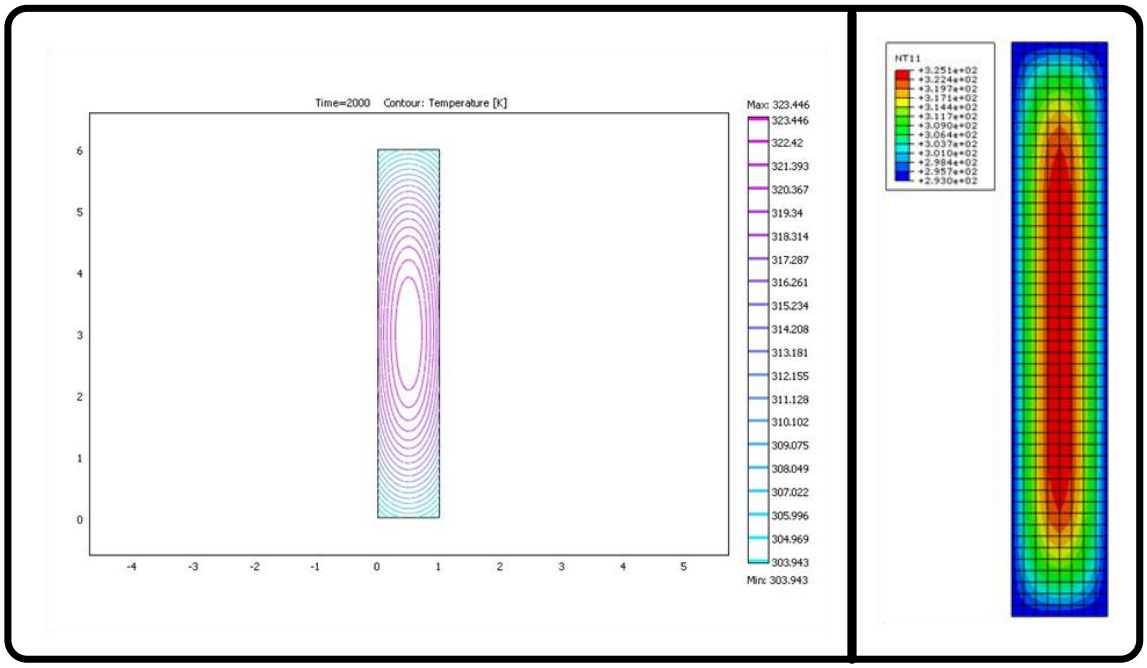

Figure 71: Results for case 4 loading at 2000 seconds elapsed time. COMSOL results on the left and ABAQUS results on the right.

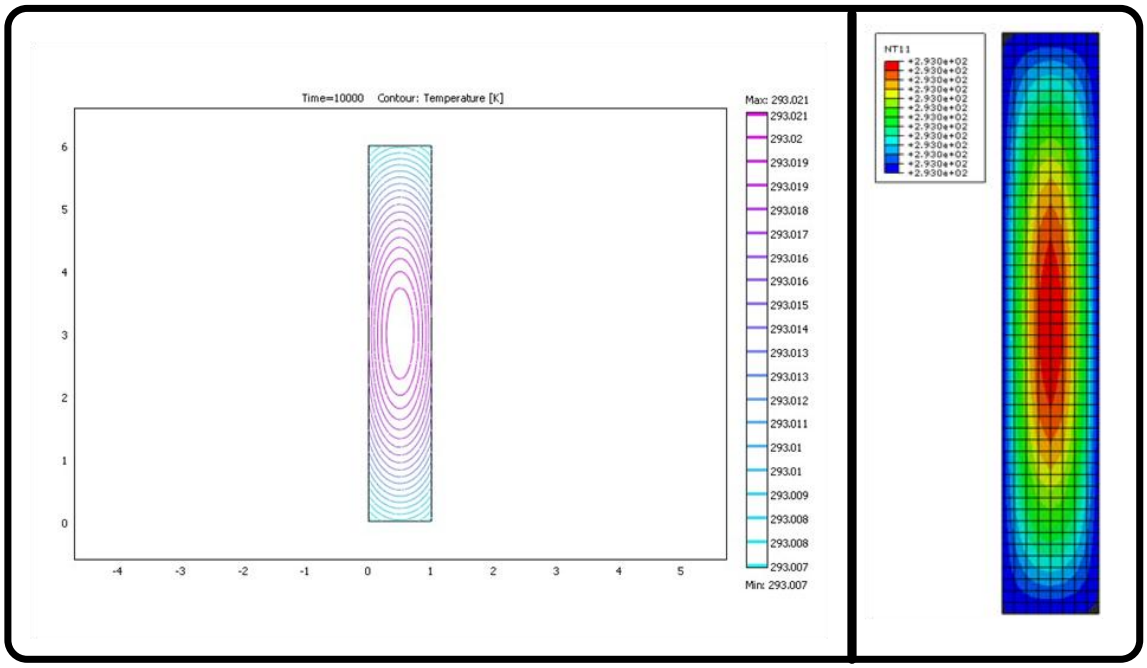

Figure 72: Results for case 4 loading at 10000 seconds elapsed time. COMSOL results on the left and ABAQUS results on the right.

Comparing temperature contours and range demonstrates that the COMSOL and ABAQUS results line up quite well. There is some deviation, though at the boundaries. In the ABAQUS model, film boundary conditions are used to apply convection. This affects the boundary different than the governing equations in COMSOL, or in analytical models for instance. This makes the boundary nodes in the ABAQUS model part of the convection. This means the edges exposed to convection in the ABAQUS model will reach the convection sink temperature more rapidly than in an analytical model. Also, there is difference in convective loading at the corners. Usually in analytical models, geometric corners in heat transfer are treated as point discontinuities where the effects along the adjoining sides are calculated and then superimposed immediately behind the node. This was attempted to be mimicked in the ABAQUS model by using only

parallelogram quadratic elements. A finer mesh was desired in the ABAQUS model, but the memory needed for each run at higher meshes caused the program to close. Since general heat transfer models in ABAQUS were validated, the next step was to model ultrasonic influence with heat generation.

Modeling heat generation was not well known to the researcher, so a combination of trial and error, and the cutting and pasting of verification codes was used. First, a desirable code or model definition was found; the exact lines of code needed were copied and then pasted into the user's new, Frankenstein code. From here, the code was verified to do as directed, or changes were made. This was, more or less, a two steps forward, one step back approach. It was found to be even more complex of a process since heat generation was a capability of ABAQUS, but in the form of a subroutine. This is in fact a section of code written in FORTRAN language and then referenced and compiled when the code is run. At MSU, there is only one computer in the college with a known FORTRAN compiler (available to students), and it is located on a separate server. Although server access is somewhat complicated, the computer accessed on this server was allocated to mainly run large batch files of ABAQUS code, taking the initial, simpler runs only seconds to calculate. Finally a code was written and shown to allow for heat generation to be accurately performed. This was reiterated by modeling an example problem from the heat transfer text book, *Introduction to Heat Transfer: Fourth Edition*, which was a two dimensional steady-state problem with heat generation on one side of the material and convection on the other exterior side (4). The problem setup and parameters are shown below in figure 70 and table 4, respectively.

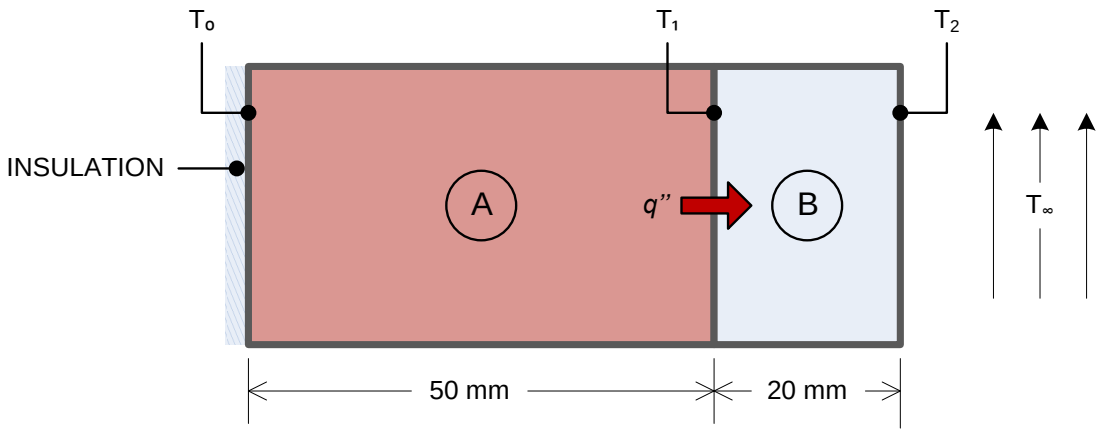

Figure 73: Heat generation problem setup. (4)

Table 4: Heat generation validation problem parameters. (4)

Validation Book Problem Material Property Values and Assumptions				
	Material A		Material B	
Conductivity	k_A	75 $^{W}/_{m\bullet K}$	k_B	150 $^{W}/_{m\bullet K}$
Material Length	L_A	50 mm	L_B	20 mm
Heat Generation	q'_A	1.5 x 10^{6} $^{W}/_{m^3}$	q'_B	0 $^{W}/_{m^3}$
Convection Coefficient	h	75 $^{W}/_{m^2\bullet K}$		
Sink Temperature	T_∞	30 ˚C		
Assumptions:	• Steady-state conditions • One-dimensional conduction in horizontal direction • Negligible contact resistance between walls • Inner surface A is adiabatic • Constant properties for materials A and B			

The problem geometry and loading was reproduced in ABAQUS. The test was run and the resulting temperature distribution is shown below.

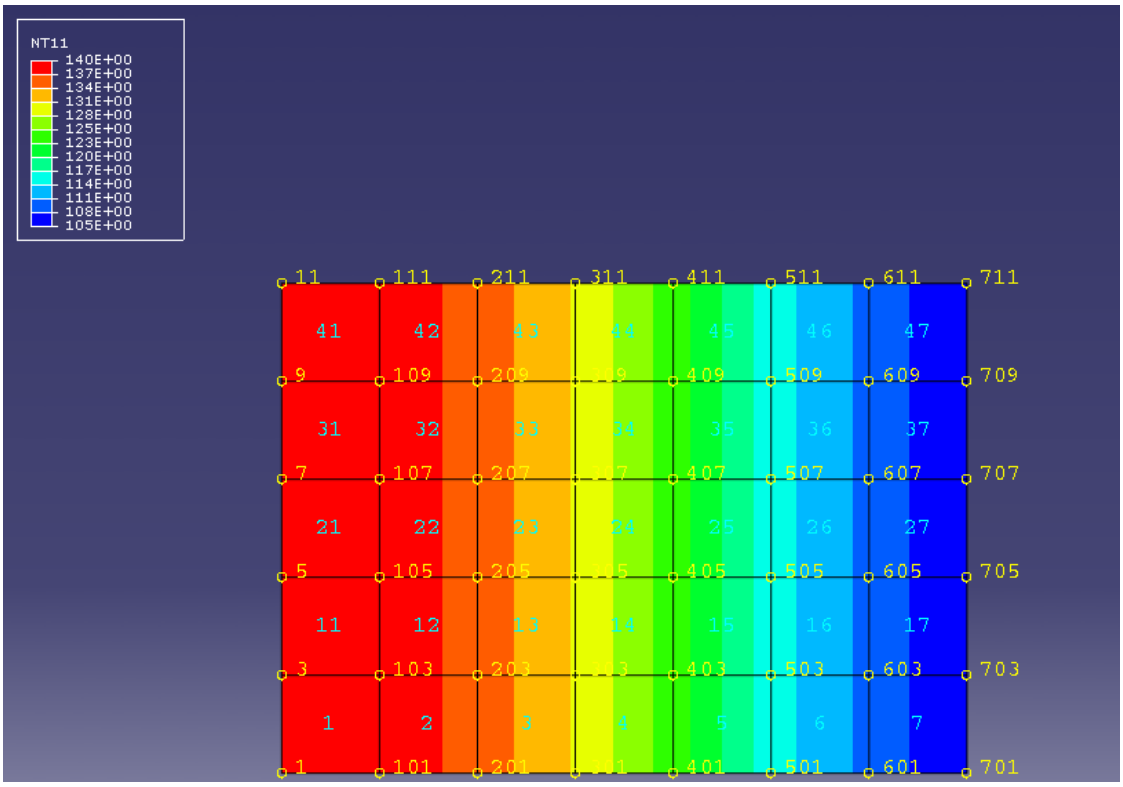

Figure 74: Heat generation validation problem results in ABAQUS.

Since the problem is one-dimensional, the nodal output at the end of the steady-state analysis was taken from a horizontal line of nodes. The nodal temperatures match the book results, and are shown below.

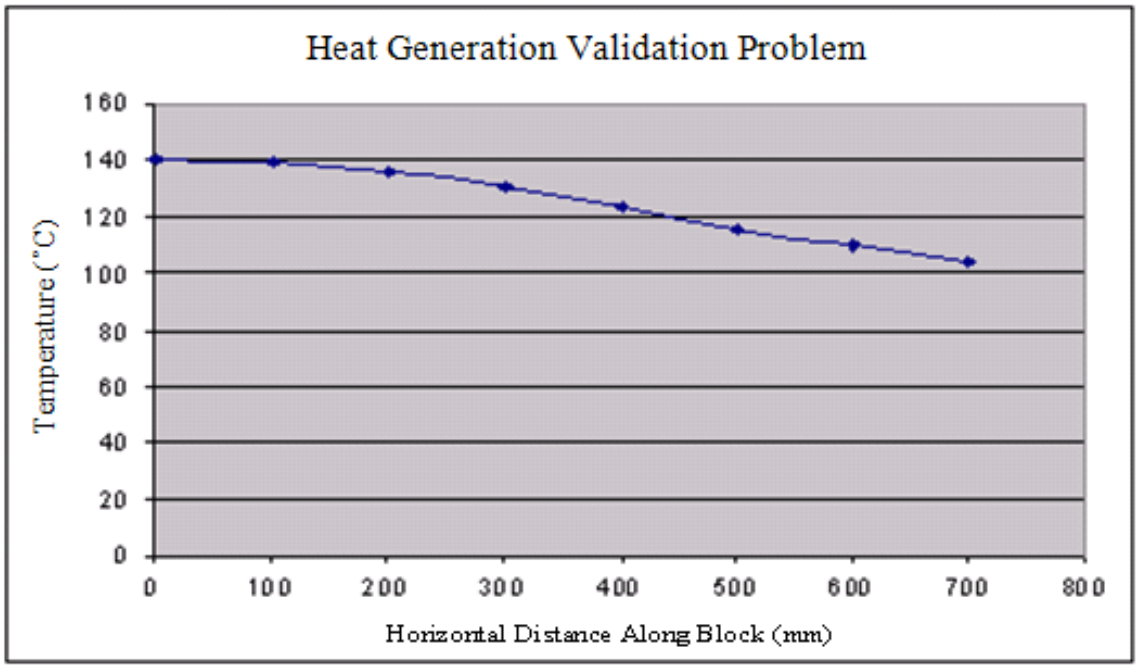

Figure 75: Nodal temperature results from heat generation validation problem.

From this point, the boundary conditions and loading definitions were changed to experiment with different situations. It should be noted here that one model was used and computation was very fast, but the transfer between the servers, and then to ABAQUS CAE to examine the results, was tedious. Therefore, an array of nine models was run at once. This made it possible to run multiple loading situations at once and examine side by side. For analysis purposes, whichever new parameter being tested was increased from sample one to sample nine. The sample array numbering is shown below.

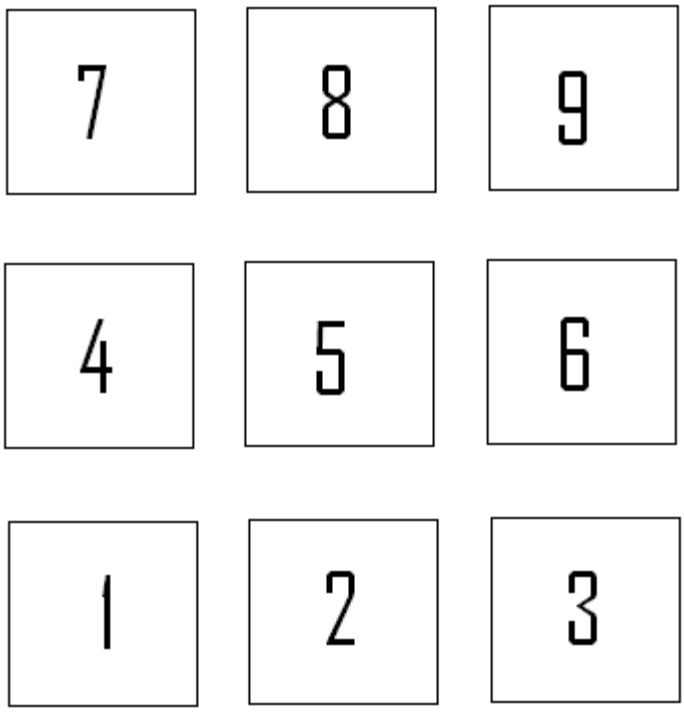

Figure 76: General model placement numbering scheme for tests involving multiple models.

The nine sample arrays were setup as coupled temperature-displacement analyses. Once the ABAQUS code was verified to other methods of modeling, other aspects of the actual experiment were modeled.

The next model created was an attempt to replicate the temperature change caused by the ultrasonic probe. The influence of the ultrasonic energy was mimicked using heat generation elements. Heat generation modeling is accomplished in ABAQUS with the use of a subroutine. Subroutines are software bundles that allow for extra modeling capability with the exception of extra coding to access. Subroutines open many modeling doors, but need extra effort to access so that their extra features do not bog down the processing strength or speed of the base ABAQUS program unless needed. The extra effort required includes FORTRAN code to initiate and direct subroutines. Initially, a test model was performed to illustrate the successful use of the heat generation subroutine

in ABAQUS. The verification model again used the nine array setup to perform 9 different models simultaneously. All nine models are rectangular areas constrained by convection on the top and bottom surfaces and a constant heat generation applied to one element. The convection on the top and bottom is controlled by a large coefficient to allow for a nearly constant top and bottom edge temperature. The difference to be observed amongst the 9 models was exactly which element is producing the heat generation. As one moves through the numbering system in the nine element array, left-to-right and bottom-to-top, the heat generation element was always produced on the left side, but at increasing vertical locations. This means that the heat generation element starts at the lower left element in location 1 of the 9 sample array, and moves up to the upper left element in position 9 of the nine element array. The heat generation element is shown by the black array, the legend corresponds to nodal temperatures, and the results from a steady state heat transfer analysis.

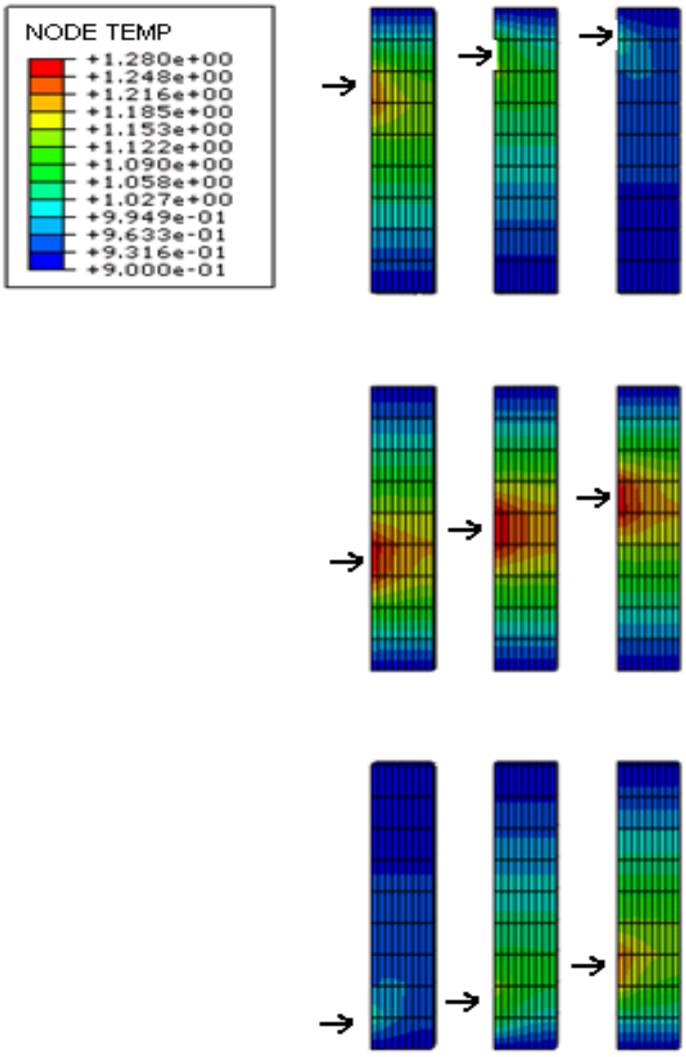

Figure 77: Heat generation model comparison. The arrow signifies the element on the leftmost side of each model providing the heat generation. The top and bottom surfaces are exposed to surface convection.

Where the heat generation is away from the convective ends, the maximum temperature was at its largest value, and the temperature gradient greater. As the heat generation element gets close to the convective influence on the ends, its influence is not as noticeable. This test illustrated that heat generation was conceptually modeled, and correctly interacted with other modes of heat transfer, in this case, namely convection. The next step was to use heat generation as a means to model the influence of the ultrasonic transducer.

The initial ultrasonic transducer test where the probe's axis was aligned with the nylon sample's length was reproduced in ABAQUS. The rectangular piece of nylon sample was modeled to the same dimensions as that of the experiment, and given the published material properties. Along the relative top of the modeled sample, elements were selected to represent the surface area contacting the ultrasonic probe. These elements were selected to provide heat generation and represent the ultrasonic wave influence.

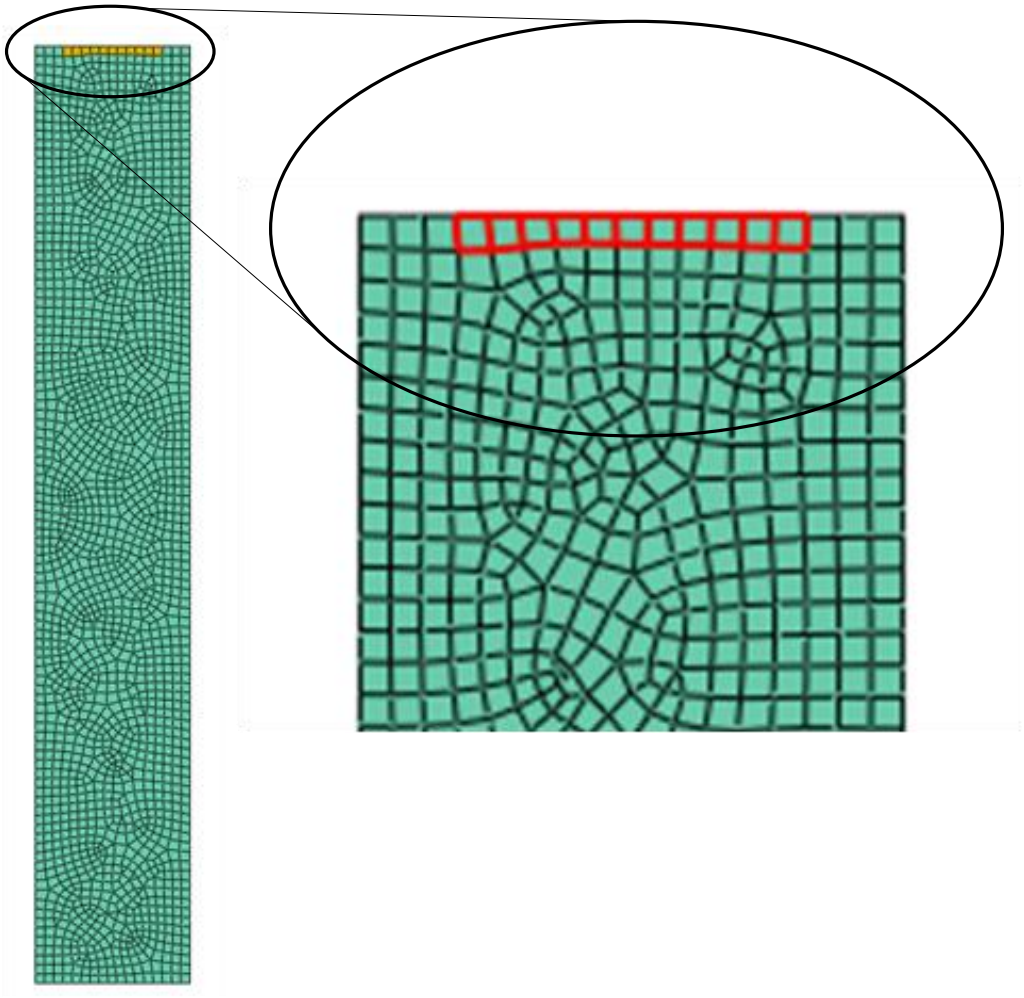

Figure 78: Elements selected for heat generation in ultrasonic influence model shown in red.

Next, 4 nodes were selected along the length of the exterior of the sample at the same positions as the thermocouples were placed along the actual experimental sample. The temperature response of these nodes was monitored for the duration of the model test.

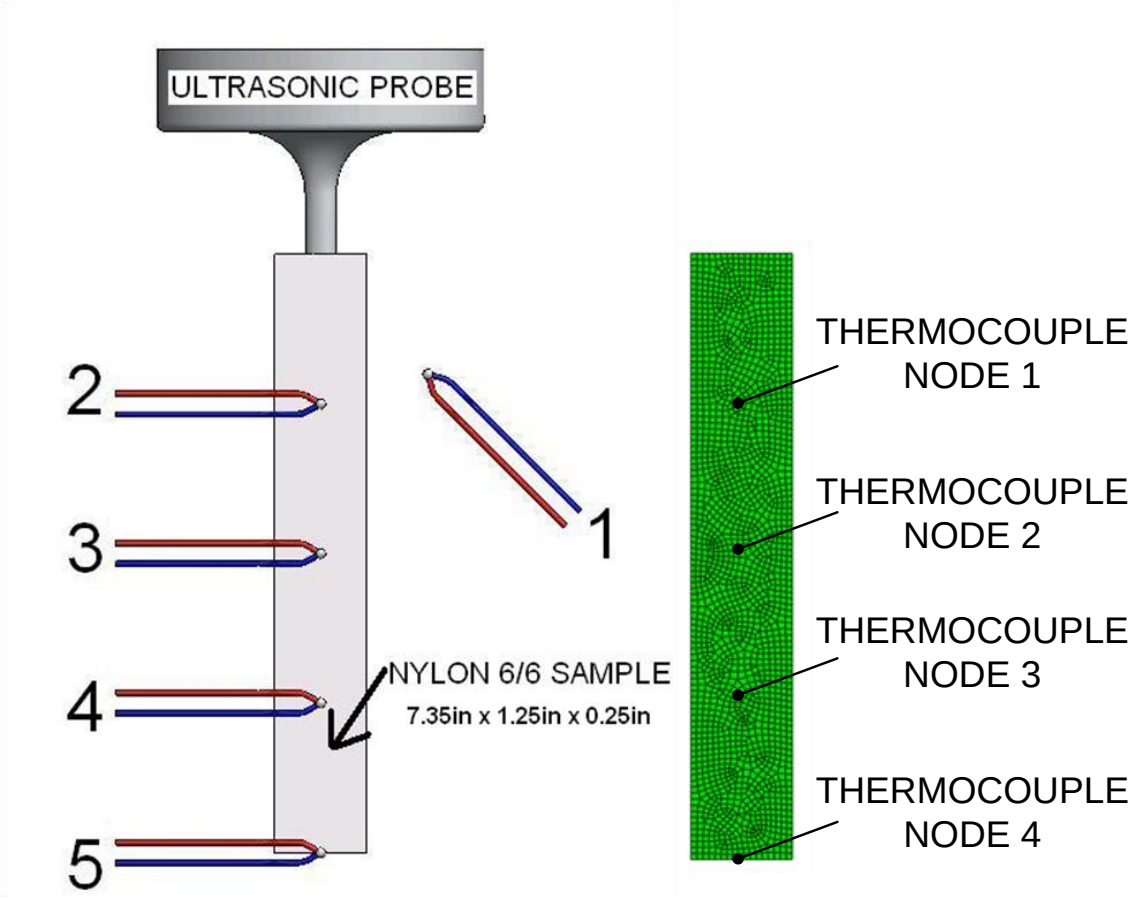

Figure 79: Model reference nodes verses experiment reference nodes.

The test was a static heat transfer test run over a period of 300 seconds, or 5 minutes, just like the actual experiment. As an additional influence, convection was added at the bottom of the model to represent the metal plate of the apparatus in the experiment. Although natural convection from the surrounding air was also considered, it was not included in the model. The model was run and the nodal response of the selected nodes representing experimental thermocouple positions was compared to that of the

experiment. The value of heat generation was then systematically adjusted and tested to compare until an acceptable representation was achieved. The general behavior was also adjusted by concurrently adjusting the convection coefficient for the bottom nodes. Although experimentation clearly showed that the ultrasonic probe has an influence on the sample, the means to correctly model it involves multiple performance parameters. Since 2 separate ultrasonic probe tests were performed, two models were completed. First, the experiment with the ultrasonic probe set to 30% of maximum power was compared. The model is shown below.

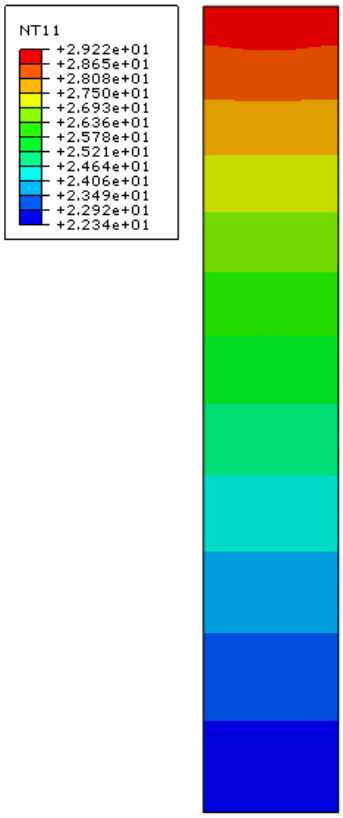

Figure 80: Temperature gradient of ultrasonic influence test at 30% power for 5 minutes.

The rainbow model after five minutes of ultrasonic application shows an increasing temperature gradient from hot to cold with a somewhat circular response near the ultrasonic probe application area, and then a more uniform temperature cross-section as

the cold end is approached. The nodal temperature values over time of the 4 specified nodes are shown below.

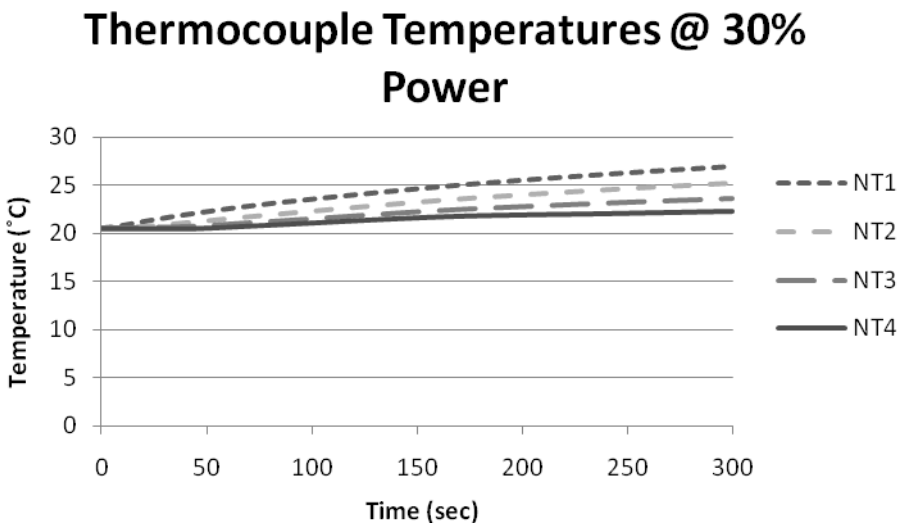

Figure 81: Temperature readout from the thermocouples in the ultrasonic influence model. The ultrasonic probe is operating at 30% of maximum power. NT stands for the nodal temperature for the associated node analysis taken from the thermal model.

The temperature results show an initial increase in temperature of the node closest to the ultrasonic application area, and then a lag by the other nodes until they all show a similar temperature progression. These model results were then compared to the experimental results and are shown below.

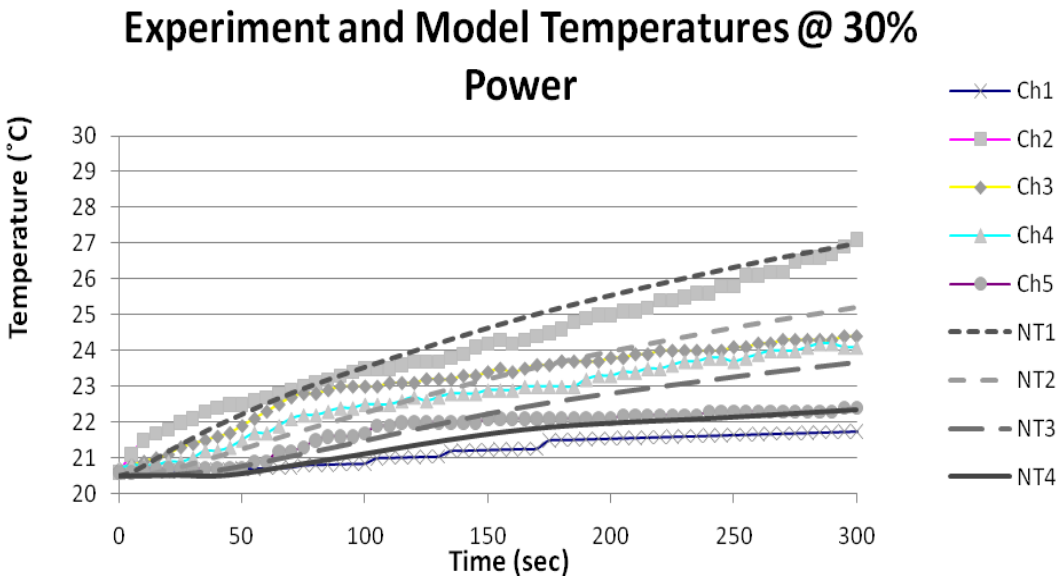

Figure 82: Temperature readout comparison from the thermocouples in the ultrasonic influence test and model. The ultrasonic probe is operating at 30% of maximum power. Note the vertical axis values. Ch stands for the channel number taken from the experimental analysis. NT stands for the nodal temperature for the associated node analysis taken from the thermal model.

The initial increase in temperature of the node nearest the probe was modeled and the following nodes follow suit. Also, the nodal temperatures at the end of the run time were lined up. Next, the experiment with the ultrasonic probe set to 50% of maximum power was compared.

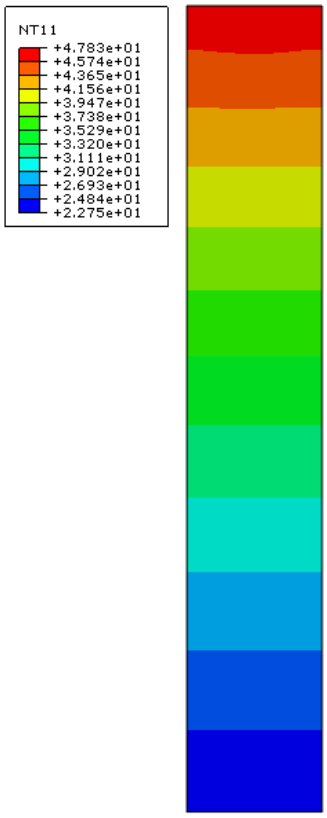

Figure 83: Temperature gradient of ultrasonic influence test at 50% power for 5 minutes.

The temperature gradient is very similar between the 30% and 50% power tests, with the only difference being the temperatures reached. The nodal temperatures also showed a similar behavior with increased values, and again the comparison between model and experiment was strong.

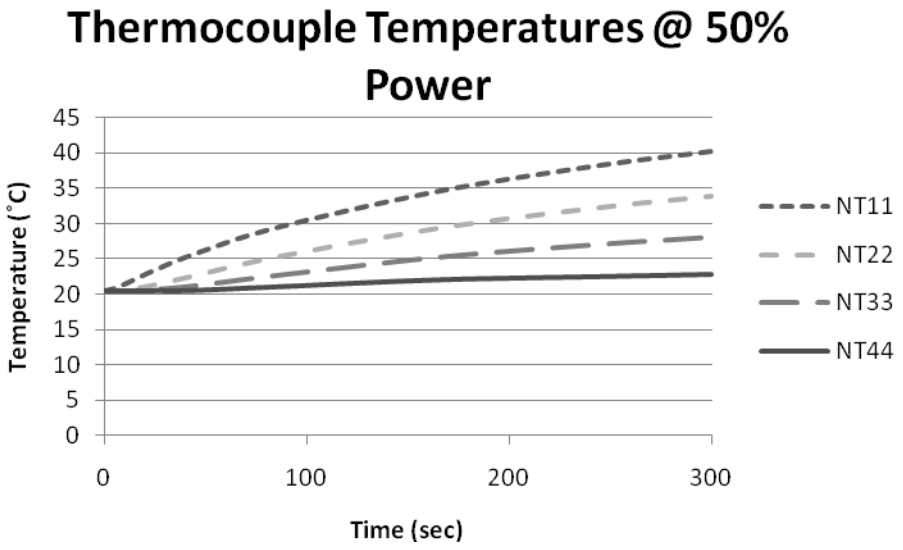

Figure 84: Temperature readout from the thermocouples in the ultrasonic influence model. The ultrasonic probe is operating at 50% of maximum power. NT stands for the nodal temperature for the associated node analysis taken from the thermal model.

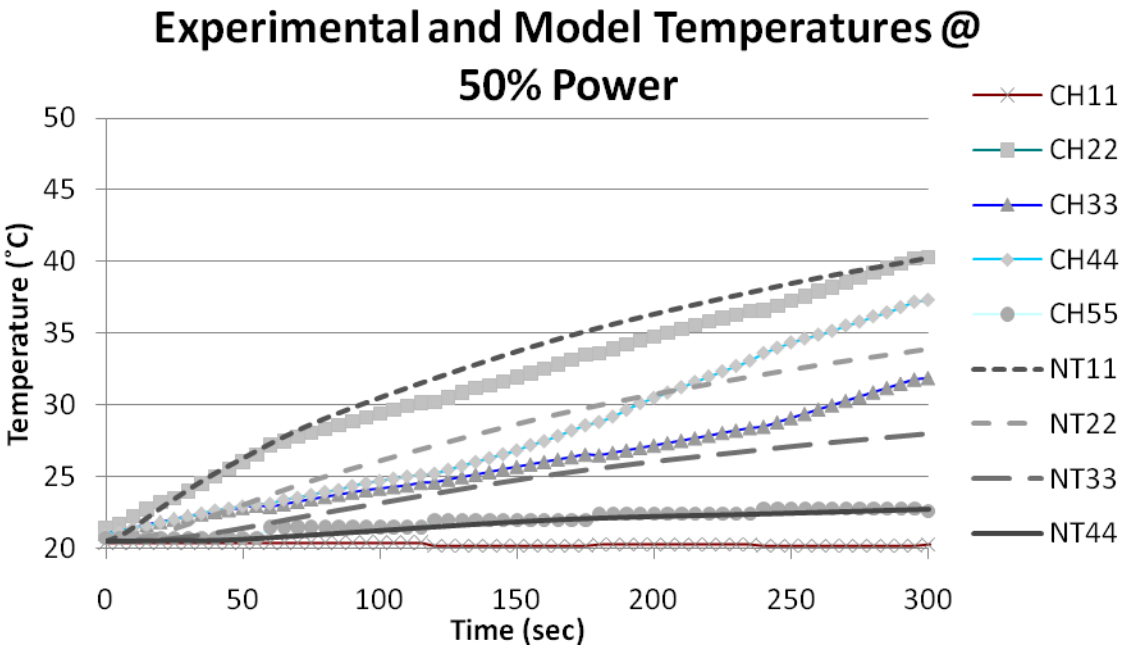

Figure 85: Temperature readout comparison from the thermocouples in the ultrasonic influence test and model. The ultrasonic probe is operating at 50% of maximum power. Note vertical axis values. Ch stands for the channel number taken from the experimental analysis. NT stands for the nodal temperature for the associated node analysis taken from the thermal model.

Again, the behavior of the nodal response from the experiment generally line up with the model data. This model data was then used to predict the material response when the ultrasonic probe was placed along the side of the damaged dogbone sample.

The rest of the modeling involves a direct prediction or model of the dogbone sample. As a means to exclude the unique geometry of the dogbone sample, only the central rectangular section of the dogbone sample was modeled. This area is shown below.

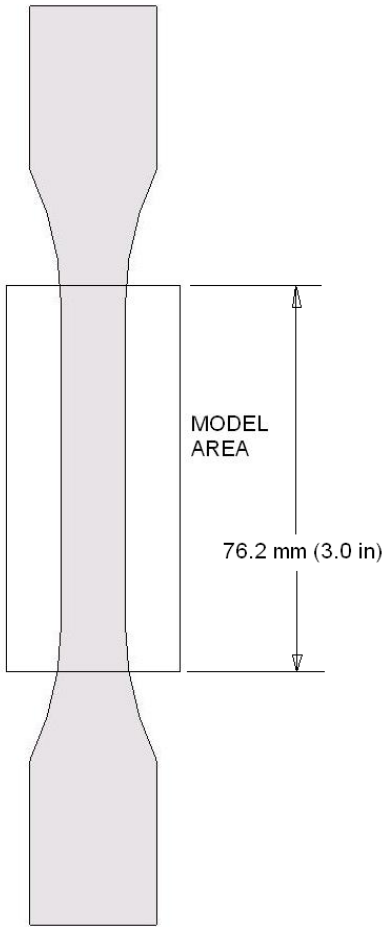

Figure 86: Illustration of finite element modeling geometry compared to dogbone sample geometry.

The resulting model areas are 76.2mm x 12.7mm (3.0in x 0.5in).

The model was changed by using the rectangular model area and moving the heat generation elements to be represented by a semi-circular region centered on the left side. This mimics the region covered by the probe tip during damage treatment.

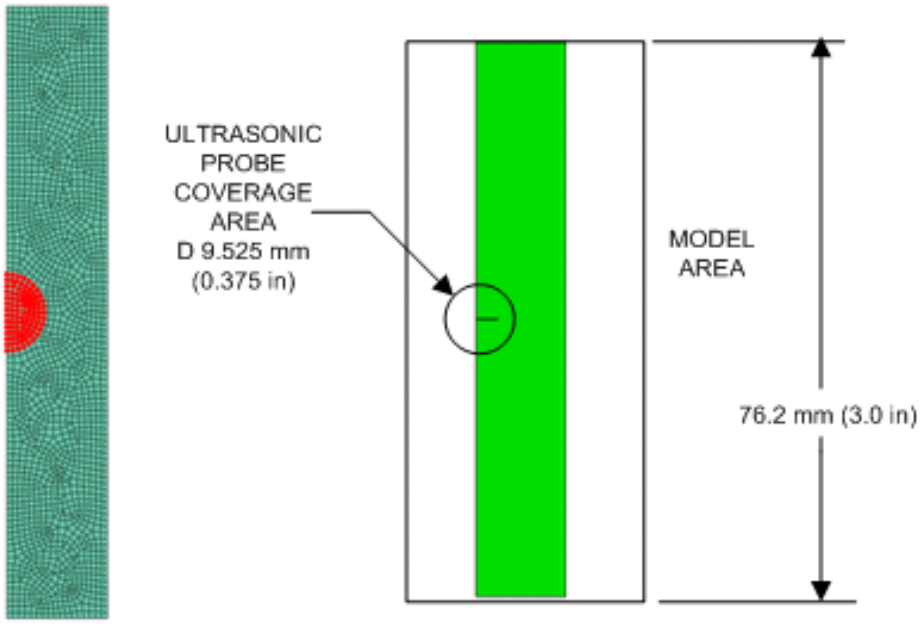

Figure 87: Heat generation area. On the left, the elements selected for heat generation. On the right, the probe coverage area is graphically represented.

The heat gradient test was performed to also mimic one of the original tests where the probe was set to level 5, or 50% of maximum power, and the test was run for 60 seconds all together. This model was meant to represent a level 5 ultrasonic probe treatment for 30 seconds a side, or 60 seconds total. Although this model is not tested in an experiment, it was important to use the correlated data. Nonetheless, the resulting heat gradient around the crack area was qualitatively analyzed. The resulting heat gradient is shown below.

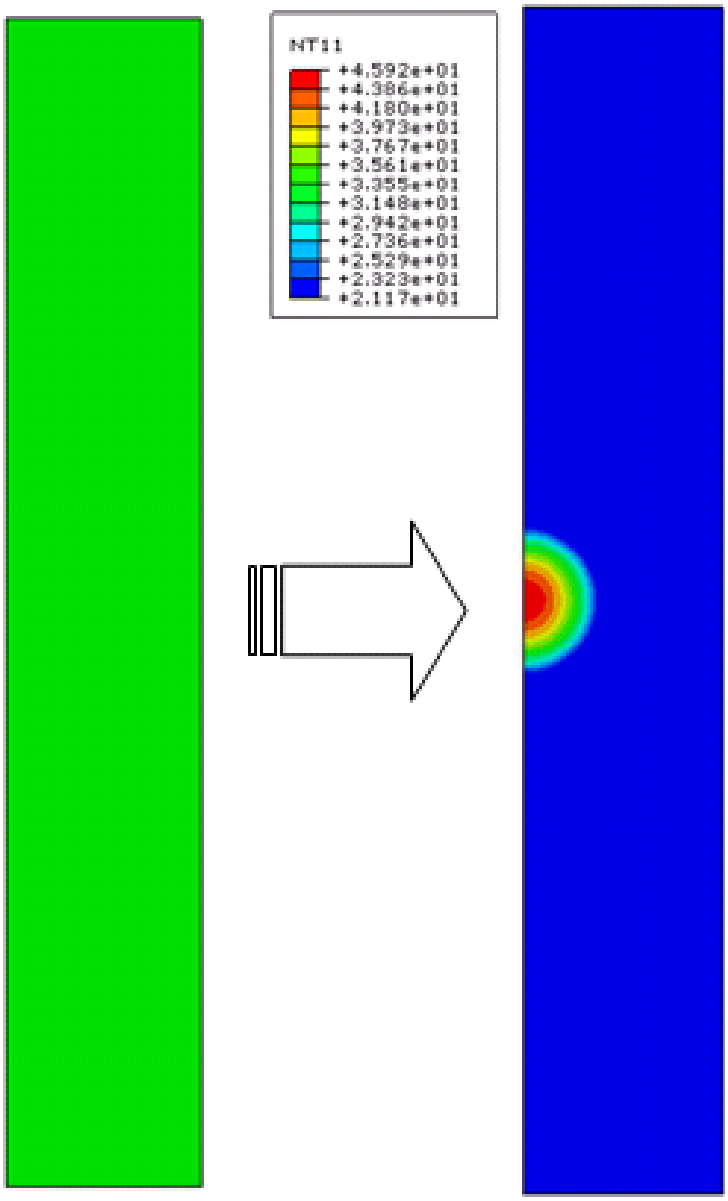

Figure 88: Temperature gradient created by ultrasonic treatment model. NT11 in the legend shows nodal temperatures.

Since some local melting was observed when treating the damaged samples and the ultrasonic probe shifted, this result was also attempted. Instead of the semicircular application area, a much smaller area was picked. The 5 heat generation elements picked are shown below.

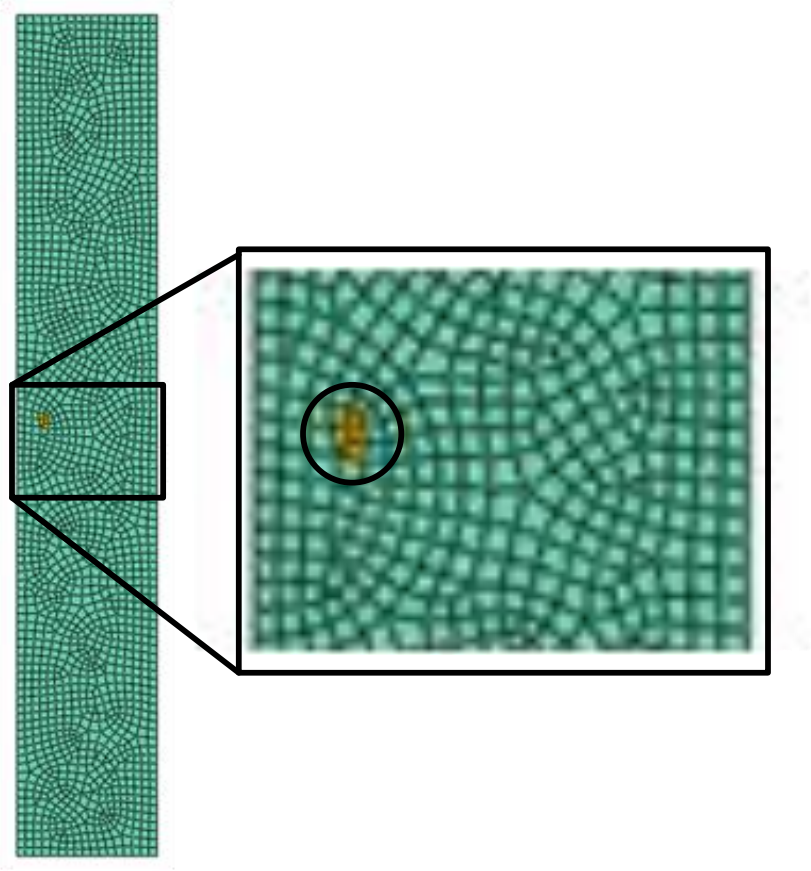

Figure 89: Localized heat generation area.

This model was run with the same heat generation factor as the semicircular region, and melting temperatures were not even approached. The local application areas was kept and the level of heat generation increased until appoximately 200ºC was reached. The resulting temperatures and gradient are shown below.

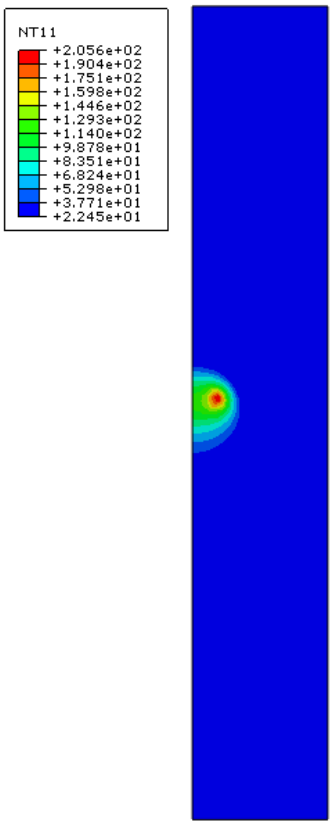

Figure 90: Temperature gradient created by ultrasonic treatment of a localized area model. NT11 in the legend shows nodal temperatures.

Since the heat generation factor needed to be increase to mimic experimental data, it is clear that although heat generation can simulate the same increase in temperature provided by an ultrasonic probe, the model needs to somehow include an intensity factor to allow for different probe tips and application areas to be correctly modeled. For the sake of interest, the heat generation value needed to create melting temperatures in the local model was then applied to the original, semicircular model. The resulting maximum temperature is above 2,000ºC.

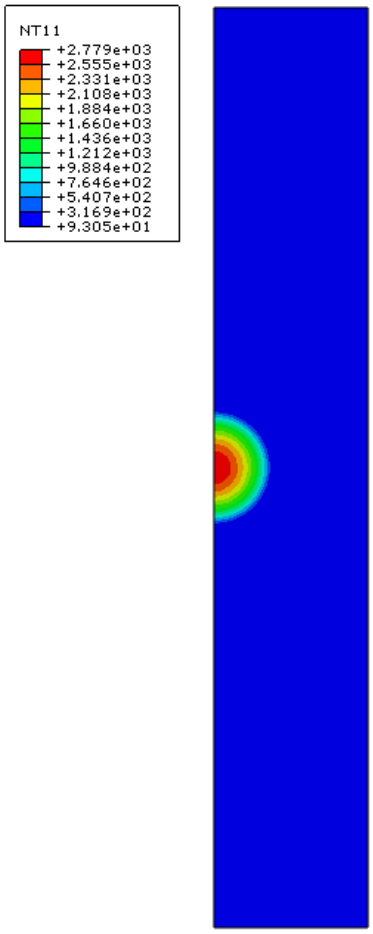

Figure 91: Temperature gradient created by ultrasonic treatment model using localized heat generation value. NT11 in the legend shows nodal temperatures.

Mechanical Modeling of Self-Healing Polymers

The actual change in mechanical properties created by the ultrasonic treatment was modeled qualitatively by a relative crack length FE model (Fig. 92). The model examined a notched sample subjected to a similar loading situation as applied by a tensile test.

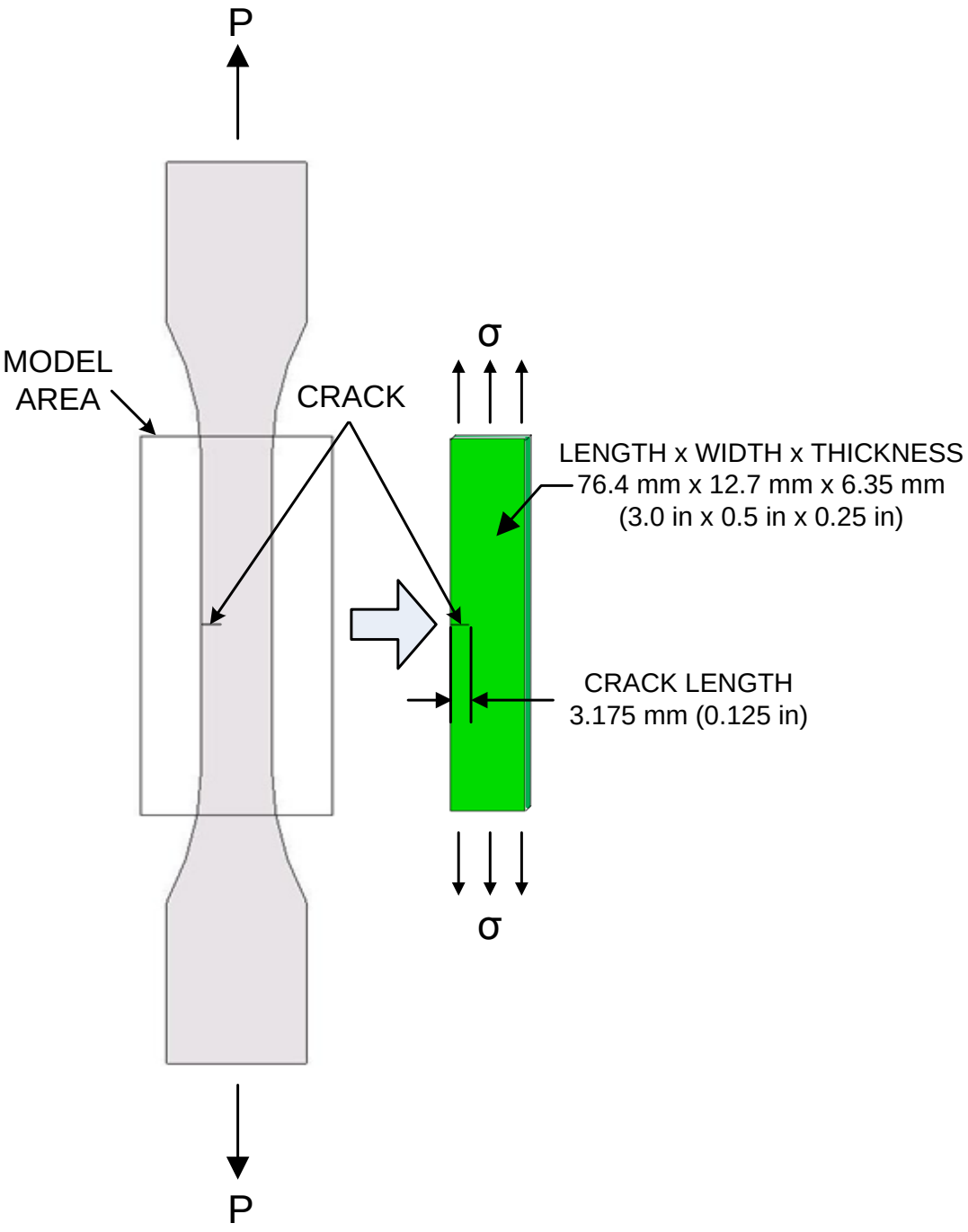

Figure 92: Definition of tensile test model section in comparison to experimental test specimen.

In this case, the bottom of the sample was held in all 3 displacement and rotation degrees of freedom, and the top of the sample was displaced directly away from the base. The cross-section of the crack and crack propagation path in the sample was represented with

cohesive elements (COH2D4) while the rest of the specimen was made from general application continuum elements (CPE4). The loading situation, just like with a tensile test was displacement controlled. The model was first configured with a full depth crack of length ($c = c_c$), then loaded in tension. The model was reconfigured with a reduced depth crack length ($c < c_c$) yielding a response that takes more displacement (strain) to reach the same final stress as the previous full crack model. This change in time represents an increase in sustainable strain and therefore a larger sustainable stress, which can be correlated to the increase in ultimate stress found in the ultrasonically treated samples. A sketch is shown below with a horizontal line drawn to represent ultimate stress (notice the axes don't start at 0).

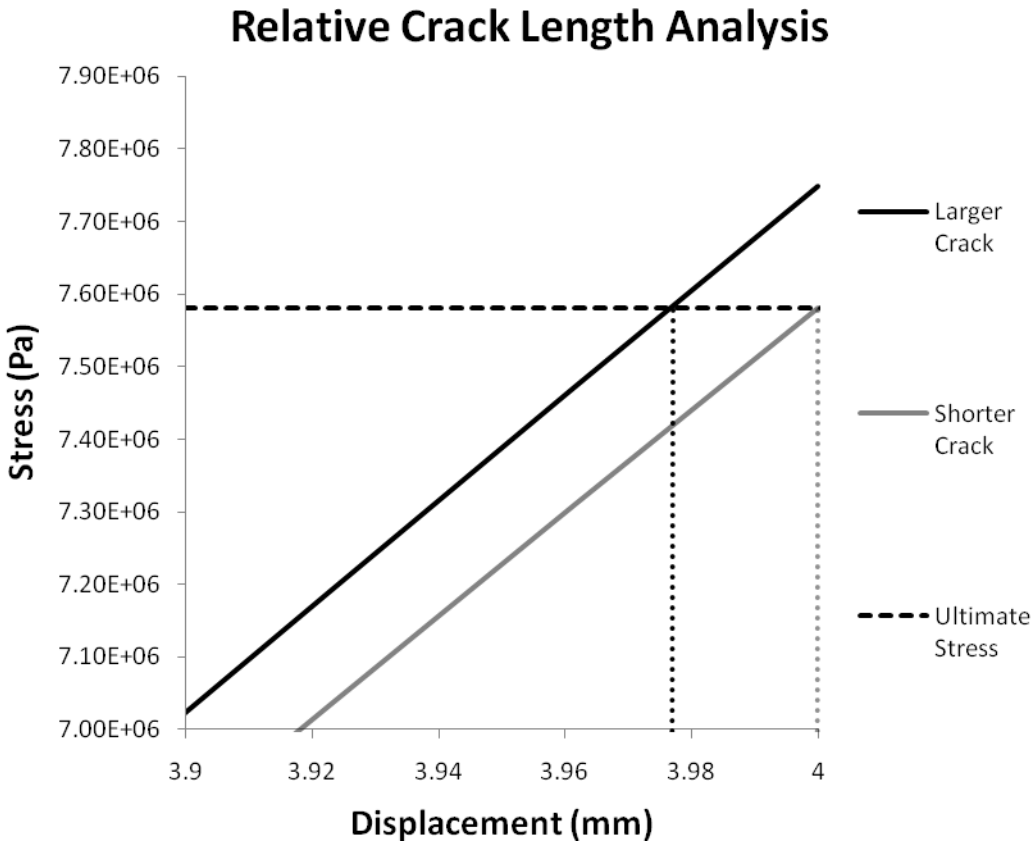

Figure 93: Concept for relative crack length analysis.

The line representing the sample with relatively more damage reaches the ultimate stress before the sample with relatively lesser damage. This means the sample with more damage fails with less displacement than the sample with less damage. The reduced displacement to failure of the brittle response also correlates to a reduced ultimate stress.

A relative crack length model was then created with the same material properties as the samples tested in the experiments. The model code used cohesive elements and an associated traction separation failure model. Cohesive elements require a surface definition and material definitions unique to the other type of elements used, continuum elements. The damage initiation was modeled with the quadratic separation-interaction criterion for cohesive elements. Since cohesive elements require a traction-separation analysis, ultimate tensile and shear values for mode I and mode II failure were used, although, as the experiment setup dictated, values for shear (mode I or II) and values for ultimate tensile stress in mode II did not have as proficient an influence as ultimate tensile stress for mode I failure. The damage evolution was a mixed mode energy evaluation constrained by the Benzeggagh-Kenane (BK) fracture criterion with linear softening.

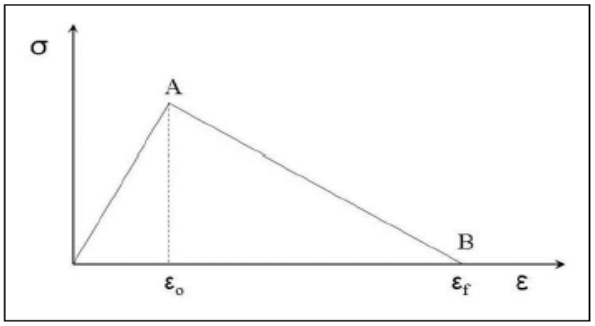

Figure 94: Bilinear softening representation for Benzeggagh-Kenane fracture criterion. The material exhibits a material response when $\varepsilon < \varepsilon_o$. Damage is initiated at A, and softening ensues for $\varepsilon_o < \varepsilon < \varepsilon_f$. The material is completely damaged and separated at B. (20)

This analysis was specified by an ideal example problem in ABAQUS, and was found to be, “particulartly useful when the fracture energies in mode II and mode III are the same, (21)” which is null in this case. The two experimental samples used were a damaged but untreated sample, and a sample damaged and treated at 50% of maximum power. The untreated model was created to mimic the stress versus displacement result of the untreated sample. All of the samples exhibited an initial lag in response until about 0.2667 mm (0.0105 in), so this lag was also modeled. The crack length model for the untreated sample mimics the same initial lag, and then follows the general path until the ultimate stress is reached. The model, not being constrained by any failure criteria, keeps increasing without bound.

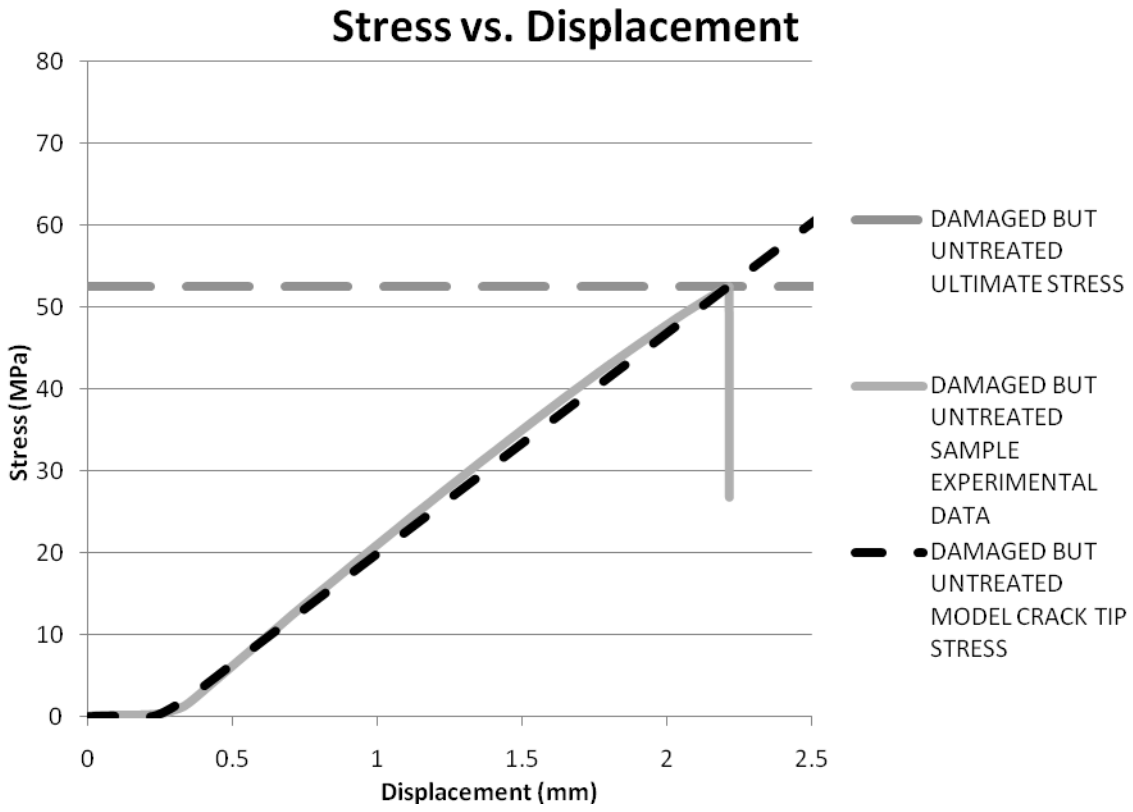

Figure 95: Stress versus displacement graph of damaged but untreated sample and associated model data.

The model of the damaged but untreated sample follows the experimental results of the damaged but untreated sample closely. Emphasis was placed on the model to pass through the ultimate stress of the experimental data. Next, the experimental results from a damaged and ultrasonically treated sample were added (Fig. 96). Specifically, the sample was treated at power level 5 for 15 seconds a side.

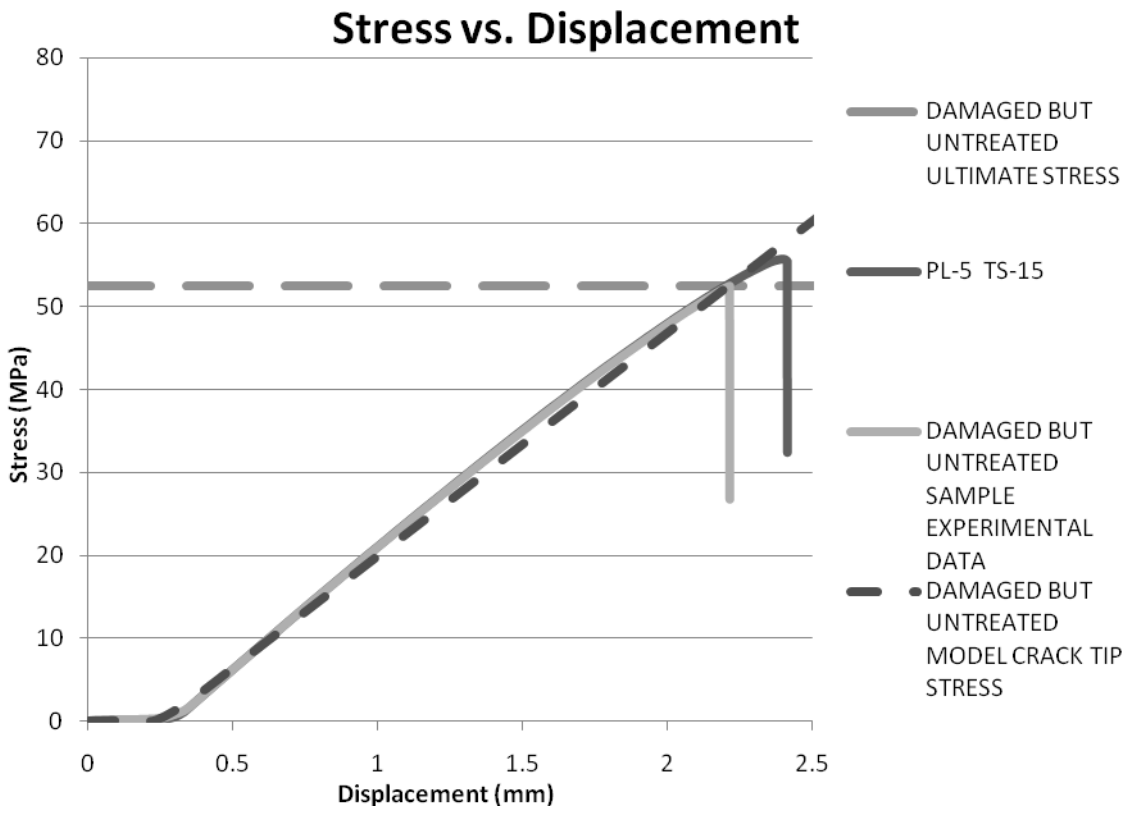

Figure 96: Stress versus displacement plot of a damaged but untreated sample, the corresponding sample's ultimate stress, a damaged and treated sample (PL-5 TS-15), and the damaged but untreated model response.

The response of the damaged and treated sample was replicated by using the untreated sample model and decreasing the crack length. More specifically, more elements were added to the crack propagation path, until the damaged and treated sample model and experimental data had a similar correlation as that between the damaged but untreated

sample experimental data and model. For example, if a model had a 13 mm (0.5 inch) cross-section width and half of that was filled with elements, then the crack length was the exposed length of half of the sample width. To decrease the crack length, adding elements to the exposed length decreases the exposed length and therefore decreases the crack length. After multiple elements were added, the model followed the damaged but treated sample's increased ductility, and ultimate stress. This can be seen in Figure 97, along with the horizontal line showing the ultimate stress of the untreated sample as before in Figure 96. The number of cohesive elements connecting the two continuum element halves was increased by 30% which decreased the untreated crack length to 15% of its original length for the ultrasonically treated model representation.

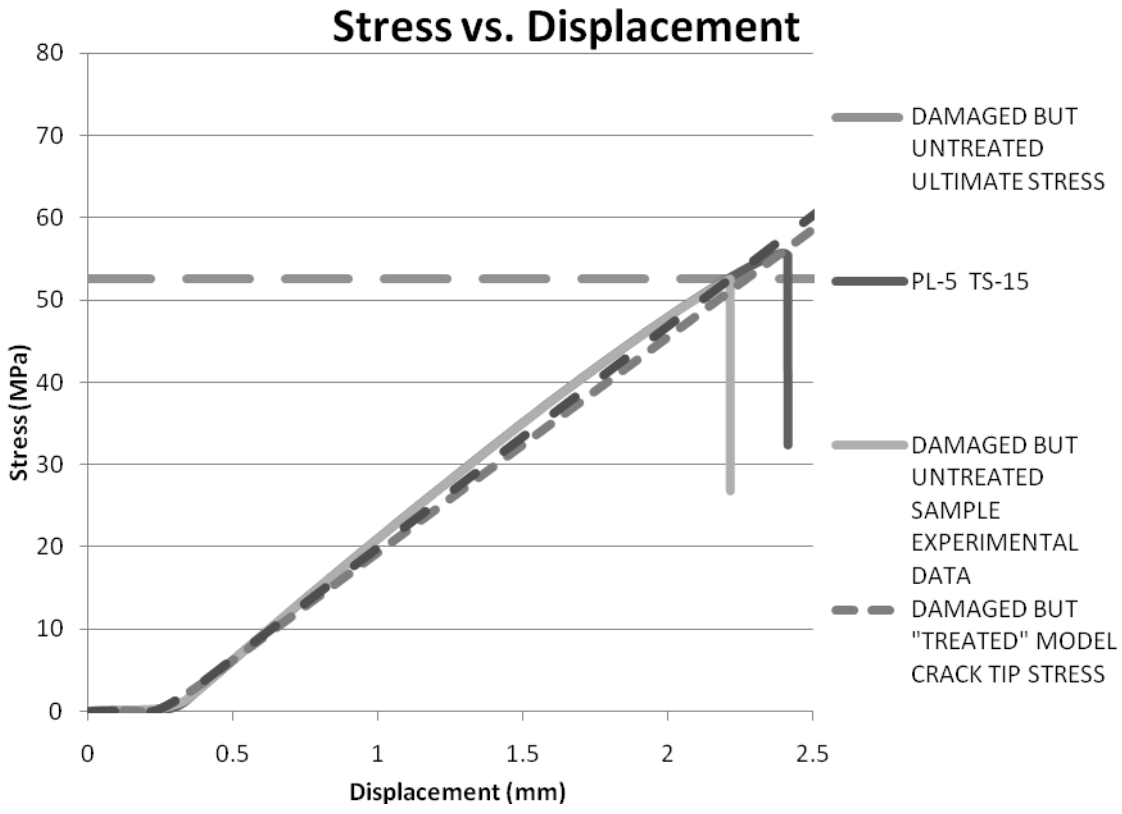

Figure 97: Stress versus displacement plot showing correlating models for a damaged but untreated and a damaged but treated (PL-5 TS-15) samples.

Note that in Figures 96 and 97, there is no failure criteria in the models, and hence the model response continues without failure. The region in Figure 97 near the crossing of the ultimate stress of the untreated sample was more closely examined in the figure below, as can be seen by the change in axes.

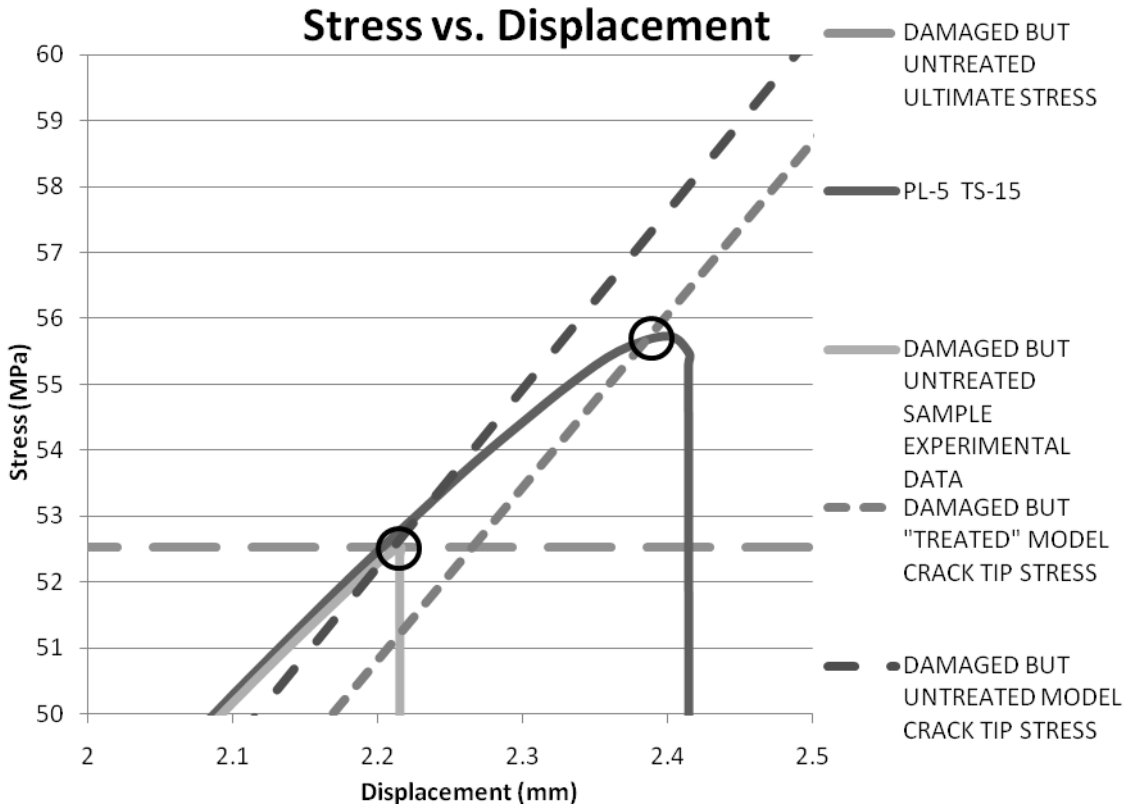

Figure 98: Close up of relative crack length model correspondence. Note the change in axes values. Circles indicate intersection of model with respective experimental ultimate stress.

Closer inspection shows that both models follow the general behavior of the tensile specimens, but, more importantly, pass through the ultimate stress point of their corresponding sample data. The point where the models intersect the ultimate stresses of the corresponding experimental data was also examined for associated displacement at intersection, as in Figure 99.

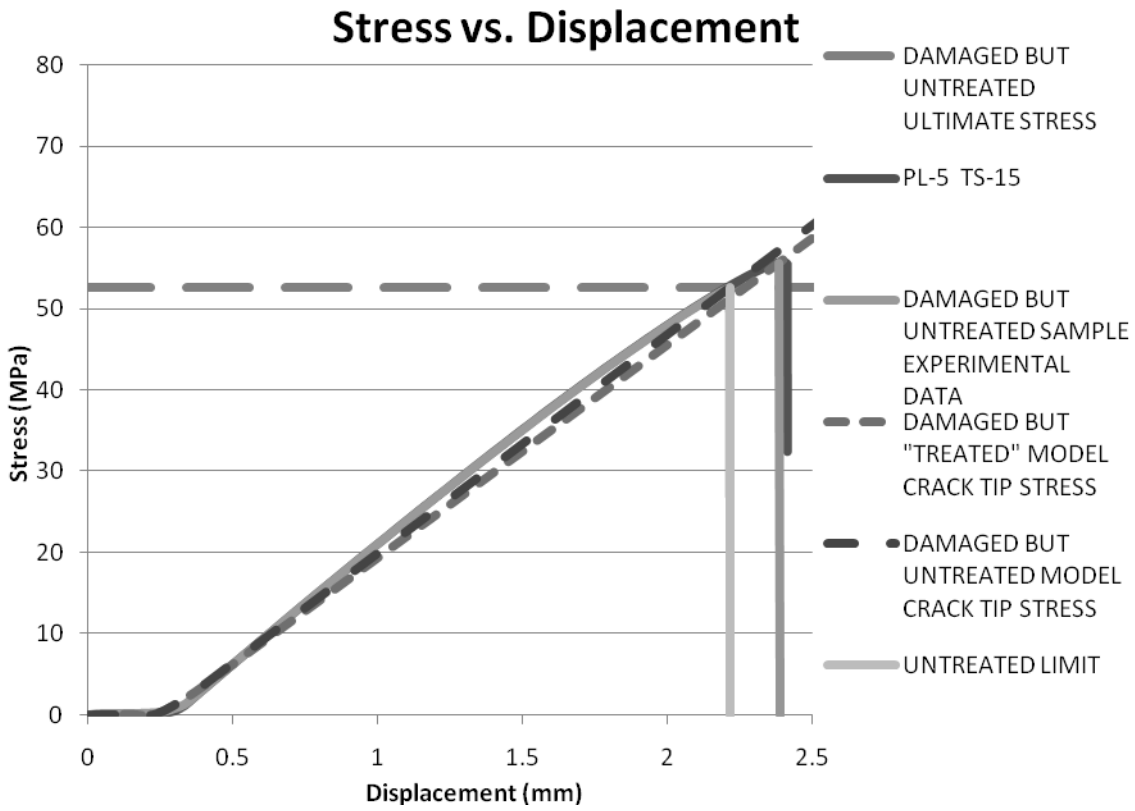

Figure 99: Relative crack length model plot showing corresponding displacement and ultimate stress intersections.

The relative crack models (damaged but untreated and damaged but "treated") reveal two points of interest. First, a model can be created and calibrated to follow the general behavior of an ultrasonically treated sample compared to an untreated sample. Also, the calibration can correlate a displacement to the ultimate stress. Multiple treated samples can be compared to tests of relative crack lengths and the data collated into an ultrasonic treatment response prediction rubric. Such a test rubric can be created for operators to know what the expected change in mechanical response results of a prescribed level of ultrasonic treatment will produce.

RESULTS

Exploring the process of ultrasonic nondestructive damage detection and healing required efforts in actual experimentation and finite element modeling. The sequence of experimentation and modeling can be seen in Table 5.

Table 5: Overall test and model progression and relations.

TESTS AND MODEL RESULTS	
Ultrasonic Influence Test 30% Power Test 50% Power Test	The ultrasonic probe creates a noticeable increase in temperature over time.
Model Validation Validate Heat Transfer Case 1 Case 2 Case 3 Case 4 Validate Heat Generation	ABAQUS modeling was validated with analytical models, additional models, and compared to a published example.
Ultrasonic Influence Model 30% Power Model 50% Power Model	The ultrasonic influence can be correlated in model by using heat generation elements.
Tensile Tests Virgin Samples Heated Undamaged Damaged Constant Period/Different Power Levels Constant Period #1/Constant Power Level Constant Period #2/Constant Power Level Overall Comparison	Ultrasonic treatment led to an increase in ultimate stress. Also, a correlation was shown that increased ultrasonic treatment period and power creates an increase in ultimate stress.

Table 5 - Continued

Heat Distribution Representative Semicircular Area Localized Area	The ultrasonic influence model was used to predict the effect the probe as while ultrasonically treating a sample.
Cohesive Zone Model	Crack propagation was modeled using cohesive elements to model the crack propagation path.
Relative Crack Representation	Cohesive zone models used to represent ultrasonic effect on ultimate stress.
DTA Crystallinity Test	Ultrasonic probe increase crystallinity of sample.

While some of the experimentation and modeling was for validation and proof of concept, much of it was related. The relations are displayed below.

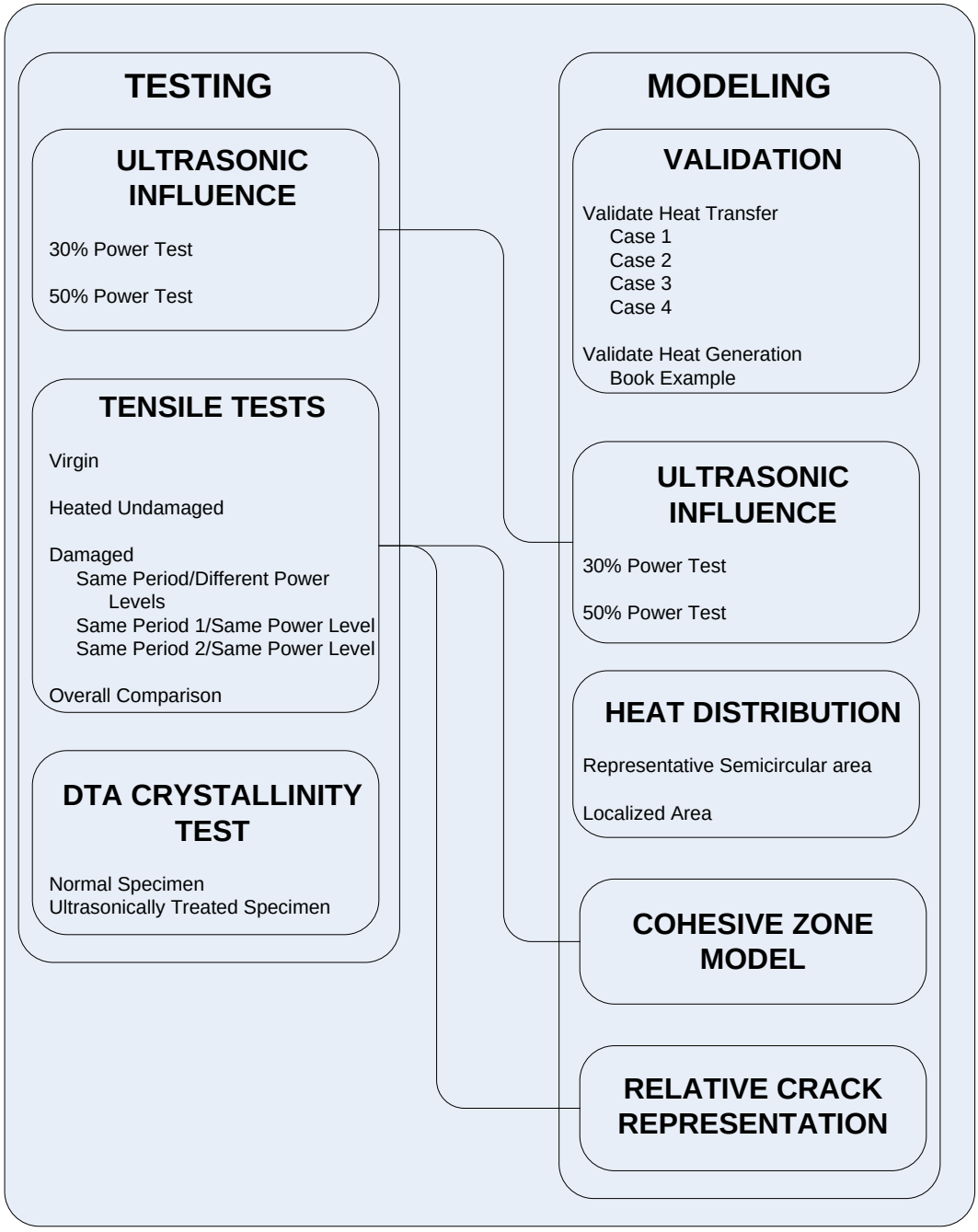

Figure 100: Chart illustrating connections between tests and models performed.

Ultrasonic energy allows for a clear increase in temperature in the nylon samples. This was exhibited by the ultrasonic influence experiments performed at both 30% and 50% of the Branson ultrasonic probe's maximum power. Although ultrasonic energy

transmission has rarely been modeled in solids for thermal response, the effect could be represented by heat generation sources within models created in ABAQUS. Accurately modeling the ultrasonic influence allowed for a model to be constructed that predicted the local change in temperature due to the ultrasonic probe application in damage treatments. This was the first step in correlating ultrasonic treatment to improved mechanical performance.

Tensile tests illustrated the increase in ultimate strength the ultrasonic energy could provide, and even produce changes in brittle versus ductile responses. Apparently, ultimate strength, or yield strength in the ductile response cases, increases with increasing ultrasonic application period and power. The ductile response was geometrically dependent as power was supplied to a more focused area. Just as the crack tip is of the highest concern in damage, locally treating this highly influential area will have a greater overall mechanical response effect than spreading the treatment out over more less influential areas.

The brittle response from the tensile tests of the damaged samples necessitated a stress intensity factor analysis. Since tensile testing actually tests mode I fracture, critical stress intensity was calculated using Equation 1:

$$K_{Ic} = \sigma\sqrt{\pi a_c} \quad (1)$$

The critical stress intensity factor for mode I fracture (K_{Ic}) equals the applied or far-field stress (σ) multipled by the square root of π times critical crack length (a_c) for a through edge crack. The ultimate stress changed for each sample while the critical crack length was the 3.18 mm (0.125 inch) controlled damage. The ultimate stresses and stress intensity factors are shown in Table 6.

Table 6: Ultimate stress and stress intensity factor for damaged samples.

Ultimate Stress and Stress Intensity Factor Comparison			
Treatment Power Level (#/10)	Treatment Time (s)	Ultimate Stress (Mpa)	KIC (MPa√m)
0	0	52.39727	5.233057
0	0	52.70622	5.263913
5	15	55.72648	5.565554
7	15	56.46141	5.638954
6	15	56.86423	5.679184
7	30	55.08442	5.50143
9	15	57.56599	5.749271
7	30	56.41526	5.634344
7	30	53.54063	5.347247
7	30	54.50364	5.443426
7	30	53.36654	5.329861
7	60	52.15293	5.208654
7	60	49.28211	4.921938
7	60	50.9879	5.092299
9	60	60.1058	6.002929

Table 6 shows the general improvement in ultimate stress and fracture stress intensity for mode I fracture with increased ultrasonic treatment power. Since the critical crack length remains the same for every test, the change in stress intensity was directly a result of change in ultimate stress. The highlighted samples are the samples with localized treatment that resulted in a more ductile response. These results are comparable to published results for critical stress intensity for nylon 6,6 of 4.0 MPa√m (22).

The increase in ultimate stength by ultrasonically treated samples was qualitatively modeled using relative crack length models of cohesive elements. Using an adjusted crack length, and concurrently adjusted amount of cohesive elements along the crack propagation path thereby altering the mechanical response. Since experiments proved the ultrasonic treatment modified the temperature and mechanical response of the

nylon, the ability to accurately model both changes creates the beginning of a completely analytical ultrasonic damage treatment process.

The third component analyzed was the small scale, the molecular scale. DTA results showed that ultrasonic treatment increased the amount of crystalline structure within the nylon sample. What's more, the ultrasonic treatment power again positively correlated to change in amount of crystalline structure.

FUTURE WORK

The course of action with any test is repetition. Data is made more concrete by additional data. It would be beneficial to repeat the ultrasonic influence experiment with more thermocouples. More temperature data points would display a more accurate representation of the ultrasonic effect on nylon. A more accurate display would allow for a more accurate model to be created, and a more accurate means to represent ultrasonic energy influence. Accuracy could be improved by also using thermocouples on the damaged sample being treated. The ultrasonic treatment represents a different ultrasonic loading situation, and the actual situation that will be later tensile tested. Accurate FE modeling is paramount to utilizing this new technology.

It is also necessary to repeat tensile tests of ultrasonically treated samples with a complete range of ultrasonic transducer power settings and application periods. Further tensile tests could further validate change in ultimate stress, yield stress, and investigate the relationship with stress intensity factors of damaged areas and stress intensity factor change of damaged but treated areas. The combination of ultrasonic treatment and loading information would allow for a complete modeling and verification database. Such a verification database would be the basis for field treatment and healing applications, making the end goal, field treatment. Along those lines, it is also important to analyze more true-to-life damage scenarios, namely, fatigue loading and crack growth. The end goal would be a situation where an operator, or an automated system, would apply an apparatus to the material to be damage detected. The apparatus would use ultrasonic waves to locate and classify the damage in terms of size and magnitude, run

the damage through a software package that determines recommended ultrasonic treatment, and then redirects ultrasonic energy back into the material focusing on the damage and initiate healing. The end goal of this research is a self-sustained, self-healing system, much like a biological system.

The effect of ultrasonic treatment has not been fully explored. Besides biomimicry, ultrasonic and acoustic energy should be analyzed for applications in local material changes. The local crystallinity change observed here allows the possibility for making a single material into a composite material with specific regions of unique, desired material properties. Ultrasonic energy has the capability to be held in the same regard as electrical, magnetic, and thermal treatments are being considered today.

CONCLUSION

The initial ultrasonic probe tests showed the clear thermal effect that ultrasonic energy can have on polymers, specifically, nylon 6,6. Ultrasonic waves easily dispersed within the nylon and allowed the molecules to vibrate enough to raise the temperature of the sample. This thermal effect was then proven to affect mechanical characteristics through tensile tests. Ultrasonic application had the effect of increasing ultimate stress, and concurrently, allowing more mechanical energy dissipation. Tensile tests of damaged dogbone samples also illustrated that the increased ultimate stress effect is positively correlated to increased ultrasonic exposure time and power. Along with time and power levels, ultrasonic treatment was also proved to be spatially dependent. When the probe tip shifted and reduced the application area, localizing the ultrasonic energy, the sample response transformed from brittle to ductile. DTA testing concluded that the ultrasonic probe was in fact increasing the level of crystallinity of the nylon, which allowed for the noticeable change in mechanical response.

Following ABAQUS validation, FE modeling attempts allowed for representative ultrasonic portrayal within a nylon sample. This permitted the model creation of the effective heat distribution caused by the ultrasonic probe to a damaged sample. The increased mechanical response was also modeled by relating the relative change in crack length creating the ultrasonically modified mechanical response.

Further modeling along with included use of time-reversed acoustics will allow for a self-healing system that although requires external energy, utilizes an active detection and healing approach.

REFERENCES CITED

1. ___. *A Philosophy of Engineering Seminar: Systems Engineering and Engineering Design.* Engineering, The Royal Academy. London, 2007.

2. ___. Wild and Natural Herbs of the Amazon Rainforest: Sangre de Drago Croton lechleri. *Amazon Superfoods.* [Online] http://www.amazonsuperfoods.com/images/sangre-de-drago-sap.gif.

3.Polymorphic Robotics Lab. Information Sciences Institutes. *Self-Healing at Polymorphic Robotics Lab.* [Online] [Cited: Month 30, 2009.] http://www.isi.edu/robots/self_heal_html/starfish2.JPG.

4. Mescher, A.L. and Neff, A.W. Loss of Regenerative Capacity: A Trade-Off for Immune Specificity? *Cellscience Reviews.* 2004, Vol. 1, 2.

5. ___. Lizards of Wisconsin: Special Tricks. *Environmental Education for Kids.* [Online] [Cited: March 30, 2009.] http://www.dnr.state.wi.us/org/caer/ce/eek/critter/reptile/images/skinkBrokenTail.jpg.

6. Company, Alexa: The Web Information. www.cartage.org.lb. *Themes>Science>Zoological Sciences>Biological Diversity>Animals I.* [Online] [Cited: March 30, 2009.] http://www.cartage.org.lb/en/themes/Sciences/Zoology/Biologicaldiverstity/AnimalsI/humanlifecyc.jpg.

7. Capewell, S. The continuuing rise in emergency admissions: Explanations and responses must be properly evaluated. *British Medical Journal.* April 26, 1996, Vol. 312.

8. ___. Polymers. *Wikipedia.* [Online] Wikimedia Foundation, Inc., January 15, 2009. http://en.wikipedia.org/wiki/Polymer.

9. Shakhashiri, B.Z. Polymers. *Chemical of the Week, SciFun.* [Online] Wisonsin Initiative for Science Literacy. [Cited: January 15, 2009.]

10.___. Polymer Crystalinity. *Polymer Science Learning Center.* [Online] The University of Southern Mississippi, Department of Polymer Science, 2005. http://pslc.ws/mactest/crystal.htm.

11. Terminology, IUPAC Compendium of Chemical. branching index (in polymers). *http://www.iupac.org/goldbook/B00726.pdf.* 2nd, 1997.

12. Wikipedia. Nylon. *Wikipedia: The Free Encyclodpedia.* [Online] Wikimedia Foundation, Inc, April 2, 2009. [Cited: January 15, 2009.] http://en.wikipedia.org/wiki/Nylon.

13. Clark, J. Polyamides. *Chemguide: Helping You to Understand Chemistry.* [Online] 2004. [Cited: January 21, 2009.] http://www.chemguide.co.uk/organicprops/amides/polyamides.html.

14. Center, Polymer Science Learning. Nylons. *Polymer Science Learning Center.* [Online] Department of Polymer Science, The University of Southern Mississippi, 2005. [Cited: January 15, 2009.] http://pslc.ws/mactest/nylon.htm.

15. Center, NDT Resource. Wave Propagation. *NDT Resource Center.* [Online] The Non Destructive Testing Resource Center. http://www.ndt-ed.org/EducationResources/CommunityCollege/Ultrasonics/Physics/wavepropagation.htm.

16. White, S., et al. *Autonomic Healing of Polymers and Composites.* s.l. : Theoretical and Applied Mechanics, University of Illinois Urbana-Champaign, Urbana, IL.

17. Alvar, S. and Qiao, Y. Effects of cooling rate on fracture resistance of nylon 6-silicate nanocomposites. *Composites: Part A.* 2005, Vol. 36.

18. ___. Thermal Analysis. [Online] Hong Kong Baptist University, 2005. http://www.hkbu.edu.hk/~matsci/thermoanal/thermoanal_files/image002.jpg.

19. Differential Scanning Calorimetry. *Polymer Science Learning Center.* [Online] The University of Southern Mississippi, Polymer Department, 2005. http://pslc.ws/mactest/dsc.htm.

20. Harwood, J.A. *Efficient Finite Element Modeling Across Optical Length Scales.* Bozeman, MT : Montana State University, 2007.

21. *Simulation of Crack Initiation and Propagation in an Adhesive Layer Using a Mesomechanical Model.* Salomonsson, K and Andersson, T. Skovde : 27th Riso International Symposium on Materials Science, Polymer Composite Materials fo rWind Power Turbines, 2006.

22. *Basic Principles in Materials Selection for Mechanical Fastening of Thermoplastics.* Kagan, V.A. and Weitzel, S.P. 1455, s.l. : Journal of Reinforced Plastics and Composites, 2003, Vol. 22.

23. Wool, R.P., O and Connor, K.M. A theory of crack healing in polymers. *Journal of Applied Physics.* 1981, Vol. 52, 10.

24. Williams, G., Trask, R. and Bond, I. *A Self-Healing Carbon Fibre Reinforced Polymer for Aerospace Applications.* Bristol : University of Bristol: Department of Aerospace Engineering, 1998.

25. White, S.R., et al. Autonomic healing of polymer composites. *Nature.* 2001, Vol. 409, 15 February.

26. Trask, R.S. and Bond, I.P. Biomimetic self-healing of advanced composite structures using hollow glass fibres. *Smart Materials and Structures.* 2006, Vol. 15.

27. *Two Distince Cohesive Layer Models in Composite Delamination Invesitgation.* Sridharan, S. and Li, Y. Honolulu, HI : AIAA/ASME/ASCE/AHS/ASC Structures, Structural Dynamics, and Materials Conference, 2007.

28. Sottos, N., White, S. and Bond, I. Introduction: self-healing polymers and composites. *The Royal Society.* 2007, Vol. 4.

29. Siddiqui, N.A., et al. Self-healing Glass Fibres with carbon Nanotube-Epoxy Nanocomposite Coating. *Key Engineering Materials.* 2007, Vols. 334-335.

30. Santos, C. *Modeling and testing of temperature behavior and resistive heating in a multi-functional composite.*

31. Rambert, G, Grandidier, J.-C. and Aifantis, E.C. On the direct interactions between heat transfer, mass transport and chemical processes within gradient elasticity. *European Journal of Mechanics A/Solids.* 2007, Vol. 26.

32. Rambert, G and Grandidier, J.-C. An approach to the coupled behavior of polymers subjected to a thermo-mechanical loading in a gaseous environment. *European Journal of Mechanis A/Solids.* 2005, Vol. 24.

33. Privman, V., Dementsov, A and Sokolov, I. Modeling of Self-Healing Polymer Composites Reinforced with Nanoporous Glass Fibers. *Center for Advanced Materials Processing and Department of Physics, Clarkson University, Potsdam, NY.*

34. *Time of Flight Diffraction - An Alternate Non-Destructive Testing Procedure to Replace Traditional Methods.* Prabhakaran, K.G., Wong, B.S. and Teng, Y.Y. Singapore : SPIE - The International Society of Optical Engineers, 2004.

35. Murugaiyan, R. *Time of Flight Diffraction (TOFD), an Advanced Non-Destructive Testing Technique for Inspection of Welds for Heavy Walled Pressure Vessels.* Kerala, India : Kochi Refineries Ltd (KRL).

36. Montaldo, G., Tanter, M. and Fink, M. Time-Reversed Acoustics. [Online] http://www.loa.espci.fr/_michael/cargese2003/Cargese_Fink_1.pdf.

37. Micciche, F. Self-healing elastomer nanocomposites. *Delft Research Center.* [Online] Delft University of Technology. http://images.google.com/imgres?imgurl=http://www.tudelft.nl/live/pagina.jsp%3Fid%3D36444f9b-9788-4973-bdf1-177684a6cde0%26lang%3Dnl%26binary%3D/img/figure2.png&imgrefurl=http://www.tudelft.nl/live/pagina.jsp%3Fid%3D36444f9b-9788-4973-bdf1-177684a6cde0%26.

38. Meo, M., Thieulot, E. Delamination modelling in a double cantilever beam. *Composite Structures.* 2005, Vol. 71.

39. ___. Definition of Thrombosis. *MedicineNet.com.* [Online] MedicineNet, Inc., October 30, 2003. http://www.medterms.com/script/main/art.asp?articlekey=25023.

40. Korde, U.A. and Barnes, K. *Accoustically Curing Self-Healing Polymers.* Rapid City, SD : SD School of Mines & Technology, 2008.

41. Keller, M.W. and Sottos, N.R. Mechanical Properties of Microcapsules Used in a Self-Healing Polymer. *Department of Theoretical and Applied Mechanics and Beckman Institute for Advanced Science and Technology University of Illinois at Urbana-Champaign, Urbana, IL.* 2005.

42. Kalista, S.J. and Ward, T. Thermal characteristics of the self-healing response in poly(ethylene-co-methacrylic acid) copolymers. *The Royal Society.* November, 2006, Vol. 4.

43. Juglal, G., Jochum, C. and Grandidier, J.C. Chemical-Thermal and Mechanical Coupling Model for the Cure of a Thermosetting Matrix: Application to FEM Simulation. *Key Engineering Materials.* 2007, Vols. 334-335.

44. Incropera, F.P. and DeWitt, D.P. *Introduction to Heat Transfer.* New York : John Wiley & Sons, Inc., 2002. ISBN 0-471-38649-9.

45. *A self-healing thermosetting composite material.* Hayes, S.A., et al. Sheffield : Joint 8th International Conference of Deformation and Fracture of Composites (DFC-8) and Experimental Techniques and Design in Composite Materials (ETDCM-7), 2007.

46. *A Method of Measuring Poisson's Ratio of Fibers1.* Frank, F.I. and Ruoff, A.L. 3, New York : Textile Research Journal, 1958, Vol. 28.

47. Fink, M. Time-Reversed Acoustics. *Scientific America.* November, 1999.

48. Fink, M., et al. Time-reversed acoustics. *Reports on Progress in Physics.* 2000, Vol. 63.

49. Fink, M. Chaos and Time-Reversed Acoustics. *Physica Scripta.* 2001, Vol. T90.

50. ___. Prokaryote Cell Division. *The Virtual Biology Course.* [Online] [Cited: April 1, 2009.] http://staff.jccc.net/pdecell/celldivision/images/binary.gif.

51. Branson Ultrasonics Corporation. Sonifier Cell Disruptors/Homogenizers. [Online] [Cited: March 30, 2009.] http://www.bransonultrasonics.com/.

52. ___. Making Native Plant Seed Available for Revegetation of Disturbed Land in the Northern Interior of British Columbia. [Online] Cybernet Communications. http://www.bulkley.net/~symbios/Newly%20logged%20area.jpg.

53. Chemistry, Michigan State University: Department of. CEM143, Experiment 11. *MSU: Department of Chemistry.* [Online] Michigan State University. http://www.cem.msu.edu/~reusch/VirtTxtJml/Images2/condpol1.gif.

54. Brunk, J.A. *Ultrasonic Nondestructive Testing and Materials Characterization.* Kansas City : National Nuclear Security Agency's .

55. Brown, E.N. Fracture Testing of a Self-Healing Polymer Composite. *Experimental Mechanics: An International Journal.* 2001.

56. ___. Biological Diversity: Protists: Stem Eukaryotes. *The Online Biology Book.* [Online] [Cited: April 1, 2009.] http://www.estrellamountain.edu/faculty/farabee/biobk/1-OLIH023P.GIF.

57. Bhadeshia, H.K.D.H. Thermal analysis technique. Differential Thermal Analysis. *University of Cambridge, Material Science and Metallurgy.* [Online] [Cited: April 11, 2009.] www.msm.cam.ac.uk/phase-trans/2002/Thermal1.pdf .

58. Beamish, D. Good Vibrations for Nondestructive Testing: Ultrasonic gages provide accurate coating thickness measurement for nonmetallic substrates. *Quality Digest.* [Online] October 2004. http://www.qualitydigest.com/oct04/Images/Features/NDT_Fig1.jpg.

59. Balazs, Anna C. Modeling self-healing materials. *Materials Today*. September, 2007, Vol. 10, 9.

60. Federal Highway Administration. Ultrasonic Testing Equipment. *General Information: Ultrasonic Testing.* [Online] United States Department of Transportation. http://images.google.com/imgres?imgurl=http://www.tfhrc.gov/infrastructure/nde/pubs/04042/images/fig07.gif&imgrefurl=http://www.tfhrc.gov/infrastructure/nde/pubs/04042/02.htm&usg=__9FxJMPRnh-zJNcIRq5rXuJk1bxc=&h=350&w=485&sz=5&hl=en&start=11&um=1&tbnid=ol.

61. National Instruments. Ultrasonic Non-destructive Testing. [Online] March 27, 2007. http://zone.ni.com/cms/images/devzone/tut/a/7e46be30706.gif.

62. Mitsubishi Heavy Industries, Ltd. No.2 TOFD Ultrasonic Testing Technique. *Power Systems Headquarters: Technology: Solutions and Services for Thermal Power Plants: Inspection Technology.* [Online] 1994-2009. http://www.mhi.co.jp/en/power/service/kensa/images/no02_01.gif.

63. Hayes, S.A., et al. Self-healing of damage in fibre-reinforced polymer-matrix composites. *Journal of the Royal Society*. 2007, Vol. 4, 13.

64. Keller, M.W., et al. Recent Advances in Self-Healing Materials Systems. *Adaptive Structures: Engineering Applications.* 2007.

APPENDICES

APPENDIX A

THERMAL MODEL VALIDATION

(By Steven Rutherford)

Date: Thursday December 4, 2008

To: Prof. Jenkins, Cody Sarrazin

From: Steve Rutherford

RE: Polymer Healing via Melt Sealing- Case Study of Heat Transfer in Nylon

Introduction: A promising method for healing damage in polymeric materials is based on the application of heat sealing techniques. This method relies on location of damage and precise application of heat at the located point of damage. Ultrasonic emissions can provide not only a method for location but also a method to subsequently generate heat at the located point. With sufficient power, ultrasonic emissions can generate heat fluxes capable of transient temperatures that exceed the melting temperature of the polymer. Local melting at the point of damage is followed by a reduction in the incident flux, allowing cooling and re-solidification to occur. By this method, a polymeric material can gain some restoration of original mechanical properties thereby allowing the polymer to be healed.

In order to understand this phenomenon in greater detail, a heat transfer model is required. In this report, a first generation model that incorporates transient heat transfer processes is developed and validated.

Model: With the ultimate goal of establishing a heat sealing technique through application of ultrasonics, a mechanical testing program has been initiated. Samples of undamaged and damaged Nylon are being tested and compared to samples repaired via ultrasonic heat sealing. The experimental program is coupled with modeling of heat transfer in Nylon. For the mechanical testing, samples of rectangular cross-section, length

6 cm by width 1cm were machined. For modeling purposes, we apply a 2 dimensional model for heat transfer.

Aim: The purpose of this report is to establish and verify a realistic model for heat transfer from Nylon. We consider a 4 step validation which is undertaken by considering 4 specific cases. Each case is modeled via numerical methods and compared with exact solutions for purposes of validation.

General Modeling Strategy: The ultimate project goal is to model the absorption of ultrasonic emissions and resulting heat flux generation in a Nylon sample. For modeling purposes, it is necessary to consider a heat source, coupled with conduction and convection. ABAQUS package readily allows modeling of point source heat generation, conduction and convection. The purpose of this report is to consider only heat conduction through the polymer and dissipation via convection. The goal is to establish a validated set of data considering only conduction and convection. This data will subsequently be used to compare, in a code to code validation, with an ABAQUS simulation under the same conditions. Heat generation can then be added to the ABAQUS model to produce a validated simulation of the mechanical test setup. This strategy is indicated diagrammatically in Figure 1.

For the conduction/convection simulations undertaken in this report, COMSOL-Multiphysics is computational package employed. Further details regarding the setup and run details appear in Appendix B.

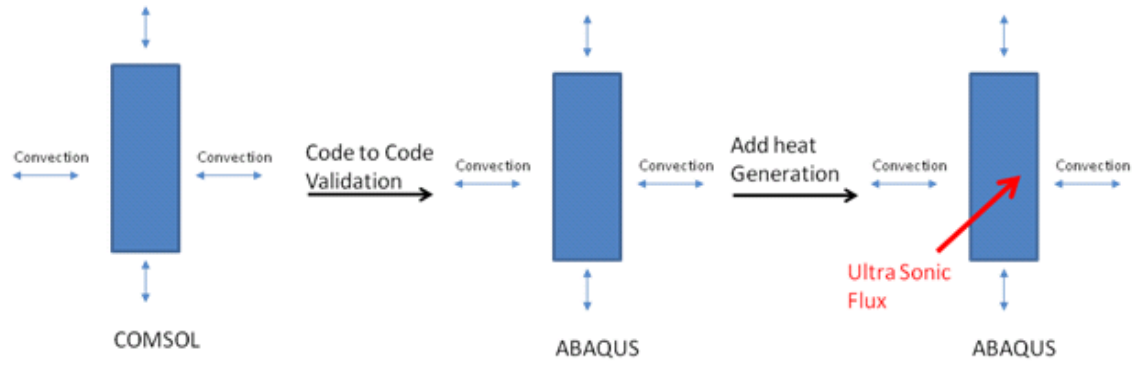

Figure 1: Validation Strategy

Validation strategy: In order to verify the COMSOL simulation results presented in this report, we have considered simplifications of the conduction/convection model resulting in several cases that are amenable to comparison with exact solutions. Our aim is to verify the results obtained for the cooling of Nylon via conduction through the polymer and dissipation via convection. We consider this scenario to be "Case 4". The addition of an insulation boundary condition to "Case 4" results in a situation where conduction through the polymer to the ends of the slab where convective cooling/heating can occur. As a result, a one dimensional model is produced. We consider this scenario to be "Case 3". An analytical solution to this problem results when we consider the limiting case where the convective transfer rate is far greater than the conductive flux. This results in a Boundary Condition of constant temperature at both ends of the slab. We refer to this scenario as "Case 2". The analytical solution to "Case 2" yields a transient and symmetric temperature profile. A steady state solution can be formed from "Case 2" when symmetry is removed, the isothermal condition at both ends is maintained, but the temperatures differ in value. The 4 cases considered in this report, together with the simplifying conditions, are displayed as Figure 2.

For all cases, COMSOL- Multiphyics package is utilized to generate solutions which can then be compared to the analytical solution.

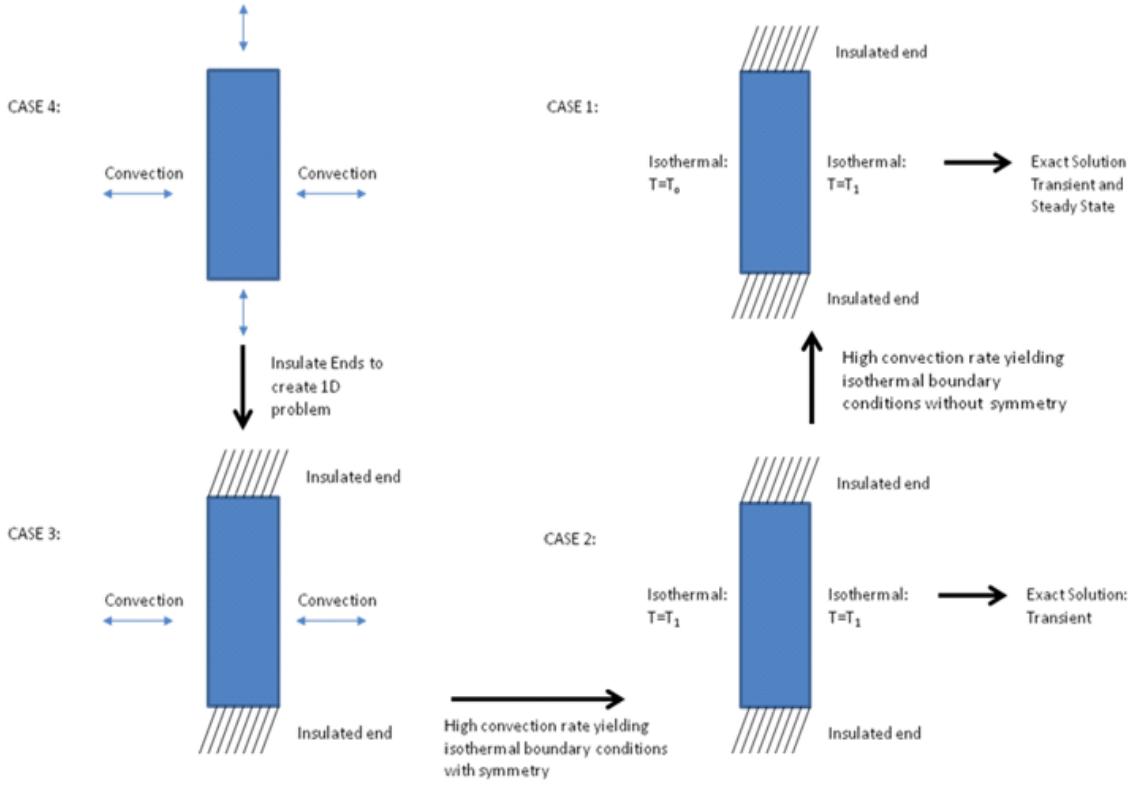

Figure 2: The four cases considered in this report and the simplifying conditions that link them

Model Details:

In this report, we consider heat transfer in Nylon whose physical properties are shown in Table 1. The lower end of the melting point range for Nylon is 200C, a temperature we would not exceed greatly in any experiment. Table 1 also indicates the Coefficient of Thermal Expansion which is listed at 8.1×10^{-5} m/mK. Coupled with an approximate temperature limit of 200C, yields a strain value on the order of less than 10^{-2}. Under these conditions, we therefore consider a constrained two dimensional model for Nylon and ignore thermal expansion.

Property	**Value**
k	0.237 W/mK
C_p	1.674×10^3 J/kgK
P	1140 kg/m^3
C.T.E.	8.1×10^{-5} m/mK
Melting Temperature range	200 C to 265 C

Table 1: Manufacturer's material specifications for Nylon

For our constrained system, we can model conduction through the Nylon with the Laplace Equation[i]:

$$\frac{\partial T}{\partial t} = \frac{k}{\rho C_p}\left[\frac{\partial^2 T}{\partial x^2} + \frac{\partial^2 T}{\partial y^2}\right] \qquad (1)$$

where we consider an isotropic material of conductivity, k, density, ρ, and heat capacity C_p. We define the thermal diffusivity as [ii]

$$D = \frac{k}{\rho C_p} \qquad (2)$$

Resulting in the conduction equation:

$$\frac{\partial T}{\partial t} = D\left[\frac{\partial^2 T}{\partial x^2} + \frac{\partial^2 T}{\partial y^2}\right] \qquad (3)$$

The four cases studied in this report differ in Boundary and Initial Conditions. We consider these cases in detail as follows:

Case 1: Transient/Steady State Conduction in a slab.

We consider a slab of length L, insulated on the y plane, such that a 1 dimensional problem results. Isothermal boundary conditions are applied at both ends of differing temperature:

$x = 0; \quad t \geq 0; \quad T = T_1$

$x = L; \quad t \geq 0; \quad T = T_0$

With the initial conditions:

$t = 0; \quad 0 < x \leq L \;\; ; T = T_0$

The transient solution is[iii]:

$$\frac{T - T_0}{T_1 - T_0} = 1 - \frac{x}{L} + \frac{2}{\pi}\sum_{n=1}^{\infty}\frac{1}{n}\sin\left(n\pi\frac{x}{L}\right)\exp\left(-n^2\pi^2\frac{Dt}{L^2}\right) \qquad (4)$$

Figure 3 shows the numerical results obtained for this Case 1 simulation generated using COMSOL compared with values obtained from equation (4) summed to 100 terms. These figures plot non-dimensional displacement $\left(\frac{x}{L}\right)$ versus non-dimensional $\left(\frac{T - T_0}{T_1 - T_0}\right)$ temperature for a variety of non-dimensional times (ndt) defined as:

$$ndt = \frac{Dt}{L^2} \qquad (5)$$

Both figures indicate that a steady state, indicated by the linear profile is approached at non dimensional times around 0.5.

Exact Solution

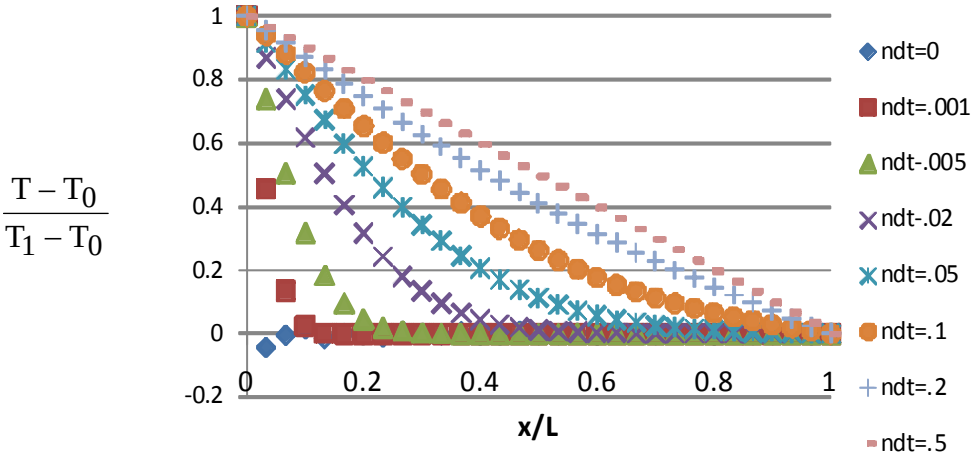

Figure 3a: Results obtained from Equation (4) summed to 100 terms

COMSOL Results

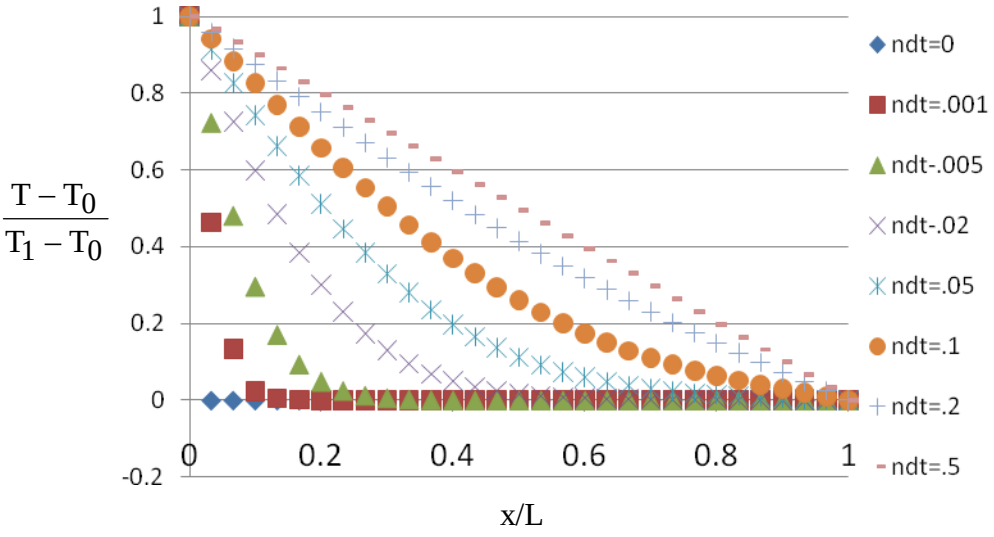

Figure 3b: Results obtained from COMSOL simulation

These figures indicate agreement between the COMSOL simulation results and the analytical solution, thereby yielding validation to the simulation results under the given conditions.

Case 2: Transient and Symmetric Conduction in a slab.

For Case 2, we consider a slab of length L, insulated on the y plane, such that a 1 dimensional conduction results. Isothermal boundary conditions are applied at both ends of the same temperature:

$$x = \pm\frac{L}{2}; \quad t \geq 0; \quad T = T_1$$

With the initial conditions:

$$t = 0; \quad -\frac{L}{2} < x < \frac{L}{2} \; ; T = T_0$$

The transient solution is[iv]:

$$\frac{T - T_0}{T_1 - T_0} = 1 - \frac{4}{\pi}\sum_{n=1}^{\infty}\frac{(-1)^n}{2n+1}\cos\left(\frac{(2n+1)\pi}{2}\frac{x}{L}\right)\exp\left((2n+1)^2\pi^2\frac{Dt}{L^2}\right) \qquad (6)$$

Figure 4 shows the values generated from COMSOL compared with values obtained from equation 6 summed to 100 terms. These figures plot non-dimensional displacement $\left(\frac{x}{L}\right)$ versus non-dimensional temperature for a variety of non-dimensional times (ndt)

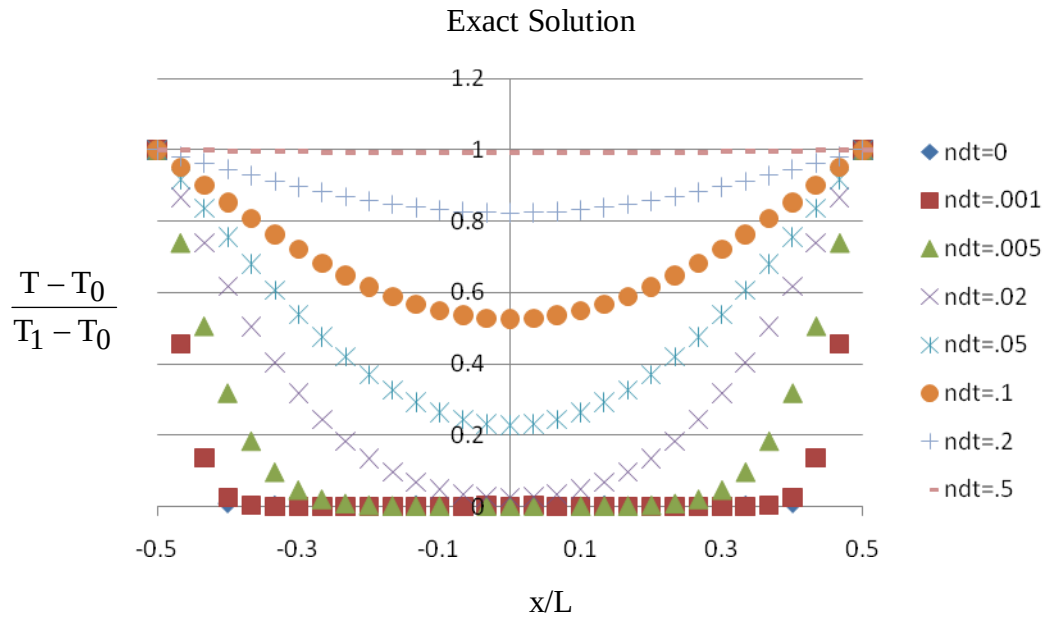

Figure 4a: Results obtained from Equation (6) summed to 100 terms

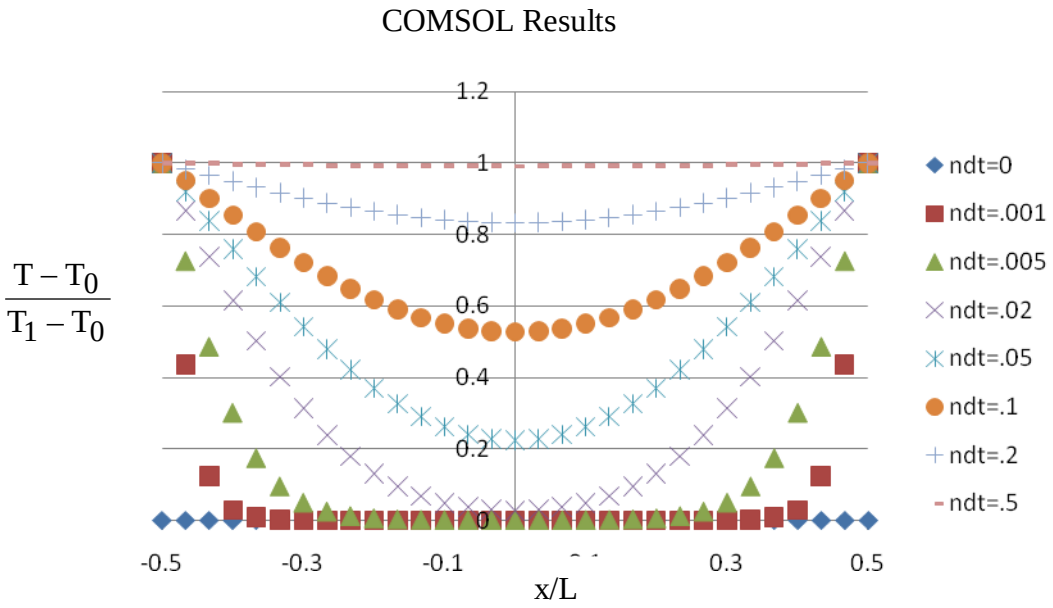

Figure 4b: Results obtained from COMSOL simulation

These figures indicate agreement between the COMSOL simulation results and the analytical solution, thereby yielding validation to the simulation results.

Case 3: Transient and Symmetric Conduction in a slab with Convection at the Ends.

We consider a slab of length L, insulated on the y plane, such that a 1 dimensional conduction results. In this case we consider non-isothermal boundary conditions and include convection at the ends of the slab to air at temperature T_1. The relevant boundary conditions are:

$$x = 0; \quad t \geq 0; \quad -k\left.\frac{dT}{dx}\right|_{x=0} = h\left(T|_{x=0} - T_1\right)$$

$$x = L; \quad t \geq 0; \quad -k\left.\frac{dT}{dx}\right|_{x=L} = h\left(T|_{x=L} - T_1\right)$$

where h is the heat transfer coefficient. This is coupled with the initial conditions:

$$t = 0; \quad 0 < x \leq L \quad ; T = T_0$$

For purposes of validation we consider the COMSOL simulation with a value of the heat transfer coefficient that is 1e6 times larger than the conductivity divide by length. This effectively simplifies the Case 3 simulation into the isothermal Case 2. The results are identical to Figure 4b and for the sake of redundancy are not repeated in this report.

Case 4: Convective Cooling of Nylon: 2 Dimensional Simulation for Comparison with ABAQUS Simulation.

At this point, we consider removal of the insulated y-plane condition and a 2 dimensional simulation results. In order to allow code to code comparison with a similar ABAQUS model, we consider the convective cooling of Nylon. For the case 4 simulation, we abandon non-dimensional analysis and consider specific dimensions and material

properties. The Nylon that is currently undergoing mechanical testing has dimensions of 6 cm by 1 cm and material properties represented in Table 1.

When considering the heat transfer coefficient, the case of natural convection from many materials into air can yield a heat transfer coefficient of around 10 W/m2/K. Under forced convection of air, values for the heat transfer coefficient can reach as high as 1000 W/m2/K. [v]

A low chosen value of this coefficient may cause the bulk of the heat transfer resistance to be lumped into conduction. Hence, we choose to consider the largest possible value of 1000 $W/m^2/K$ in this simulation to allow a mixed mode of heat transfer that allows conduction and convection to contribute to cooling.

The boundary conditions for this case can be represented on all sides as:

$$n.(k\nabla T) = h(T_1 - T)$$

We will consider the cooling of a hot Nylon sample, heated to just below its melting temperature (ie. 200C). Cooling takes place in air kept at 20C. The results for this case are indicated in Appendix A as contour plots for values of time ranging from 50 to 10000 seconds. These results can be compared with ABAQUS output in order to generate a code to code validation.

Appendix A1

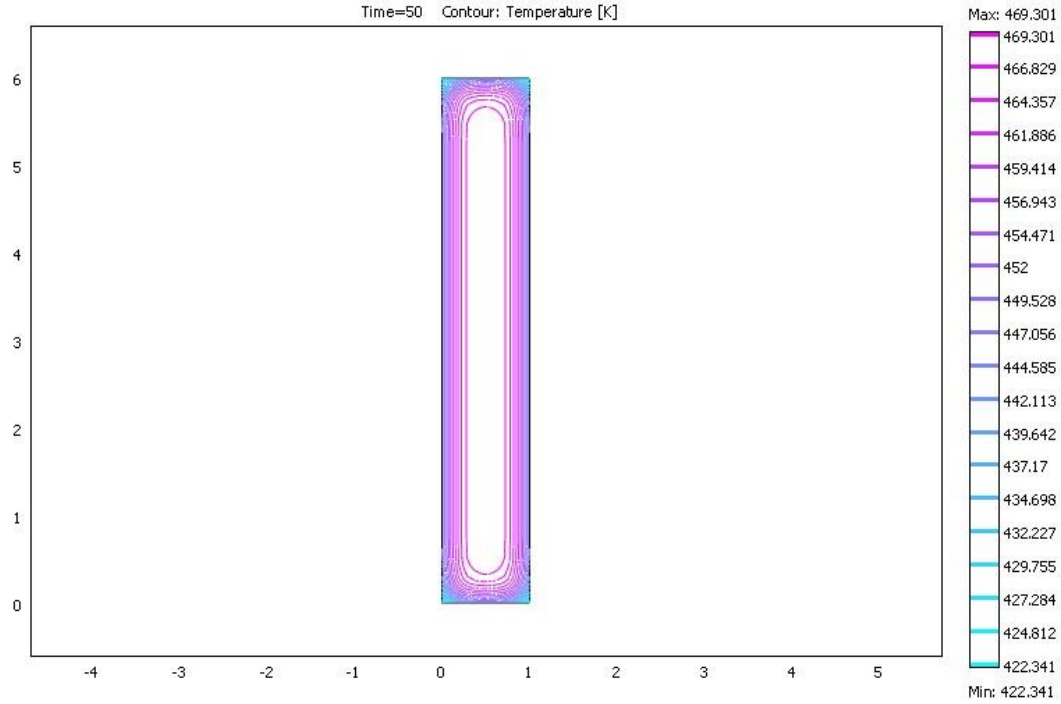
Time=50 Contour: Temperature [K]
Max: 469.301
469.301
466.829
464.357
461.886
459.414
456.943
454.471
452
449.528
447.056
444.585
442.113
439.642
437.17
434.698
432.227
429.755
427.284
424.812
422.341
Min: 422.341
6
5
4
3
2
1
0
-4
-3
-2
-1
0
1
2
3
4
5

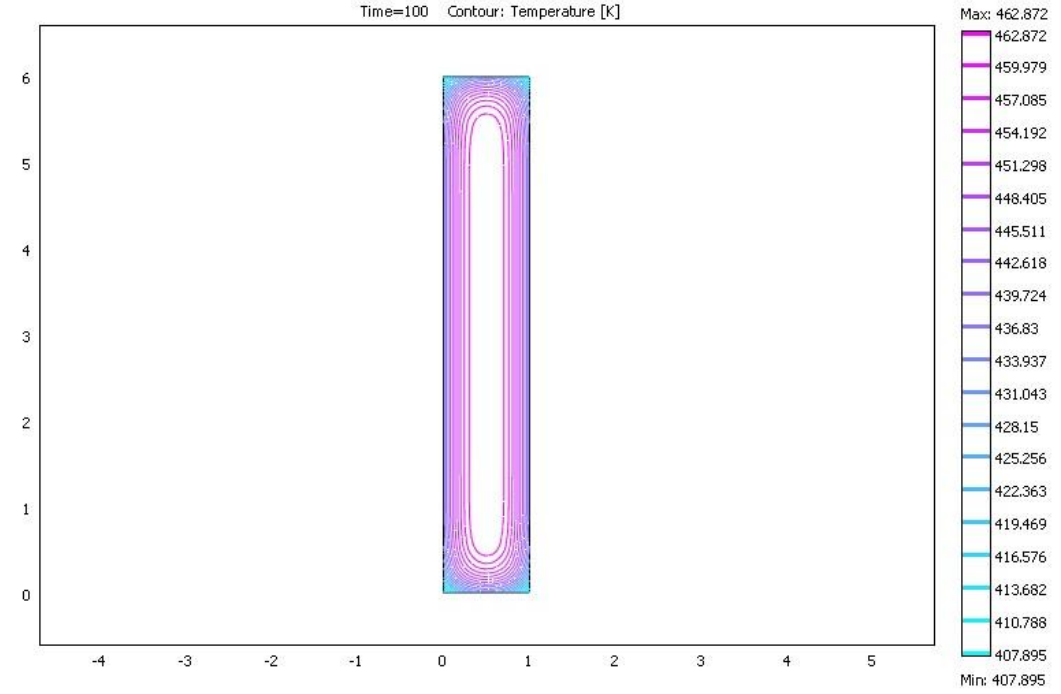
Time=100 Contour: Temperature [K]
Max: 462.872
462.872
459.979
457.085
454.192
451.298
448.405
445.511
442.618
439.724
436.83
433.937
431.043
428.15
425.256
422.363
419.469
416.576
413.682
410.788
407.895
Min: 407.895
6
5
4
3
2
1
0
-4
-3
-2
-1
0
1
2
3
4
5

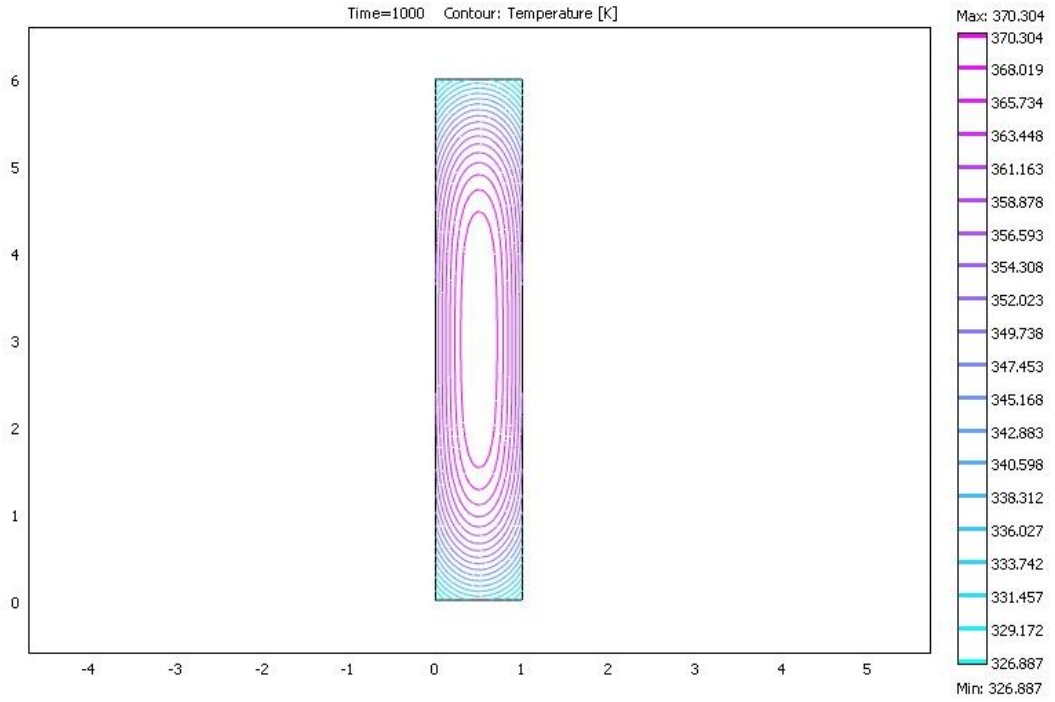
Time=1000 Contour: Temperature [K]
Max: 370.304
370.304
368.019
365.734
363.448
361.163
358.878
356.593
354.308
352.023
349.738
347.453
345.168
342.883
340.598
338.312
336.027
333.742
331.457
329.172
326.887
Min: 326.887
6
5
4
3
2
1
0
-4
-3
-2
-1
0
1
2
3
4
5

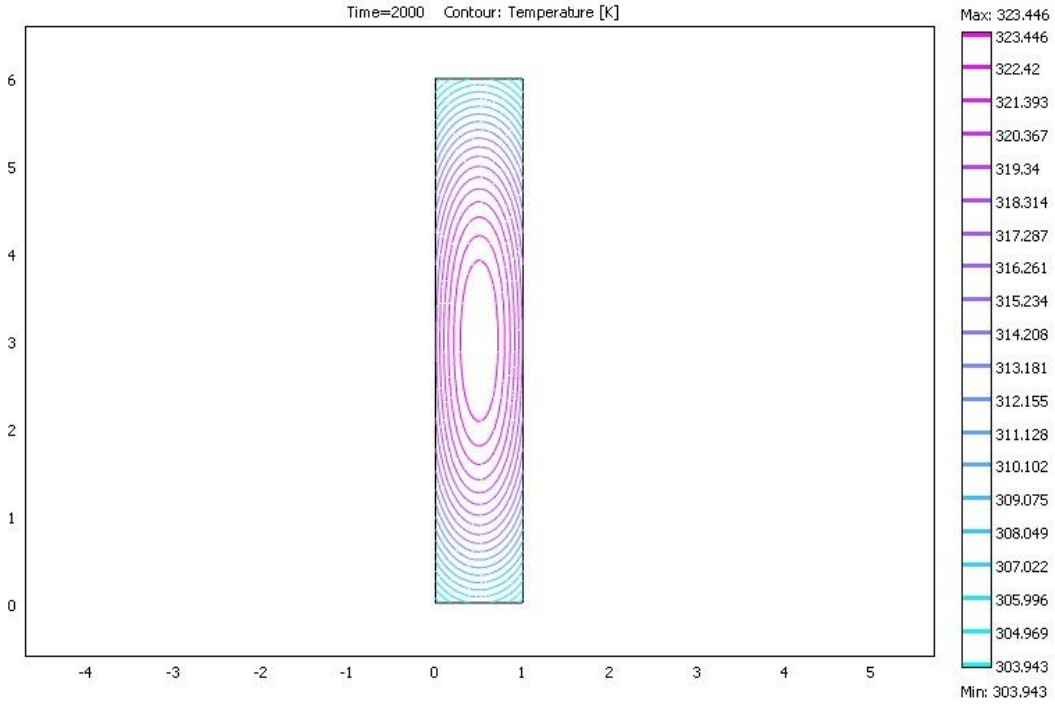
Time=2000 Contour: Temperature [K]
Max: 323.446
323.446
322.42
321.393
320.367
319.34
318.314
317.287
316.261
315.234
314.208
313.181
312.155
311.128
310.102
309.075
308.049
307.022
305.996
304.969
303.943
Min: 303.943
6
5
4
3
2
1
0
-4
-3
-2
-1
0
1
2
3
4
5

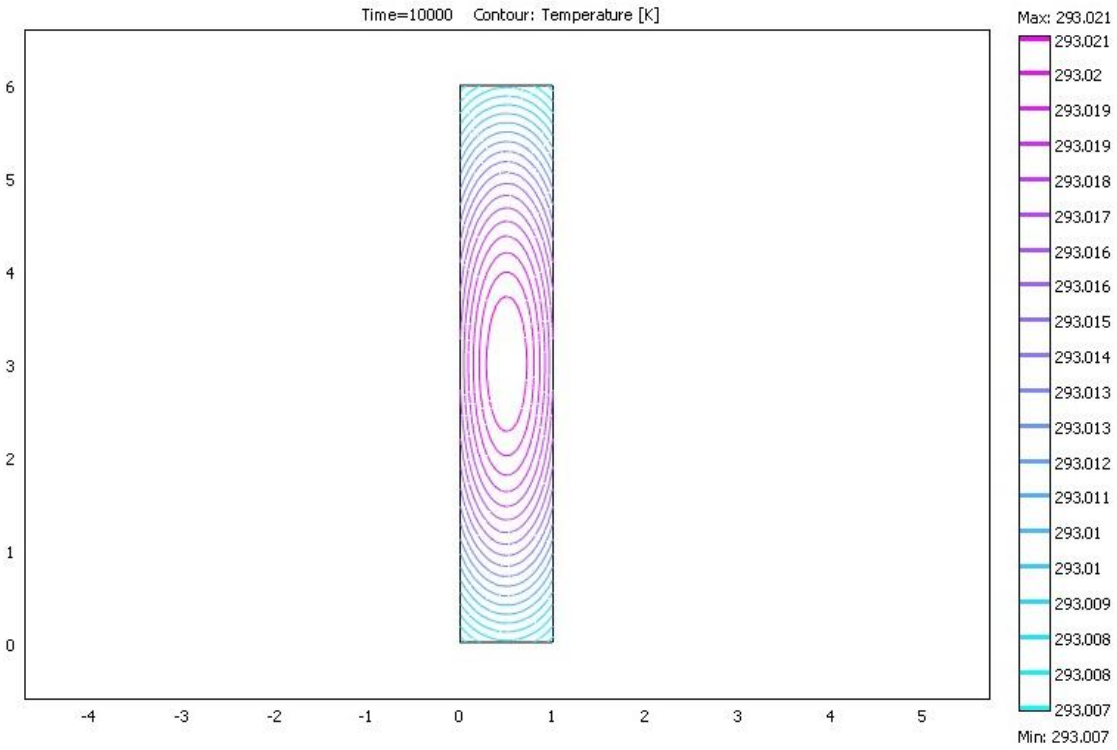
Time=10000 Contour: Temperature [K]
Max: 293.021
293.021
293.02
293.019
293.019
293.018
293.017
293.016
293.016
293.015
293.014
293.013
293.013
293.012
293.011
293.01
293.01
293.009
293.008
293.008
293.007
Min: 293.007
6
5
4
3
2
1
0
-4
-3
-2
-1
0
1
2
3
4
5

Appendix A2: COMSOL INSTRUCTIONS FOR CASE 4: (Adapted from web available Help Files (Find web address)

1. Start COMSOL by double clicking on the COMSOL Multiphysics icon on the Desktop

2. Select 2D next to Space Dimension
   (Note: COMSOL can do 1D problems, however to give you a better understanding of COMSOL we'll model the problem as 2D)

3. Single Click on COMSOL Multiphysics >> Heat Transfer >> Conduction >> Transient Analysis. Transient Analysis under conduction is selected as we intend to solve a time dependent conduction problem (Equation 2).

   Click on the Settings Tab

5. Set the Unit system to SI

   6. Click OK. COMSOL Window opens up.

   7. Under File, click on Save as…

   8. Create your own folder

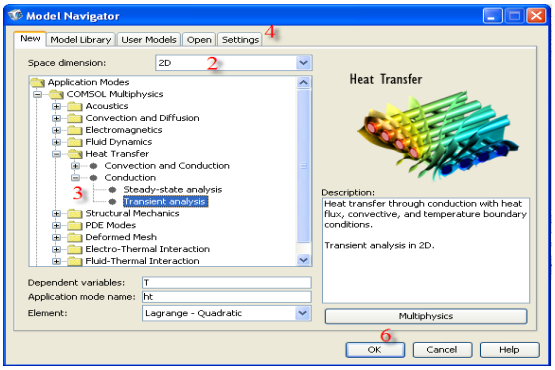

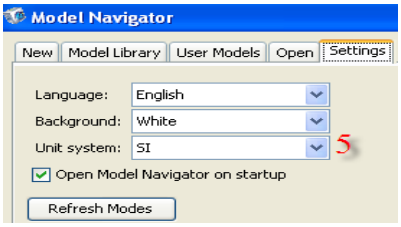

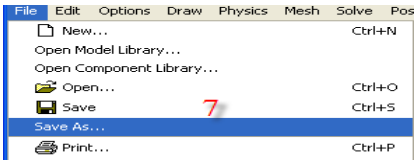

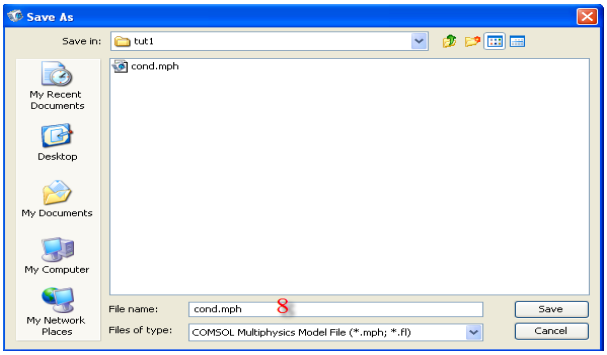

Step 2: Creating the Geometry

For the 2D problem we use 6 cm in y-direction and 1cm in x direction.

1. Click on Draw >> Specify Objects >> Rectangle. Rectangle window opens up.
2. Specify width as 0.06 and height as 0.01. These are the dimensions of the slab in m.
3. Click on OK.
4. Click on Zoom Extents to fit the geometry in the window.

The geometry that is created is shown in the figure.

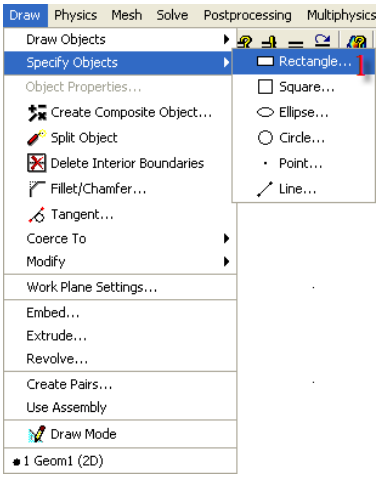

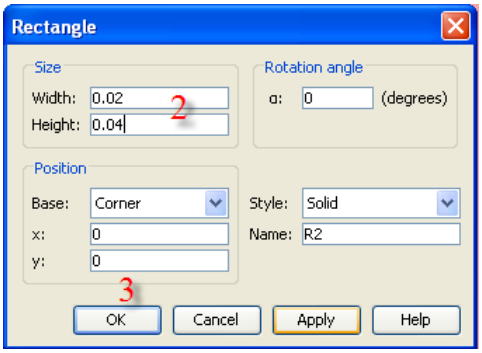

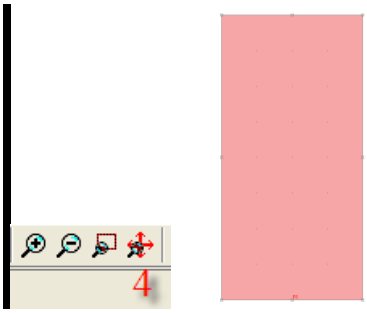

Step 3: Meshing

We will mesh the edges first and then the face. This method is used to control the number of elements in certain parts of the geometry like the boundaries and interfaces. In many cases we need a finer mesh near the boundary and so we mesh the edge accordingly and what we get is a non-uniform mesh. However in this case we mesh the geometry with a uniform mesh with a spacing of 0.002 between the nodes.

1. Under Mesh, click on Mapped Mesh Parameters…
2. Click on the Boundary Tab
3. In Boundary Selection, select 1 and 4 by left clicking and holding the Ctrl key. We will specify 20 elements each on the left and right edges.
4. Check the box for Constrained edge element distribution
5. Click on Number of edge elements, and type in 20 in the box below.
6. For boundary 2 and 3, use number of edge elements as 10. We specify 10 elements each on the top and bottom edges.
7. Press the 'Remesh' Button on the bottom. The mesh that is obtained is shown in the figure.
8. Click 'Ok'

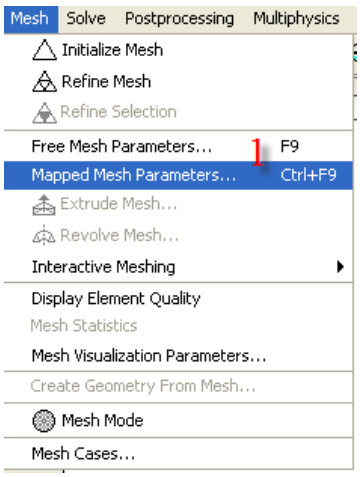

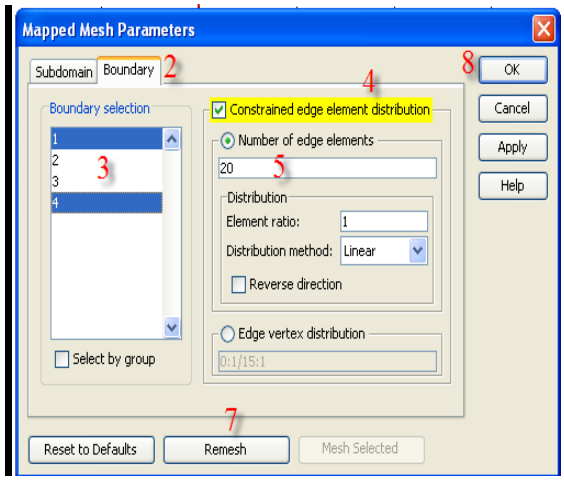

9. Screen should now look like this.	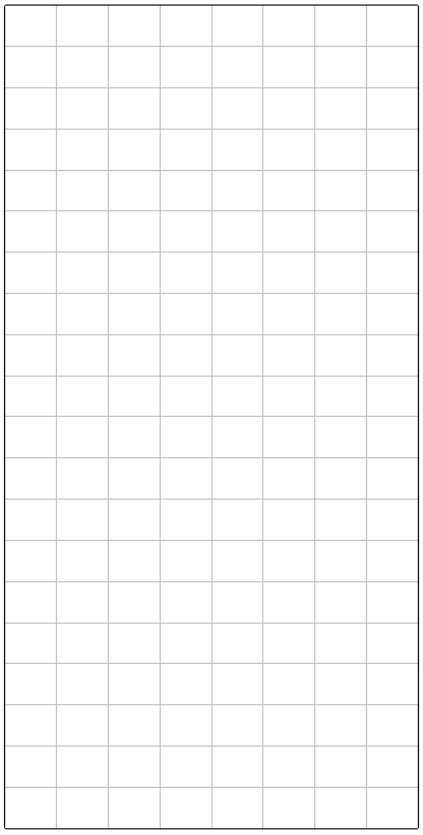

Step 4: Defining Material Properties and Initial Condition

We are solving the energy equation and so we need to provide the solver with the appropriate material property values required for the analysis. These properties are:

(i) *Density (ρ)*: The density of the material of the slab is 1150 kgm^{-3}

(ii) *Thermal Conductivity (k)*: The thermal conductivity is 0.237 W(mK)$^{-1}$

(iii) *Specific Heat (c_p):* The specific heat is 1690 J (kgK)$^{-1}$

The Slab is initially at a temperature of 200^{0}C.

1. Under Physics, click on Subdomain Settings…
2. Click on 1 to select the slab.
3. Left click on the text field next to **Thermal Conductivity** and type **0.237**
4. Left click on the text field next to **Density** and type **1150**
5. Left click on the text field next to **Heat Capacity** and type 1690
6. Click on the Init Tab
7. In the box under Initial Value, fill in 473. The slab is initially at a temperature of 200 ^{0}C .
8. Click Ok

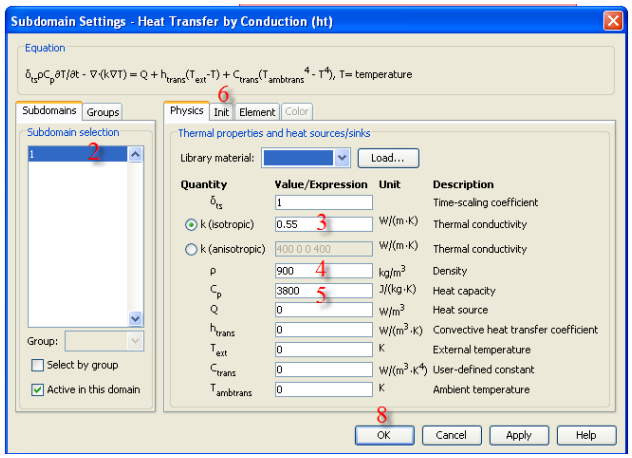

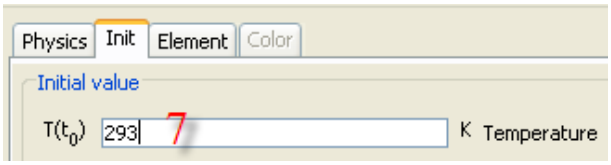

Step 5: Defining Boundary Conditions

The boundary conditions for the problem are convection on all sides:

1. Under Physics, click on Boundary Settings…
2. Click on 2 in the Boundary Selection box
3. Change the Boundary Condition to Heat Flux
4. In q_0=0, h=1000, Tinf=293K, const=0, Tamb=0, T0=0.
5. Repeat for all sides
6. Click on OK

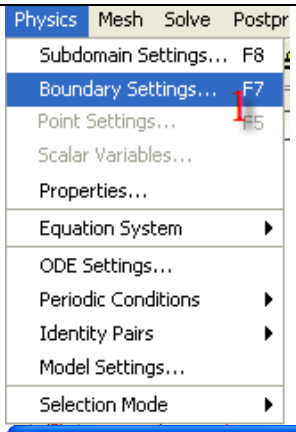

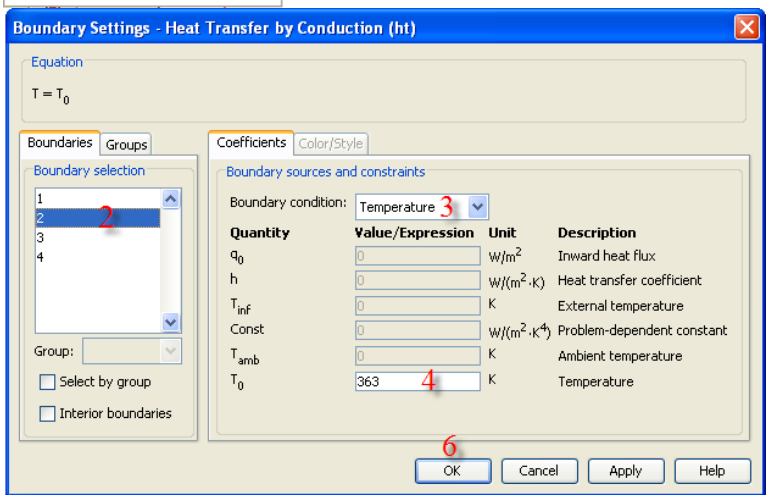

Step 6: Specifying Solver Parameters

1. Under Solve, click on Solver Parameters.
2. Under the General Tab, select Transient under Analysis if it is not already selected
3. Select Time dependent under Solver.
4. In the Times: box, type in 0:10:10000. This tells the solver to start at 0 seconds, then save the solution every 10 seconds until it reaches 10000 seconds.
5. Click Ok
6. Click on Get Initial Value under Solve. This step initializes the solver with the value provided when the initial conditions were specified (Step 4).
7. Under Solve, click

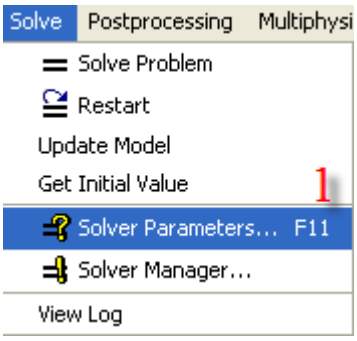

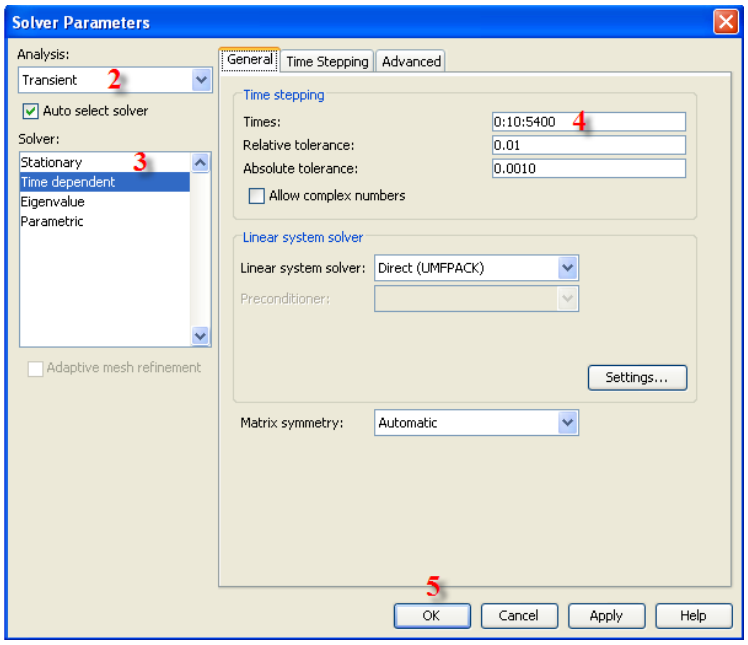

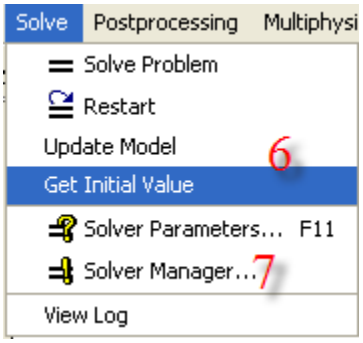

on Solver Manager.

8. Click on the Solve For tab.
9. Select T for temperature if it is not already selected. By selecting T, we are directing the solver to solve for the temperature.
10. Click on the Output tab.
11. Select T for temperature if it is not already selected. By selecting T, we are directing the program to save the temperature values.
12. Press Solve. Once Solve is pressed, the solver solves the transient heat transfer equation

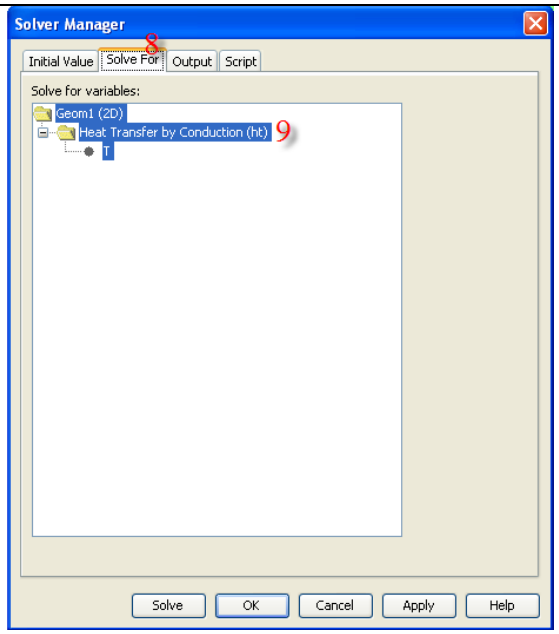

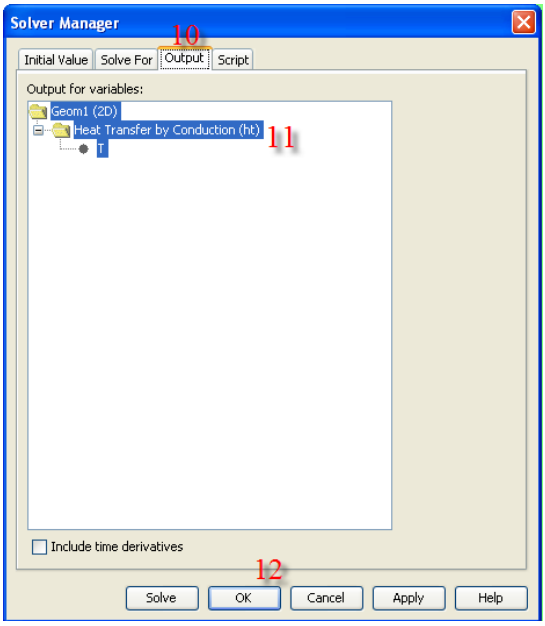

Step 7: Postprocessing

Post-processing is viewing the results obtained on running the simulations of the problem. We will generate graphs and charts based upon our simulation.

Displaying the Mesh

1. To display the mesh, simply click on the Mesh Mode button. Mesh mode can also be selected by clicking on Mesh >> Mesh Mode.

The mesh is shown in the figure below.

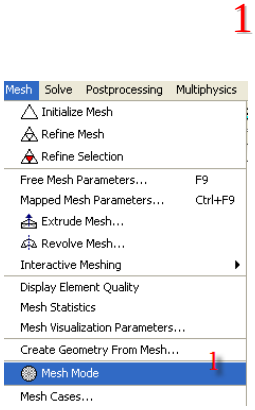

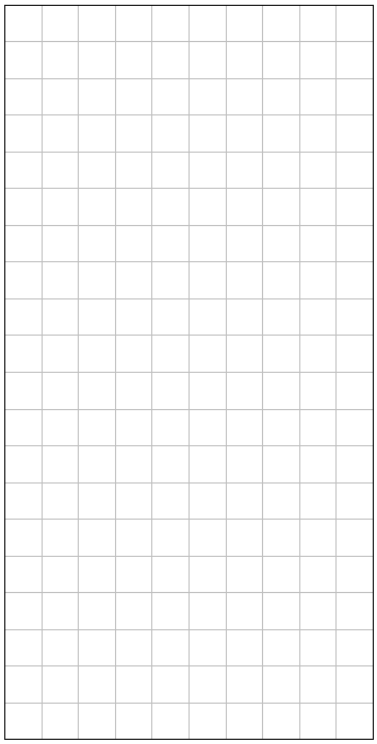

Obtain the surface plot at the last time step

We now plot the temperature contour in the slab at the end time (i.e. after 1.5 hrs or 5400 s).

1. Under Postprocessing click on Plot Parameters.
2. Click on the General Tab
3. Check the box for Surface under Plot Type.
4. Next to Solution at time: select 5400.
5. Click on the Surface Tab.
6. Select Temperature next to Predefined quantities, if it is not already selected.
7. Click on OK.

The contour plot that is obtained is shown on the next page.

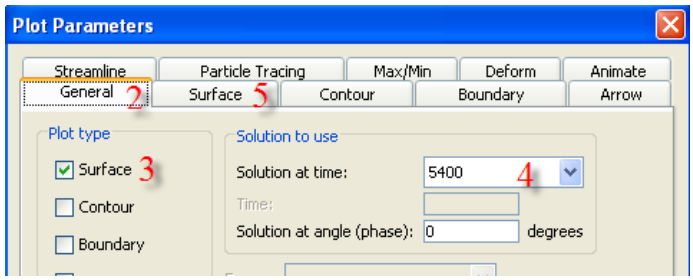

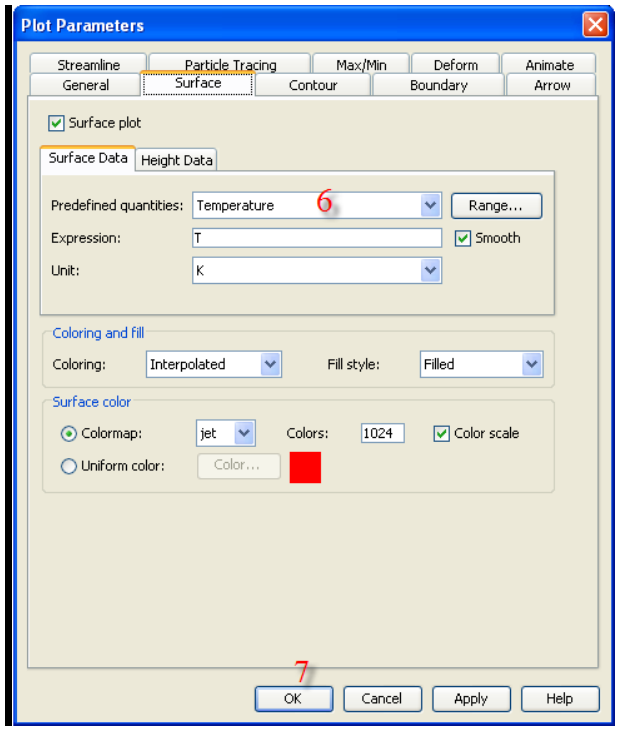

References

[i] H.S. Carslaw and J.C. Jaeger, Conduction of Heat in Solids, Oxford University Press, 1946.
[ii] H.S. Carslaw and J.C. Jaeger, Conduction of Heat in Solids, Oxford University Press, 1946.
[iii] H.S. Carslaw and J.C. Jaeger, Conduction of Heat in Solids, Oxford University Press, 1946.
[iv] H.S. Carslaw and J.C. Jaeger, Conduction of Heat in Solids, Oxford University Press, 1946.
[v] Incropera FP and Dewitt DP, Introduction to Heat Transfer, 1985.

APPENDIX B

DIFFERENTIAL SCANNING CALORIMETER TESTING

(By Rukiye Tortop)

Ultra-Sonic Self-Healing of Polymers

Work with Differential Scanning Calorimeter

Supervisor: Dr. Chris Jenkins
Rukiye Tortop
April 2009

Purpose of this paper:

It is to explain why the use of a DSC on Ultra-Sonic Self-Healing of Polymers research was helpful. This document gives detail of the work accomplished by using a DSC, as well as the results by the analyzing data.

It also provides counsels and techniques to use the DSC.

CONTENTS

Abbreviations:

DSC : Differential Scanning Calorimeter

DTA : Differential Thermal Analysis

INTRODUCTION

In the research of Ultra-sonic Self-healing of Polymers, we used exclusively this polymer: nylon 66 (polyamide 6-6, $C_{12}H_{22}O_2N_2$).

Below are some characteristics of this material given by the supplier

Melting point	491°F - 255°C
Glass transition	162°F - 72.2°C
Density (lbs/in^3)	0.0412
Water Absorption (%) @ 24 hours, 73°F	1.2
@ Saturation, 73°F	8.5

This information is useful to analyze the data coming from the DSC.

The aim of this work was to observe property changes in the material after it was ultrasonically heated. In that case, a DSC is very useful to detect property changes in materials.

OBJECTIVES

The objective of this work was to find how we can detect property changes in the material with a DSC. Some studies tend to use this apparatus to find crystallinity changes, showing that a different degree of crystallinity was synonym to higher or lower strength of material (See references: resource 1).

This work was composed of two parts:

First, I worked on virgin samples of nylon 66, heated three times to detect any changes in the differential thermal analysis (DTA) curves given by the Evaluation software of the DSC apparatus.

Then, my work came closer to our research, and I studied the property changes of ultrasonically heated samples, compared to virgin samples.

ACCOMPLISHMENT

1. First part of work

The purpose was to detect any difference in behavior if a sample goes through the heating-cooling process several times. Two small samples of approximately 50mg were tested.

The heating-cooling process was simple:

A virgin sample was heated (10°C per min heating rate) to a maximum of 190°C, and cooled down with no dwelling time (10°C per min cooling rate).

Once the sample was at room temperature, the process was repeated two more times.

Thus, one sample was heated three times with the same process. The DTA showed differences between samples that had already been heated and virgin samples.

Here is a typical output for one sample run through the process three times:

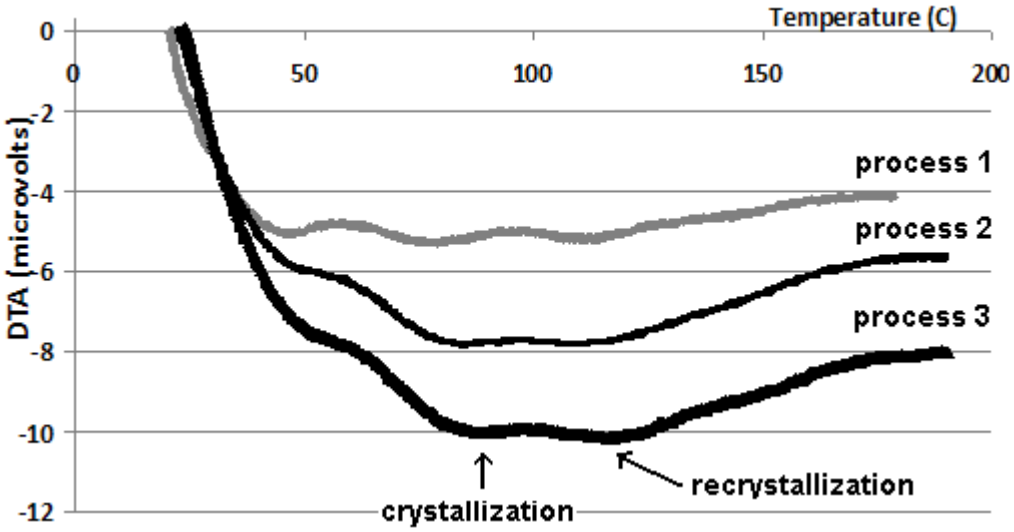

Figure 1

After heating, the nylon sample changed color. The curve corresponding to the first heating process was different from the other curves. The second and third curves were similar.

The process was the same for the second sample and the results were the same.

2. Second part of work

The aim of this part was to find any differences in crystallinity between virgin samples and ultrasonically heated ample.

By referring to resource 1, melting the samples by using a DSC would help to find the degree of crystallinity of each sample.

In this part, 4 samples were studied:

- One small sample of approximately 50mg heated ultrasonically;

- Two samples cut around ultrasonically heated zone, one at 10% of power (low power) and the other one at 50% of power (high power), these two sample weighted approximately 80mg;

- The last sample was a virgin sample of approximately 50mg.

The melting process was the following:

An ultrasonically heated sample was heated (10°C per min heating rate) to a maximum of 300°C, and cooled down with no dwelling time (10°C per min cooling rate).

Below is the DTA of ultrasonically heated samples and of a virgin sample (upper curve of figure 2).

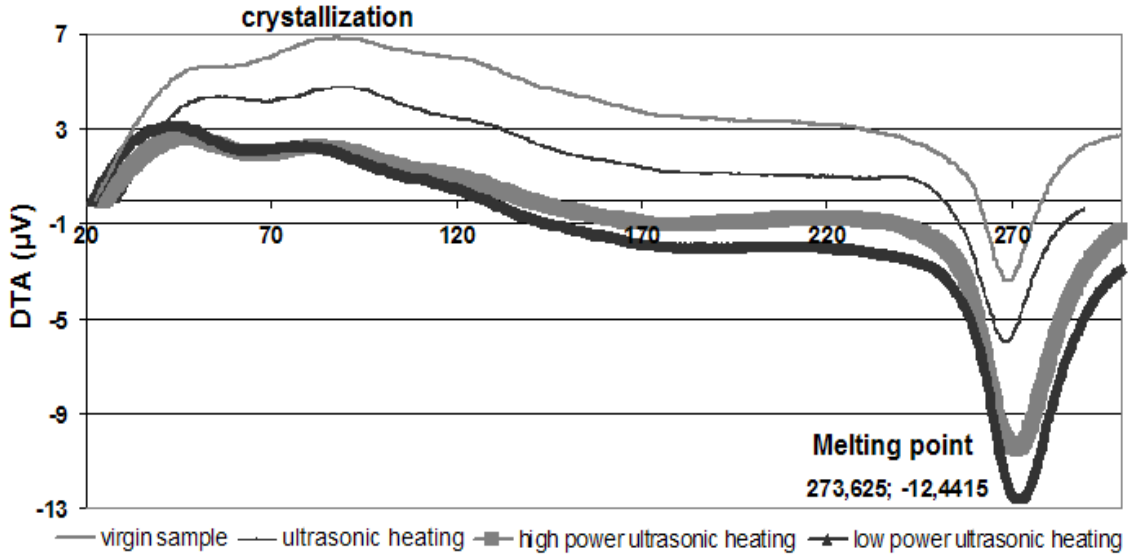

Figure 2

To calculate the crystallinity of each sample, the method given in resource 1 was followed.

The evaluation software gave area under the peak of crystallization and melting.

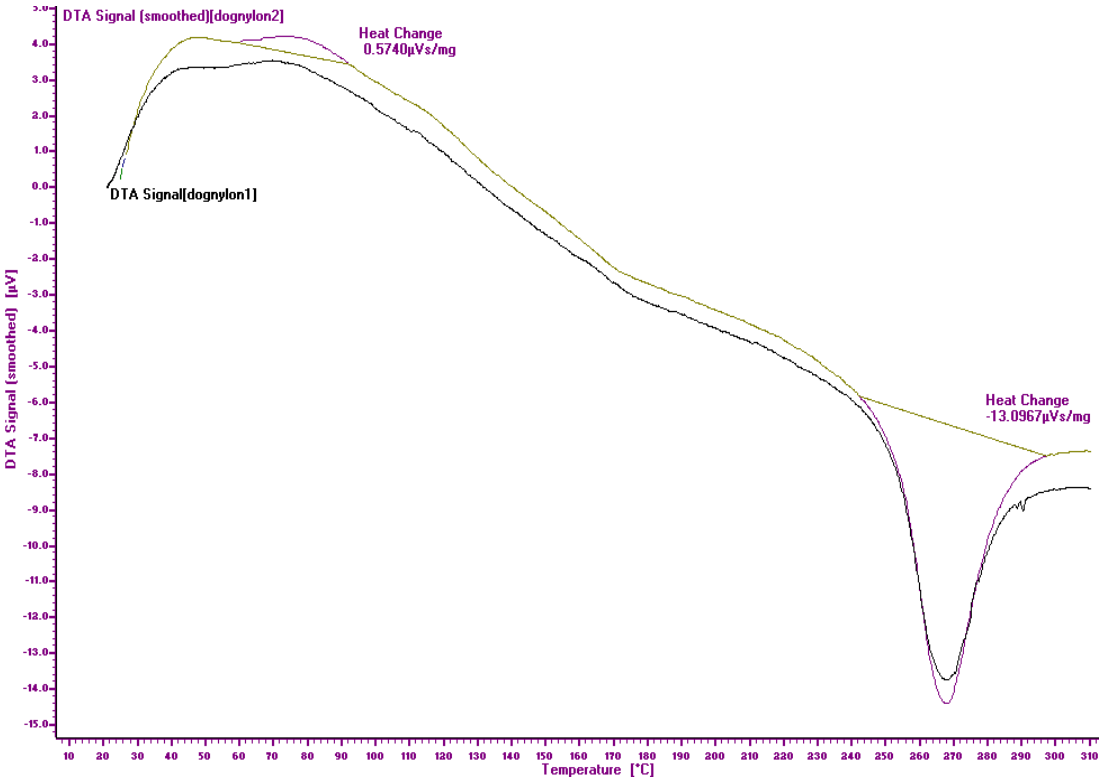

Figure 3 – DTA evaluation output with area under the peak

These data are use as following, to find the percent of crystallinity.

First, we calculate the total heat given off by the sample during melting H_m :

$$H_m = \frac{A_m * m_{total}}{h}$$

With A_m = area under the peak of melting (µVs/mg)

m_{total} = mass of the sample (mg)

h = heating rate (°C/min)

Second, we calculate the heat given off by one gram of this sample:

$$H_m^* = \frac{H_m}{m_{total}}$$

Third, we calculated the total heated absorbed during crystallization:

$H_c = \frac{A_c * m_{total}}{h}$, with A_c the area under the peak of crystallization (μVs/mg)

Fourth, we subtract:

$$H_m - H_c = H'$$

This is the heat given off by the part of the sample which was already crystalline before the sample was heated above crystallization temperature (Tc).

Fifth, we divide and:

$$\mathrm{m_c} = \frac{H'}{H_m^*}$$

This is the total amount of grams of polymer that were crystalline below Tc.

Finally, we get the percent of crystallinity: $\frac{\mathrm{m_c}}{m_{total}} * 100$

Following this process, the percent of crystallinity of the seven samples were found:

83% of crystallinity for the ultrasonically heated sample,

95% of crystallinity for the low power ultrasonically heated sample,

95% of crystallinity for the high power ultrasonically heated sample,

73% of crystallinity for the virgin sample,

97.7%, 95.6%, 96.8% for three samples of a heated dogbone (190°C at 10°C/min).

Another virgin sample was melt and the percent of crystallinity was lower than 70%.

These results showed that ultrasonically heated samples were more crystalline than virgin sample.

Below is a table of detailed results:

sample	Percent of crystallinity	Area under CRYSTALLIZATION peak (μVs/mg)	Area under MELTING peak (μVs/mg)
VIRGIN 1	73.6	4.3945	16.6846
VIRGIN 2	47	10.3489	19.5754
HIGH ULTRASONIC	95.7	0.6690	15.4067
LOW ULTRASONIC	95.6	0.7036	15.9383
ULTRASONIC	83	2.5798	15.2038
DOGBONE 1	97.7	0.2364	10.5388
DOGBONE 2	95.6	0.5740	13.0967
DOGBONE 3	96.8	0.3495	11.0280

We see that the area for crystallization is lowest for these samples with very high percent of crystallinity, and that the area of melting is lower for these same samples.

Also according to resource 1, higher crystallinity means better strength of material.

To conclude, the strength of ultrasonically heated samples were higher than strength of virgin samples.

3. Problems with reading the curves

- Why the curves are different from the first part and the second part of work

Before the first part of the work was done, the peak given by the software was known as reversed, but still accurate.

Not knowing how to fix this little problem, the first part of the work was thus accomplished.

After that, this problem was fixed and a control made to ensure the accuracy of older results. The curves before and after repairing the apparatus were symmetric about the 0 µV x-axis.

- Glass transition temperature:

In all the DTA curves, the glass transition point is not obvious as it is showed in resources.

The glass transition is defined by a shift in the DTA like figure 3.

Figure 3

There is no shift particularly in healed samples. (see resource 1)

If we consider the melting curve of the virgin sample, and if we take in account the *transient* period at the beginning of the curve (period of instability at the start of a run before a stable heating rate is established - see resource 2), meaning we do as if the curve start at 50°C, we can observe the glass transition point (Figure 4):

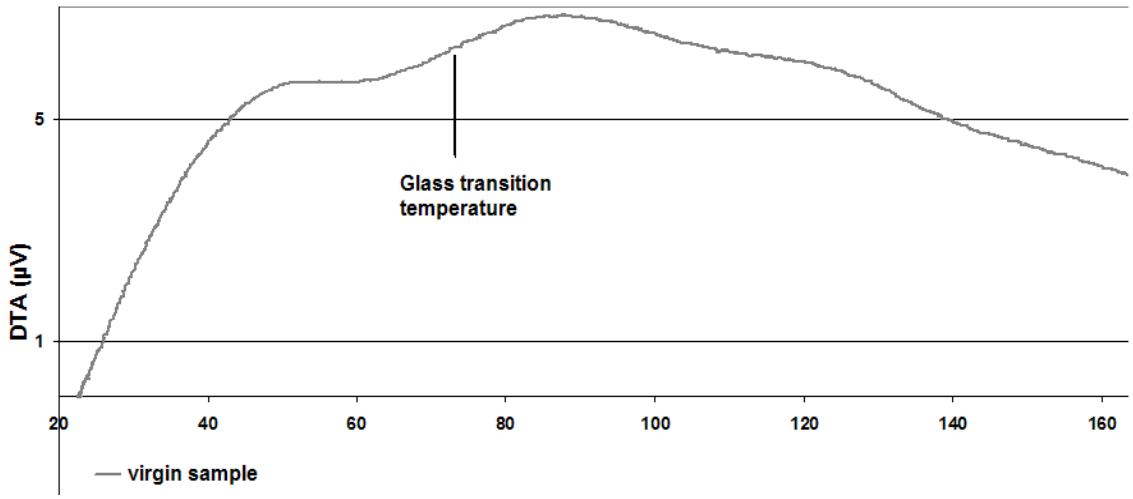

Figure 4

There are factors affecting the glass transition point Tg: (refer to resource 2)

i. Additives, for example plasticisers like moisture,
ii. Chemical bond such CH_2-CH_2,
iii. Heating rate: good determination of Tg with a heated rate of 5°C/min.

Moreover, fully crystalline materials do not show glass transition in DTA, but show melting point. Only semi-crystalline materials show both glass transition and melting point and nylon 66 is highly crystalline.

HOW TO USE A DSC

1. Checking performance

To ensure the accuracy of the results, a performance check is necessary, approximately every 10 measurements. This will consist on running a Calcium-Oxalate (type DTA+TG sample) and comparing the results with the reference curve given in the manual file (see Annexe 1).

If the curves are not the same, you will have to run calibration runs following the documentations in Annexe 2.

2. Steps to be followed in order to run a test

Next to the DSC apparatus is a complete manual and a sheet that resumes steps to follow to do a measurement. Below is the same procedure with illustrations:

Sample measurement procedure

1. Switch on amplifier, computer, cooling water

2. Unlock the balance by pressing the A/M button on the amplifier to M until the red LED is on (needs approx. 5sec)

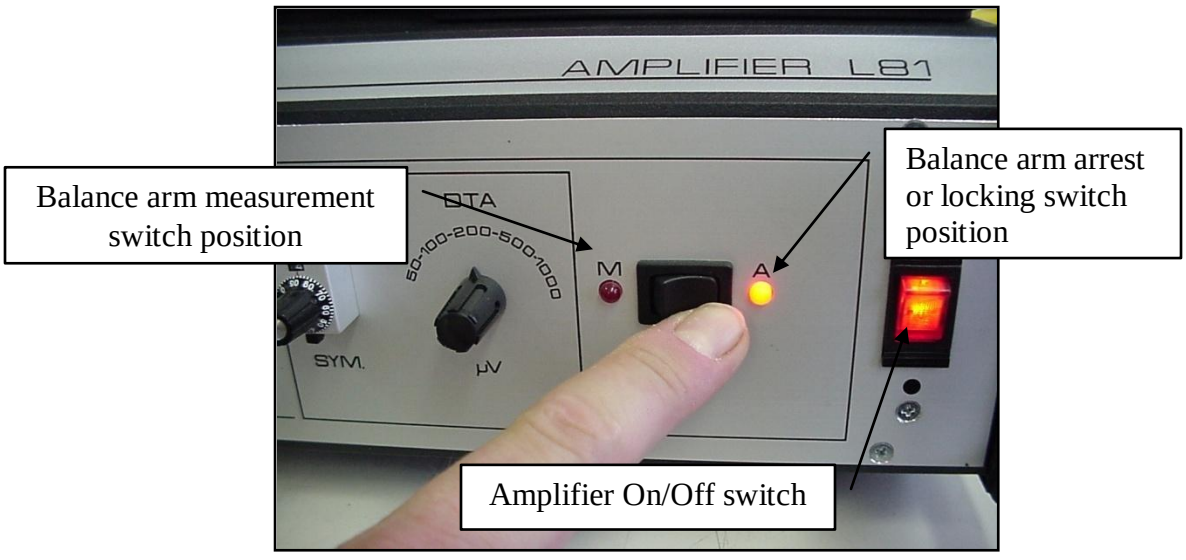

3. Lift the furnace with the protection tube carefully by pressing Up/Dow button

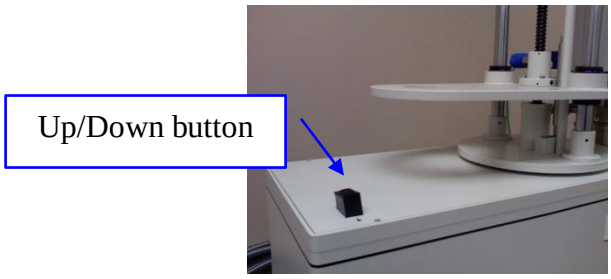

4. Remove sample crucible and clean

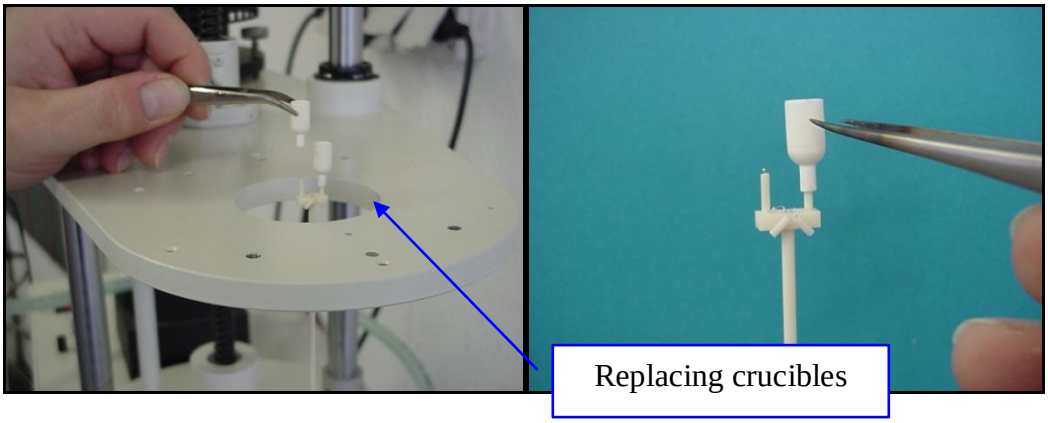

5. Be careful, reference always on the right, sample on the left.

6. Weigh the new sample
7. Place sample crucible onto measuring system
8. Check if the measuring system is centred.

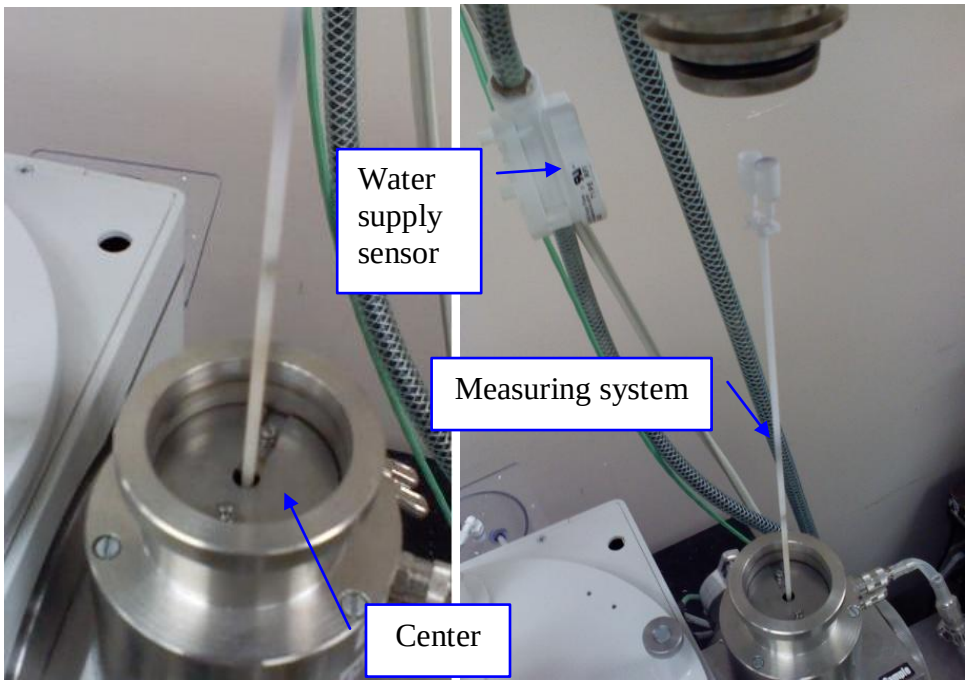

9. If not, unlock balance (point 2.) and wait couple seconds. If not centred go to paragraph number 3 after this instruction.
10. Lower the furnace with protection tube
11. select measuring range to amplifier for TG +/-25mg, +/-250mg or +/-2500mg
12. select measuring range to amplifier for DTA between +/-50 uV and +/-1000uV

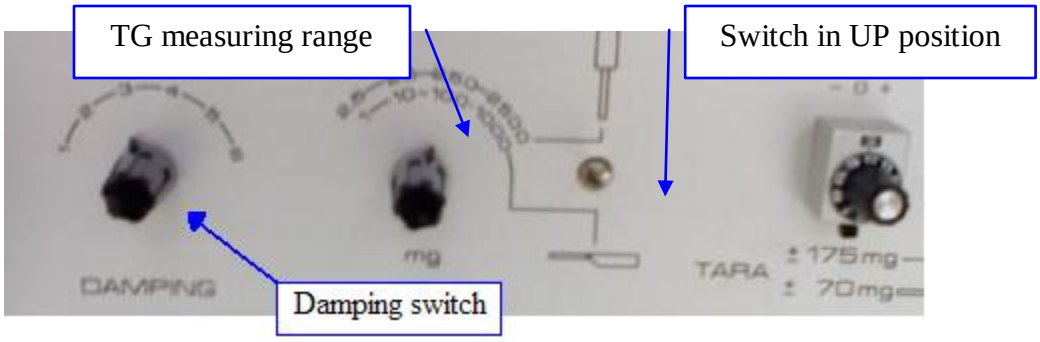

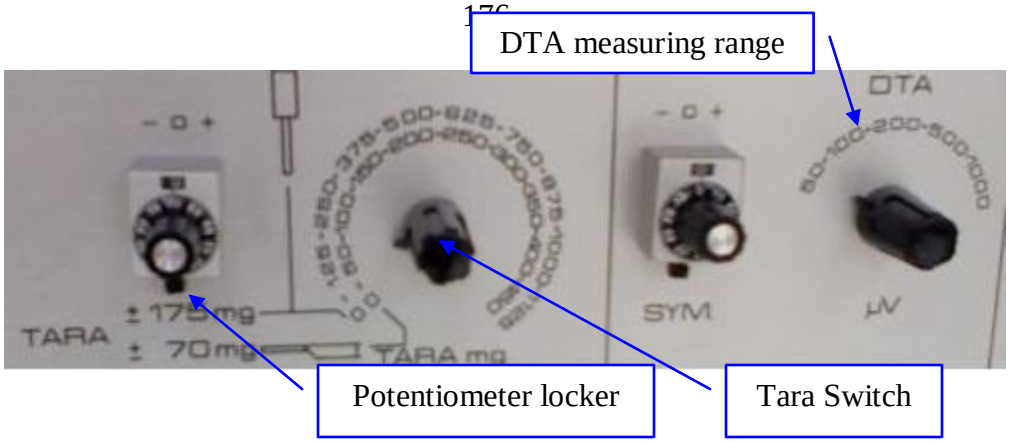

13. Start DATA COLLECTION SOFTWARE
14. Select DATA ACQUISITION, TYPE, SAMPLE TG+DTA
15. Enter the DATA ACQUISITION, SETTNGS

    sample file name, zero file name (if ZERO type test), weight of sample, duration, end temperature, and ranges for TG and DTA (Value must match at amplifier settings)
16. Enter the CONTROLLER, TEMPERATURE PROFILE

    always program one heating rate with 30K/min down to 700C as the last segment. This controlled cool protects the heating element and alumina tube protection.
17. Check CURRENT VALUE for temperature of sample and furnace the values should be at room temperature
18. Select OPTIONS, SETUP SCALES to find the tara of the balance
19. Switch damping to 1 on amplifier
20. Use Tara switch and potentiometer to adjust cursor to the center or within +/- 100% of the range

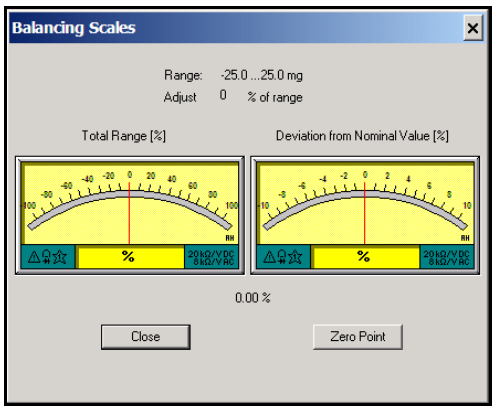

21. Lock the Tara potentiometer. If the tare adjustment is not possible, check the balance lock switch, (M/A Switch)
22. If the tare still can not be done, add or remove weight at the left side of the balance (see paragraph 4 after the instruction)
23. Switch damping to back to 3 for the measurement
24. Make sure the switch is in UP position
25. Start measurement with START (if there is nothing on the page, stop the run and wait until the temperature come back to room temperature to restart the measurement)
26. Monitor measurement with CONTROLLER CURRENT VALUES or real time graphic
27. Raise the furnace with protection tube only if temperature is below 200C
28. Shut off the water supply only if temperature is below 200C
29. Lock balance at the amplifier if you do not use the machine by pressing the A/M button at the amplifier to A until the LED is on (approx. 5sec)
30. Record run in the “user log” excel file on the desktop

3. Tips about the software

- SETTINGS:

Data of the run will be recorded in the file you have chosen or created when you named the file. It is in “my documents”.

- DATA EVALUATION software:

When using this software, your saved data will be in:

“My Documents\Tawin\STA\DATA”

When you start the software for the first time, right the name of your file, then go to FILE, LOAD DATA and load from your recorded files either TG or DTA…Don’t forget to save your work.

- Most useful tools of Data Evaluation:

You can load several curves in one sheet by clicking on FILE, LOAD DATA.

To adjust the curves to the same axis click on TRACE, Adjust range.

To do a glass point or a data peak evaluation, you have to SMOOTH the curve first by clicking on EVALUATION, (make sure of the right function group, DTA-evaluation or TG-evaluation), SMOOTHING, DERIATION. Then click on glass point evaluation or DATA PEAK EVALUATION, of Evaluation.

Delete or Hide curve by clicking on TRACE, HIDE…or DELETE…

To export your file onto excel for example, click on ASCII-Export

4. What to do if the measuring system is not centred

Open the inspection port and the side measurement port.

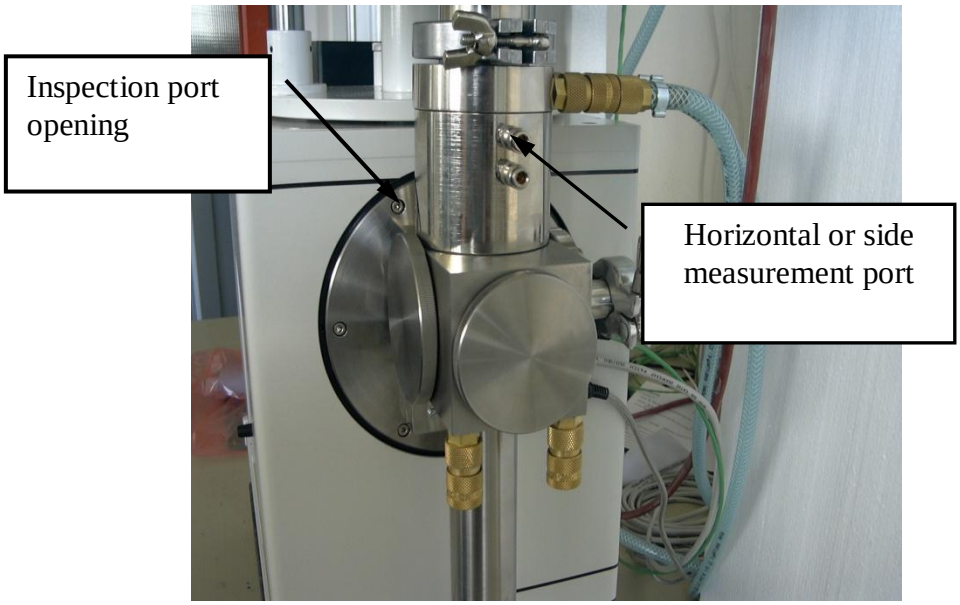

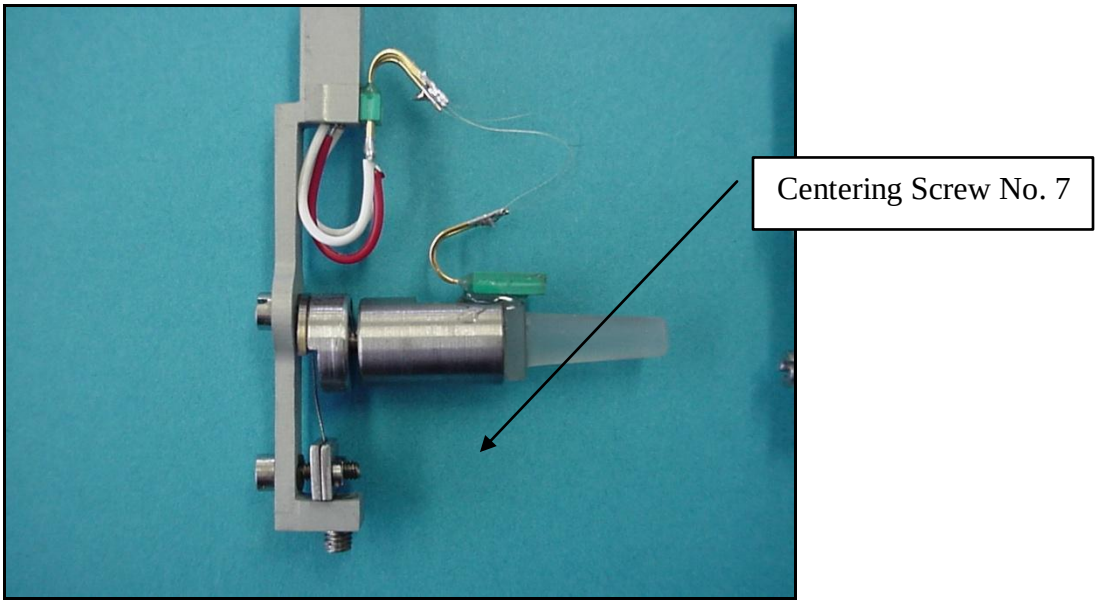

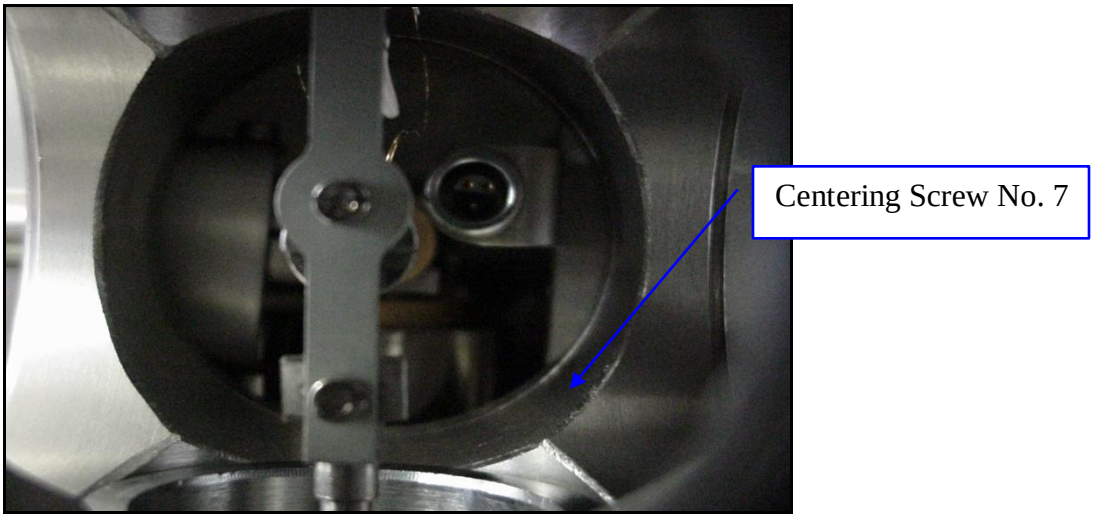

Use screws no 6 and 7 with the Allen key provided to center the measurement system.

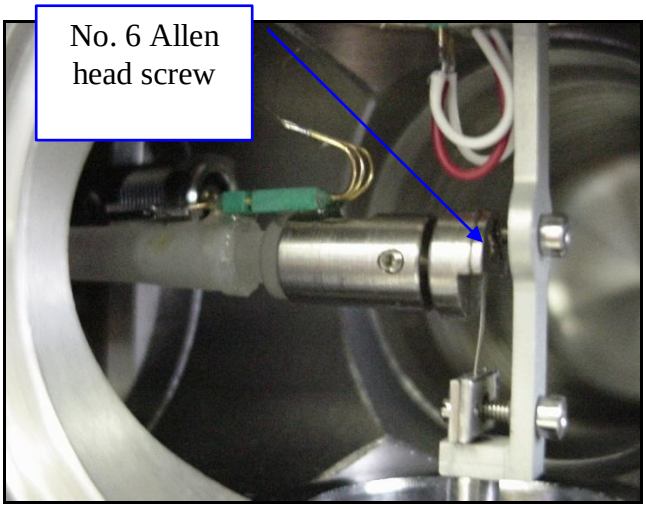

5. What to do if unable to setup the scales

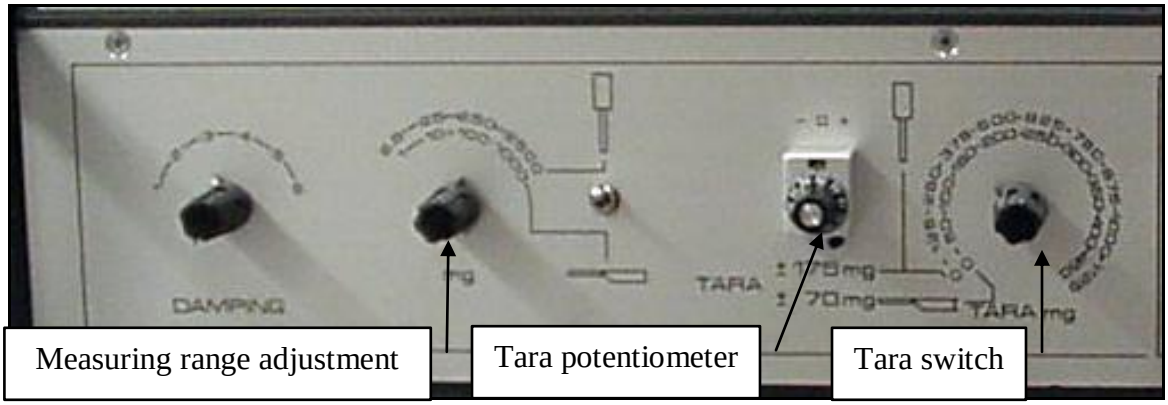

- Confirm that the vertical operation switch is in the “up” position
- Adjust the measuring range TG to +/- 2500 mg
- Adjust TARA potentiometer to 5.0
- Adjust TARA switch to 0 mg
- Remove balance counter weight glass cover at the left side of the balance

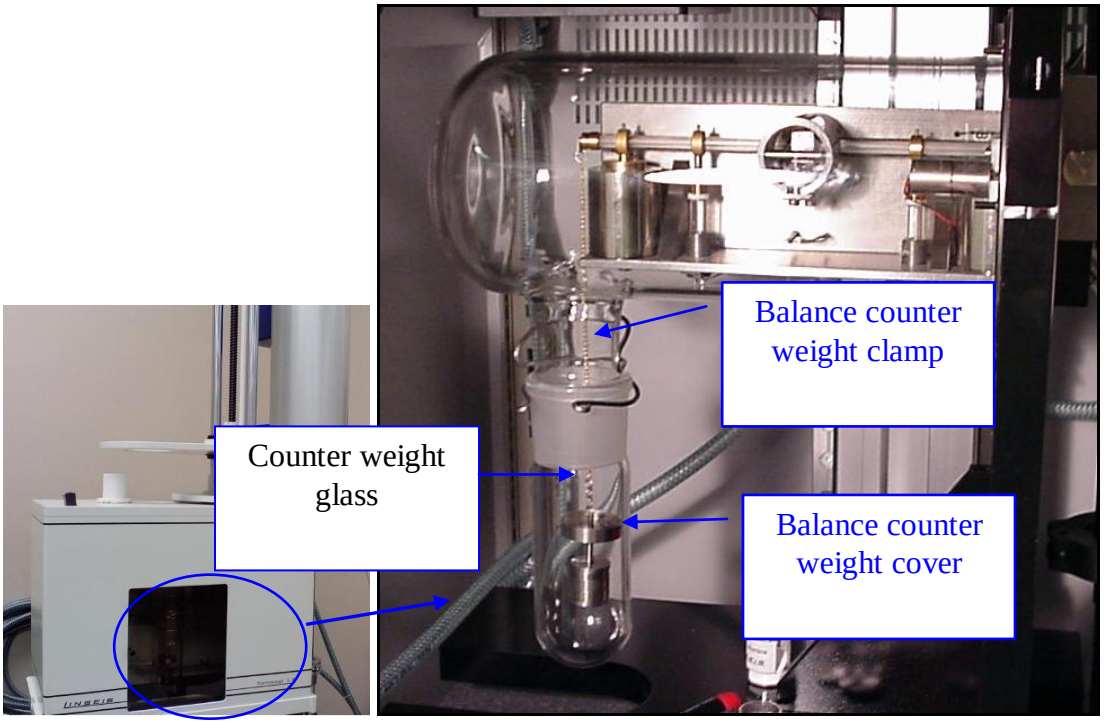

Add or remove weights (metal sleeves and/or lead balls) until the cursor is centered.

Once the cursor is within +/- 5% change the measuring range TG to +/- 250 mg.

Use the small balls to adjust the cursor to the center of the scales as close as possible to 0%.

Carefully close the balance counter weight glass cover at the left side of the balance and secure with the metal spring clamp. Try to eliminate any sway of the weight as you close the cover.

ANNEXES

Annexe 1- DTA reference of calcium oxalate

Thermo-balance measurement of Calziumoxalate
Calziumoxalate: $CaC_2O_4+1H_2O$
1. Stage: Dehydration: $CaC_2O_4 + 1H_2O \Rightarrow CaC_2O_4 + H_2O\uparrow$
Mass change: -12.3%

2. Stage: Building carboante: $CaC_2O_4 \Rightarrow CaCO_3 + CO\uparrow$
Mass change: -19.2% (-31.5% total)

3. Stage: Decarbonation: $CaCO_3 \Rightarrow CaO + CO_2\uparrow$
Mass change: -30.1% (-61.6% total)

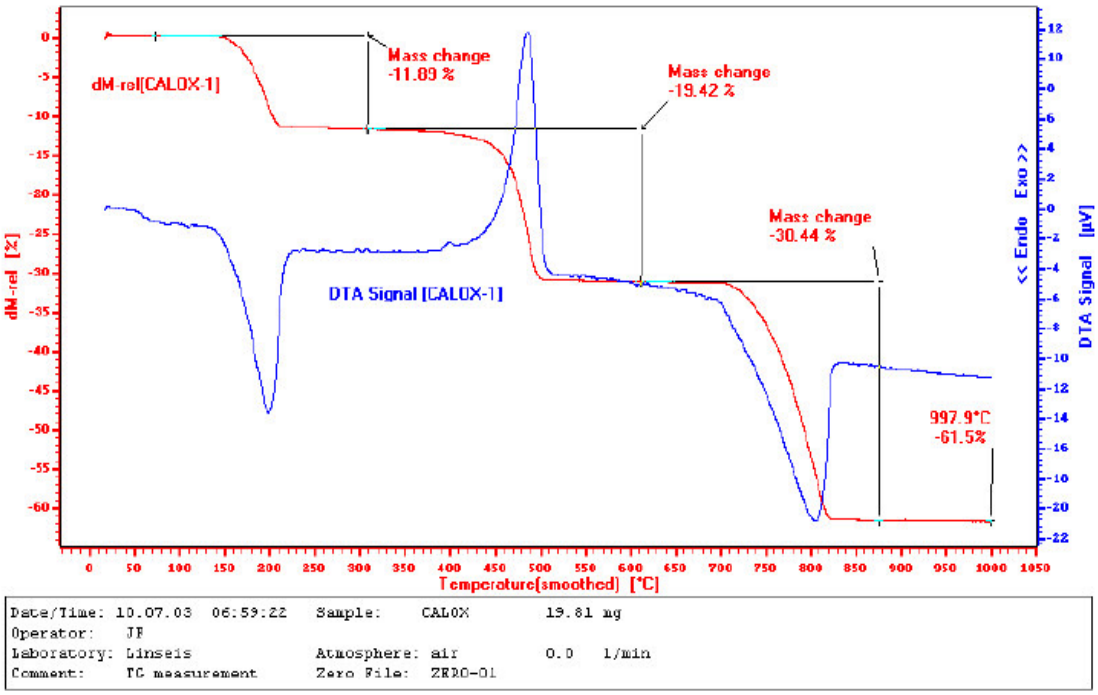

Heating rate: 10°C/min

Annexe 2 – improving the slope

Improving the baseline of the DTA if the slope is constantly up, or constantly down.

Below is an example of an upward slope.

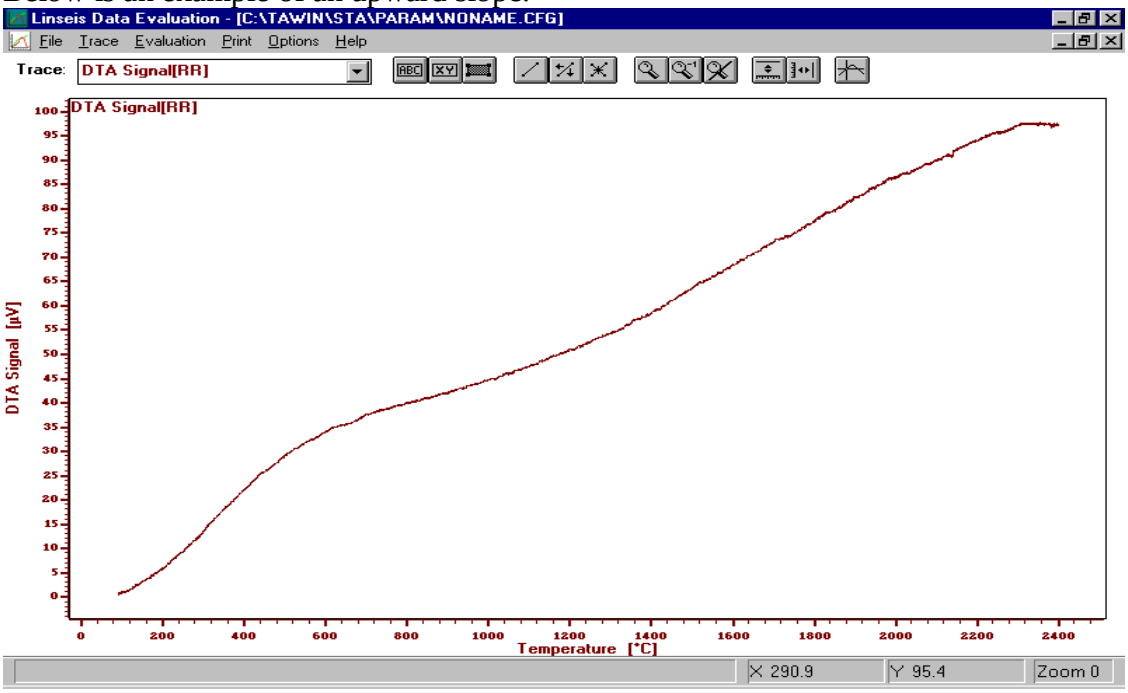

If your baseline has constant slope up or down and is repeatable it is easy to improve the baseline by following these steps:

Install the TGA/DTA sample holder

Place the same amount of reference material (Al_2O_3) in both crucibles.

Center the sample holder with the counter weights using the aluminum centering tool supplied with the instrument.

Run a zero curve with a heating rate of 5°C/min. to 1500°C

At approximately 1200°C turn the Sym potentiometer to bring the DTA signal back to 0µV

Improving the baseline of the DTA if the slope is not constantly up or constantly down.

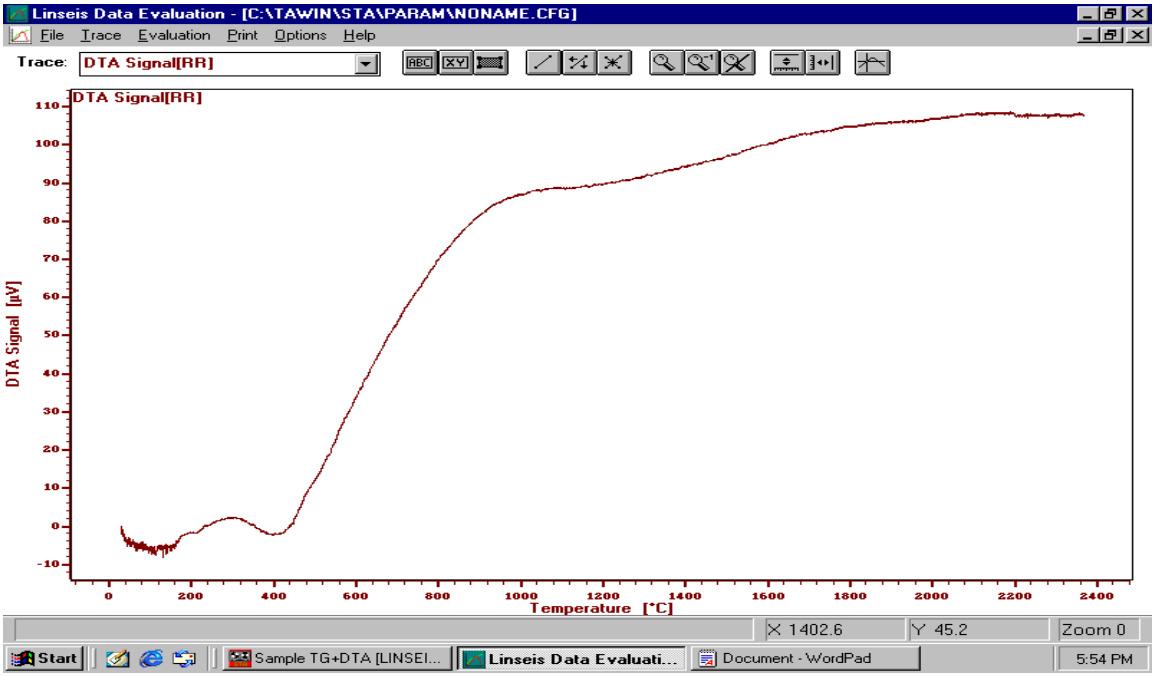

If the baseline is similar the above example without a constant slope, the procedure is different.

The adjustment should be made at the point in the curve where you want a straight baseline.

In the above example it would be better to repeat the measurement and at about 2000 C to use the potentiometer to bring the value back to 80µV. This would give you a horizontal baseline for the high temp range. If the value was adjusted to 0µV it would cause a neg.

REFERENCES

Resource 1

Website about polymers:

http://pslc.ws/mactest/dsc.htm

Resource 2

Principles and Applications of Thermal Analysis, Paul Gabbott

MSU Library reference: QD117.T4.A67 2007

APPENDIX C

MODEL CODE TEMPLATE FOR RELATIVE CRACK LENGTH MODEL

```
*HEADING
  RELATIVE CRACK LENGTH MODEL
  DOGBONE test model using 2D cohesive elements
*PREPRINT,MODEL=YES,HISTORY=YES
**Input parameters for tensile test analysis
*parameter
** Ultimate strenth in tensile and mode II:
 ultI  =  X
 ultII =  X
** cohesive layer modulus:
 Emod = X
** Fracture toughness:
GIc   = X
 GIIc  = X
** B-K parameter:
eta=X
** width in the plane strain direction
 width =X
**

**Define nodes for both models
**Model 1
*NODE
NODE ASSIGNMENTS FOR DAMAGED CRACK MODEL
NODE ASSIGNMENTS FOR DAMAGED BUT TREATED MODEL
*NSET
GENERATE NODE SETS TO DISCRIMINATE COHESIVE SECTIONS
CREATE NODE SETS FOR BOUNDARY LOADING CONDITIONS


**Define elements for each model
*ELEMENT,TYPE=CPE4
ELEMENTS FOR REGULAR SECTIONS
*ELEMENT,TYPE=COH2D4
ELEMENTS FOR COHESIVE SECTION
*ELSET
GENERATE OR DEFINE SECTION FOR STRESS ANALYSIS

**Section Definitions
*SOLID SECTION
DEFINE SECTION FOR NORMAL CONTINUUM ELEMENTS
```

```
**Material Definitions for Main Body Nylon
*MATERIAL,NAME=NYLON
*DENSITY
*ELASTIC, TYPE=ISO

**Define surfaces for cohesive sections
**After defining surfaces, define surface interactions and cohesive section parameters
*SURFACE,NAME=BOTTOM1
*SURFACE,NAME=TOP1
*SURFACE,NAME=BOTTOM2
*SURFACE,NAME=TOP2
*CONTACT PAIR, INTERACTION=FRACT
 BOTTOM1, TOP1
 BOTTOM2, TOP2
*SURFACE INTERACTION, NAME=FRACT
INTERACTION ZONE THICKNESS
*COHESIVE SECTION, elset=X, material=X, response=traction separation,
thickness=specified
 THICKNESS SPECIFICATION

**Material Definitions for Cohesive Material
*MATERIAL,NAME=adhesive
*ELASTIC,TYPE=TRACTION
 <Emod>,<Emod>,<Emod>

**Define Damage Criterion
*DAMAGE INITIATION,CRITERION=QUADS
 <ultI>, <ultII>
*DAMAGE EVOLUTION,TYPE=ENERGY,MIXED MODE
BEHAVIOR=BK,POWER=<eta>,SOFTENING=LINEAR
 <GIc>, <GIIc>
**

**Define Amplitude for Displacement Tensile Test
*AMPLITUDE, NAME=AMP1
 0.0,0.0   1.0,1.0

**Define Step
**----------------------------------------------------------------------
*STEP,NLGEOM, INC=120,convert sdi=no
*STATIC
DEFINE TIME STEP PARAMETERS

**Restrain Bottom and Pull Top Directly away from Base
```

```
*BOUNDARY
 DEFINE BOTTOM EDGES ENCASTRE AND TOP IN ALL BUT Y AXES
*BOUNDARY, OP=MOD, AMPLITUDE=AMP1
 DEFINE TOP SURFACE DISPLACEMENT FOR TIME PERIOD

**Define Outputs for Step
*output,field, freq=10
DEFINE DESIRED NODE AND ELEMENT FIELD OUTPUTS
*output, history
DEFINE DESIRED NODE AND ELEMENT FIELD OUTPUTS
*END STEP
**----------------------------------------------------------------------------
```

APPENDIX D

MODEL CODE TEMPLATE FOR ULTRASONIC INFLUENCE BY HEAT GENERATION

```
*Heading
HEAT GENERATION CODE
** Job name:  X  Model name:  X
** use with user=X.f
*Preprint, echo=NO, model=NO, history=NO, contact=NO
CLEAR PAST INFO
**
** PARTS
**
*Part, name=PART-1-1
DEFINE PART
*Node
DEFINE NODES
*Element, type=DC2D3
DEFINE ELEMENTS
*Nset, nset=INTERNAL, internal
DEFINE NODE REGION(S) FOR DIFFERENT MATERIAL PROPERTIES
  *Elset, elset=INTERNAL, internal, generate
DEFINE ELEMENT REGION(S) FOR DIFFERENT MATERIAL PROPERTIES
**
** Section: Section-1-INTERNAL
*Solid Section, elset=INTERNAL, material=MATERIAL-1
DEFINE SECTION(S) FOR DIFFERENT MATERIAL PROPERTIES
**
*End Part
**
** ASSEMBLY
*Assembly, name=Assembly
*Instance, name=PART-1-1, part=PART-1-1
*End Instance
**
*Nset, nset=BOTTOM, internal, instance=PART-1-1
*Elset, elset=BOTTOM, internal, instance=PART-1-1
DEFINE NODE OR ELEMENT SETS FOR BOUNDARY CONDITIONS AND LOADS
*Surface, type=ELEMENT, name=BOT
DEFINE SURFACE(S) IF NEEDED
*End Assembly
**
**
** MATERIALS
**
*Material, name=MATERIAL-1
```

*ELASTIC
X,X
*CONDUCTIVITY
X
*DENSITY
X
*SPECIFIC HEAT
X
*HEAT GENERATION
**
** PREDEFINED FIELDS
**
** Name: Predefined Field-1 Type: Temperature
*Initial Conditions, type=TEMPERATURE
DEFINE INITIAL CONDITION(S)
** --
*Step, name=Step-1
*Heat Transfer
DEFINE STEP PARAMETERS
*Boundary
BOUNDARY CONDITIONS AND/OR FLUXES
** OUTPUT REQUESTS
**
** FIELD OUTPUT: F-Output-1
DEFINE FIELD OUTPUT(S)
** HISTORY OUTPUT: H-Output-1
DEFINE HISTORY OUTPUT(S)
*End Step

APPENDIX E

MODEL CODE TEMPLATE FOR HEAT GENERATION SUBROUTINE IN FORTRAN

```
      SUBROUTINE HETVAL(CMNAME,TEMP,TIME,DTIME,SVAR,FLUX,PREDEF,
     1                  DPRED)
C
      INCLUDE 'ABA_PARAM.INC'
C
      CHARACTER*80 CMNAME
      DIMENSION TEMP(2),SVAR(1),PREDEF(1),TIME(2),FLUX(2),DPRED(1)
C
      FLUX(1)=FLUX VALUE
      RETURN
      END
```